An introduction to FLUKA physics models and applications

Rossendorf, 29 August 2002

A. Ferrari

CERN, Geneva Switzerland (on leave from INFN-Milan)

Topics

- Hadronic interactions in FLUKA: short description and examples
- Neutrino interactions
- Photonuclear reactions
- (*Ionization Energy losses, multiple scattering, EM showers, muons)*
- Complex benchmarks
- The atmospheric neutrino calculations and other "cosmic ray" applications
- Heavy ion interactions: work in progress

FLUKA

Authors: **A. Fassò[†], A. Ferrari[&], J. Ranft[*], P.R. Sala[&]**
[†] CERN, [&] INFN Milan and CERN, [*] Siegen University

Interaction and transport MonteCarlo code

- Hadron-hadron and hadron-nucleus interactions 0-100 TeV
- Nucleus-nucleus interactions 0-10000 TeV/n: *under development*
- Electromagnetic and μ interactions 1 keV-100 TeV
- Neutrino interactions
- Charged particle transport including all relevant processes
- Transport in magnetic field
- Combinatorial (boolean) geometry
- Neutron multigroup transport and interactions 0-20 MeV
- Analogue or variance reduction calculations

A multipurpose code

The program can be used in different fields such as shielding, dosimetry, high energy experimental physics and engineering, cosmic ray studies, medical physics, etc.

- Each radiation component is treated as far as possible with the same level of accuracy (it's like having 4 different programs in one, for pure neutron, electron-photon or muon problems – and hadrons, of course!)
- FLUKA can be run in fully analog mode, for calorimetry. It can calculate coincidences and anticoincidences
- It can also be run in biased mode, for shielding design

  But also experimental high energy physicists need sometimes to make studies of deep penetration or rare events: hadron punchthrough, radiation background in underground experiments, muon production over short decay lengths

FLUKA History

- *Beginning of the* FLUKA *history : 1962* Johannes Ranft (Leipzig) and H. Geibel (CERN): MonteCarlo for high energy beams
- *The name* FLUKA *: 1970*: calorimeter fluctuations on an event-by-event basis (FLUKA = FLUktuierende KAskade).
- *From the the beginning of the 70's* J. Ranft and coworkers(Leipzig), with contributors from Helsinki (J. Routti, P. Aarnio) and CERN (G.R. Stevenson, A. Fassò) till $\approx$ 1987.
- *The present code : since 1990* mostly INFN-Milan : little or no remnants of older versions. Link with the past: J. Ranft, A. Fassò
- *The GEANT-FLUKA interface:* 1993 the FLUKA hadronic package interfaced with GEANT3. *no development/update thereafter*
- *In MCNPX:* High energy hadronic FLUKA generator, 1990 status
- *The FLUKA project: since Sept. 2001* FLUKA is an official INFN project

The FLUKA hadronic models

Hadron-Nucleon

Elastic, exchange	P<3-5GeV/c	low E π,K	High Energy
Phase shifts,	Resonance prod.	Special	DPM
data,eikonal	and decay		hadronization

Hadron-Nucleus

P<4-5GeV/c	High Energy
PEANUT:	Glauber-Gribov
Sophisticated GINC	multiple interactions
preequilibrium	Coarser GINC

Evaporation/Fission/Fermi break-up

γ deexcitation

Hadron-nucleon interaction models

Elastic, charge exchange and strangeness exchange reactions:

- Available phase-shift analysis and/or fits of experimental differential data
- At high energies, standard eikonal approximations are used

Particle production interactions: two kind of models

- Those based on "resonance" production and decays, which cover the energy range up to 3–5 GeV
- Those based on quark/parton string models, which provide reliable results up to several tens of TeV

Nucleon–nucleon cross sections I

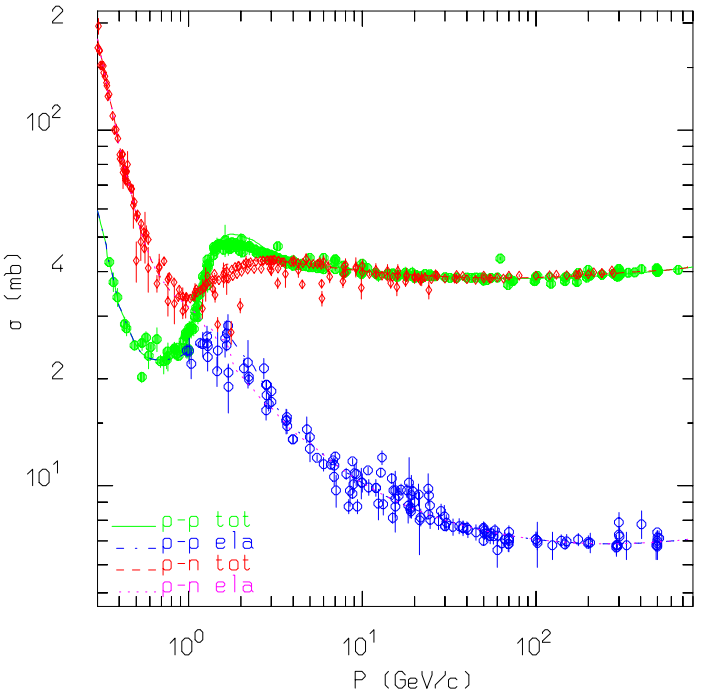

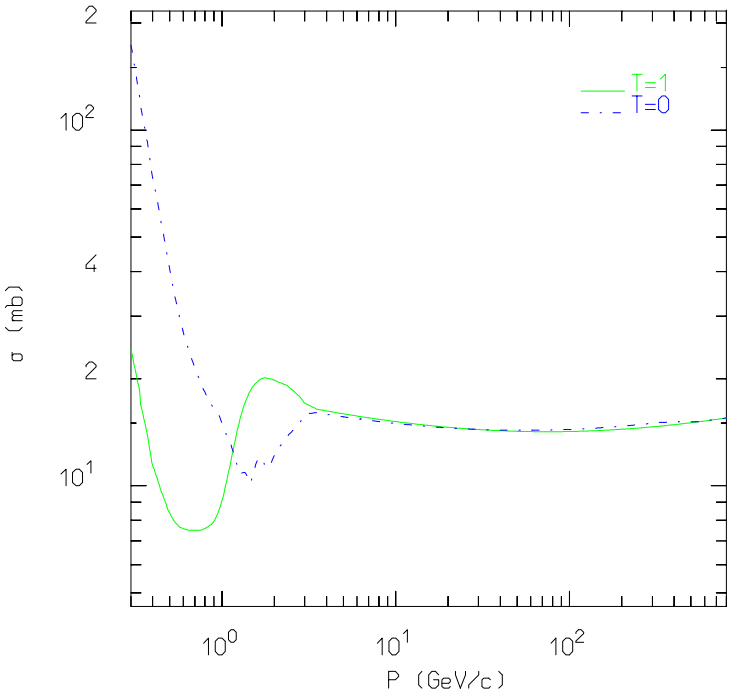

Total and elastic cross section for p–p and p–n scattering, together with experimental data (left), isospin decomposition in the T=0 and T=1 components (right)

π–nucleon cross sections I

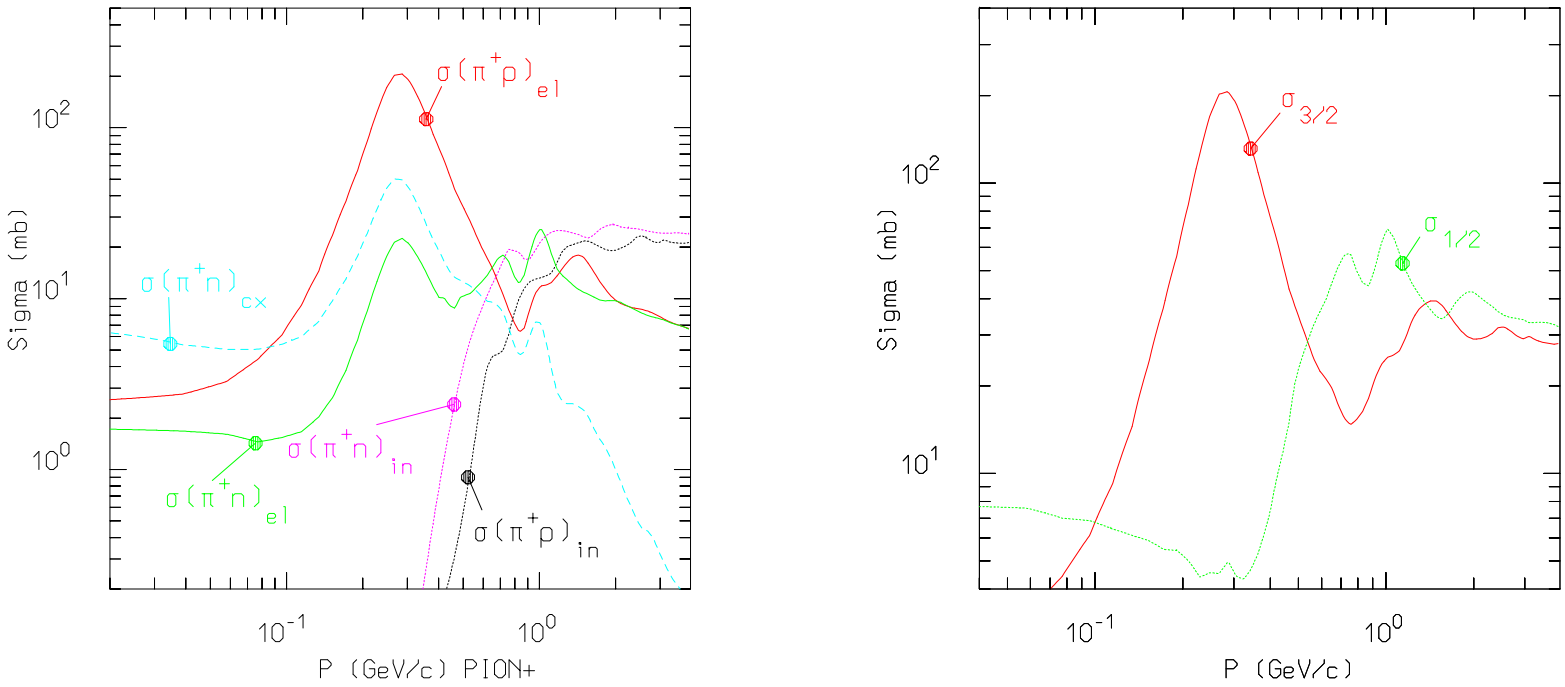

Elastic, chx and inel. cross sections for π–N scattering (left), isospin decomposition in the T=1/2 and T=3/2 components (right)

Nonelastic hN interactions at intermediate energies

- $N_1 + N_2 \to N_1' + N_2' + \pi$ threshold around 290 MeV, important above 700 MeV,
- $\pi + N \to \pi' + \pi'' + N'$ opens at 170 MeV.

Dominance of the Δ resonance and of the N^* resonances $\to$ reactions treated in the framework of the isobar model $\to$ all reactions proceed through an intermediate state containing at least one resonance.

$$\begin{aligned} N_1 + N_2 &\to N_1' + \Delta(1232) \to N_1' + N_2' + \pi \\ \pi + N &\to \Delta(1600) \to \pi' + \Delta(1232) \to \pi' + \pi'' + N' \\ N_1 + N_2 &\to \Delta_1(1232) + \Delta_2(1232) \to N_1' + \pi_1 + N_2' + \pi_2 \end{aligned}$$

Resonance energies, widths, cross sections, branching ratios from data and conservation laws, whenever possible. Inferred from inclusive cross sections when needed

Inelastic hN at high energies: (DPM, QGSM, ...)

- Problem: "soft" interactions $\rightarrow$ no perturbation theory.
- Solution : Interacting strings (quarks held together by the gluon-gluon interaction into the form of a string)
- Interactions treated in the Reggeon-Pomeron framework
- At sufficiently high energies the leading term corresponds to a Pomeron (IP) exchange (a closed string exchange)
- Each colliding hadron splits into two colored partons $\rightarrow$ combination into two color neutral chains $\rightarrow$ two back-to-back jets
- Physical particle exchange produce single chains at low energies
- Higher order contributions with multi-Pomeron exchanges important at $E_{lab} \geq$ 1 TeV

From resonance production to DPM

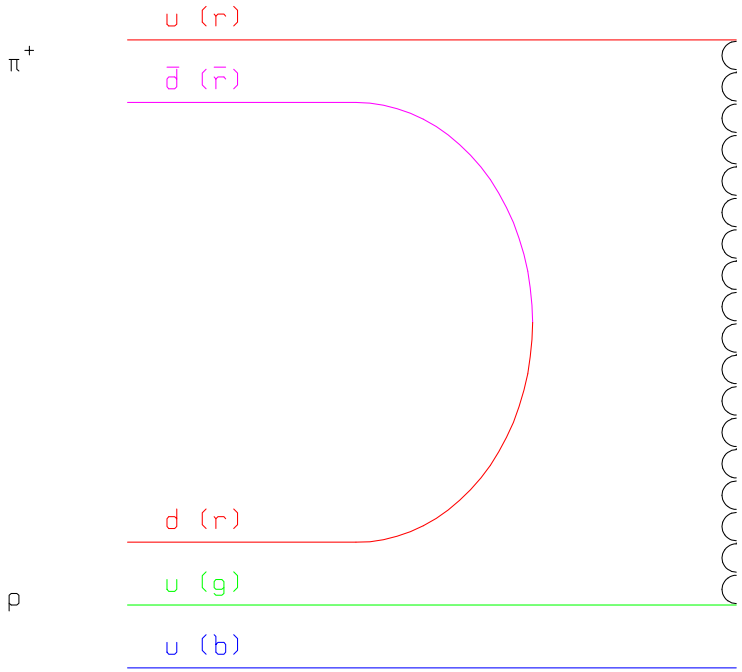

Single chain diagram for $\pi^+ - p$ scattering, corresponding to a physical particle exchange. The color (red, blue, and green) and quark combination shown in the figure is just one of the allowed possibilities

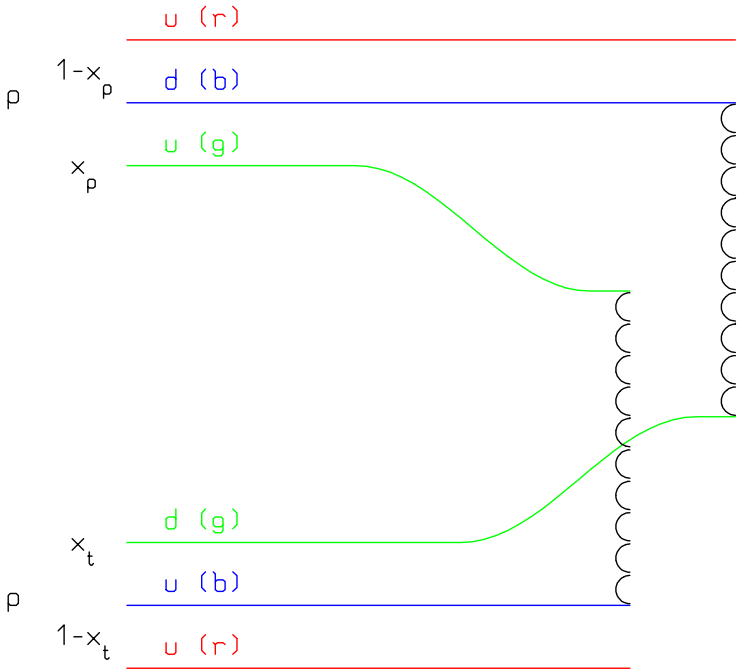

Leading two-chain diagram in DPM for $p - p$ scattering. The color (red, blue, and green) and quark combination shown in the figure is just one of the allowed possibilities

DPM: chain examples

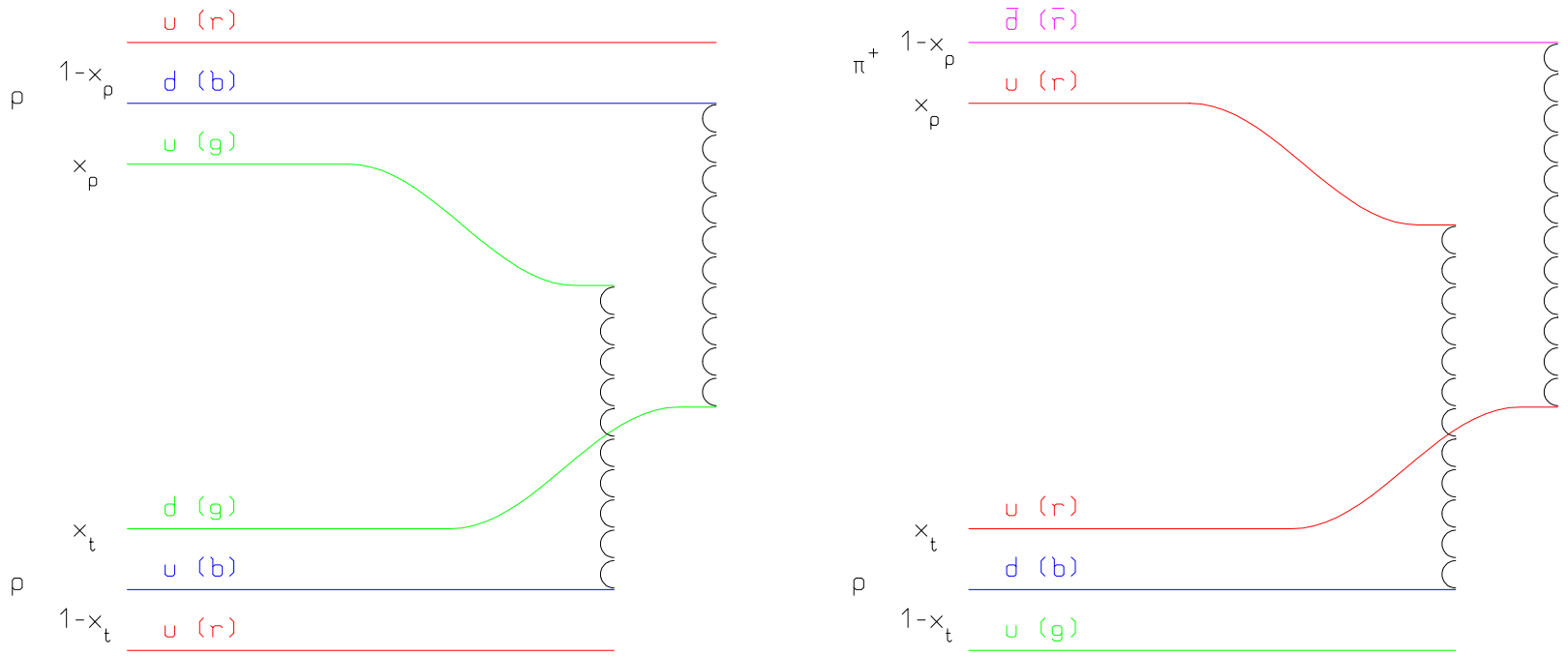

Leading two-chain diagrams in DPM for $p-p$ (left) and $\pi-p$ (right) scattering. The color (red, blue, and green) and quark combinations shown in the figure are just one of the allowed possibilities

DPM and hadronization

from DPM:

- Number of chains
- Chain composition
- Chain energies and momenta
- Diffractive events

Almost No Freedom

Chain hadronization

- Assumes chain universality
- Fragmentation functions from hard processes and e^+e^-
- Transverse momentum from uncertainty considerations
- Mass effects at low energies

The same functions and (few) parameters for all reactions and energies

Nonelastic hN at high E :(π^+ p), 7-22 GeV

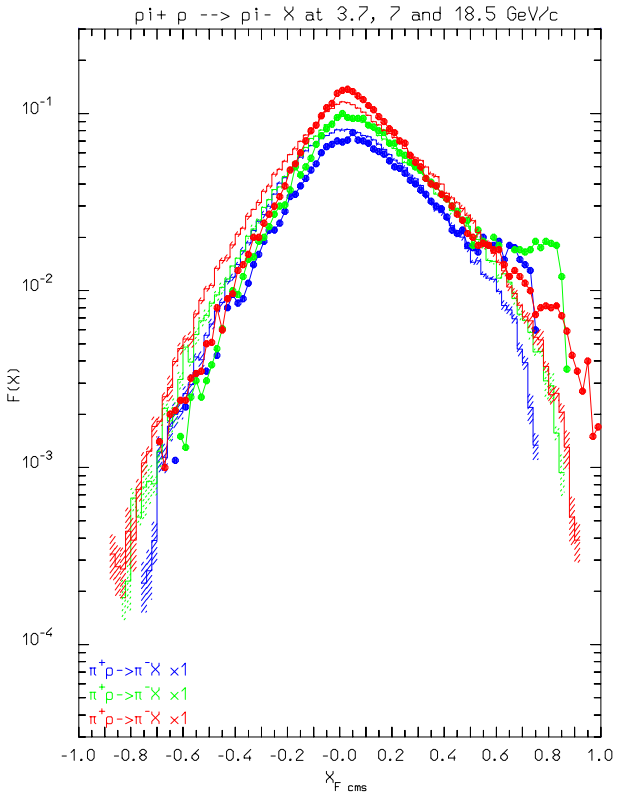

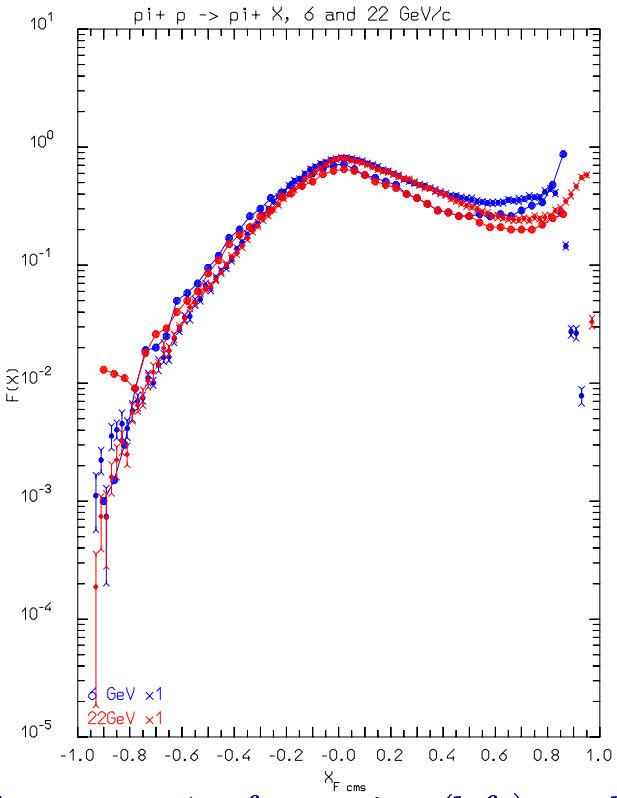

Invariant cross section spectra, as a function of Feynman x_F^* of negative (left), and positive (right) pions emitted for π^+ on protons at various momenta. Data from M.E Law et al. LBL80 (1972).

Nonelastic hN high E: (K^-p) , (π^-p) 10-16 GeV, p_T

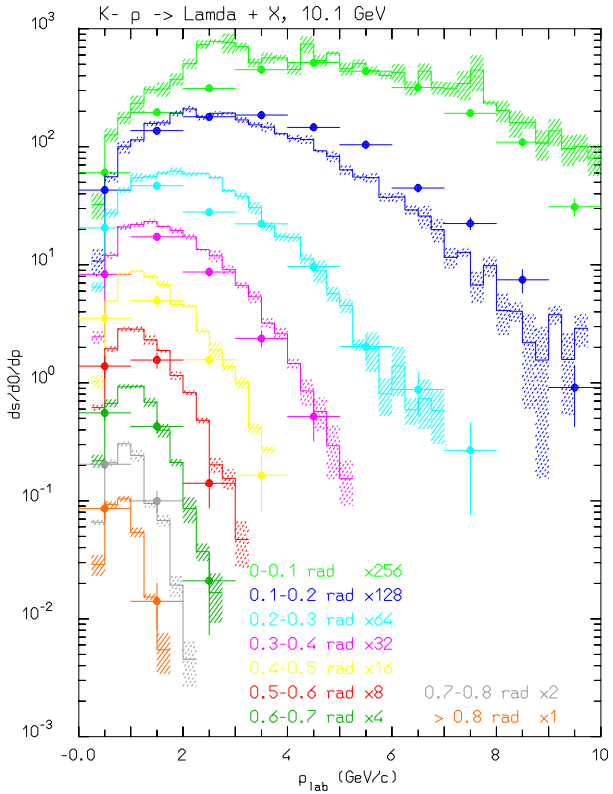

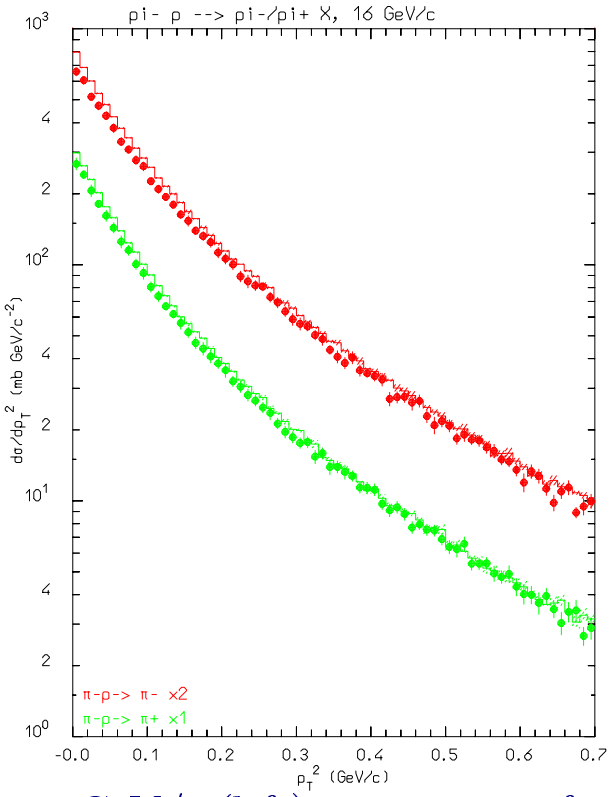

Double differential cross section for $K^-p \to \Lambda X$ at 10 GeV/c (left), p_T spectra of π^+ and π^- produced by 16 GeV/c π^- incident on an hydrogen target. Data from M.E Law et al. LBL80 (1972).

Nonelastic hN high E: (π^+ p) 250GeV, x_F and p_t

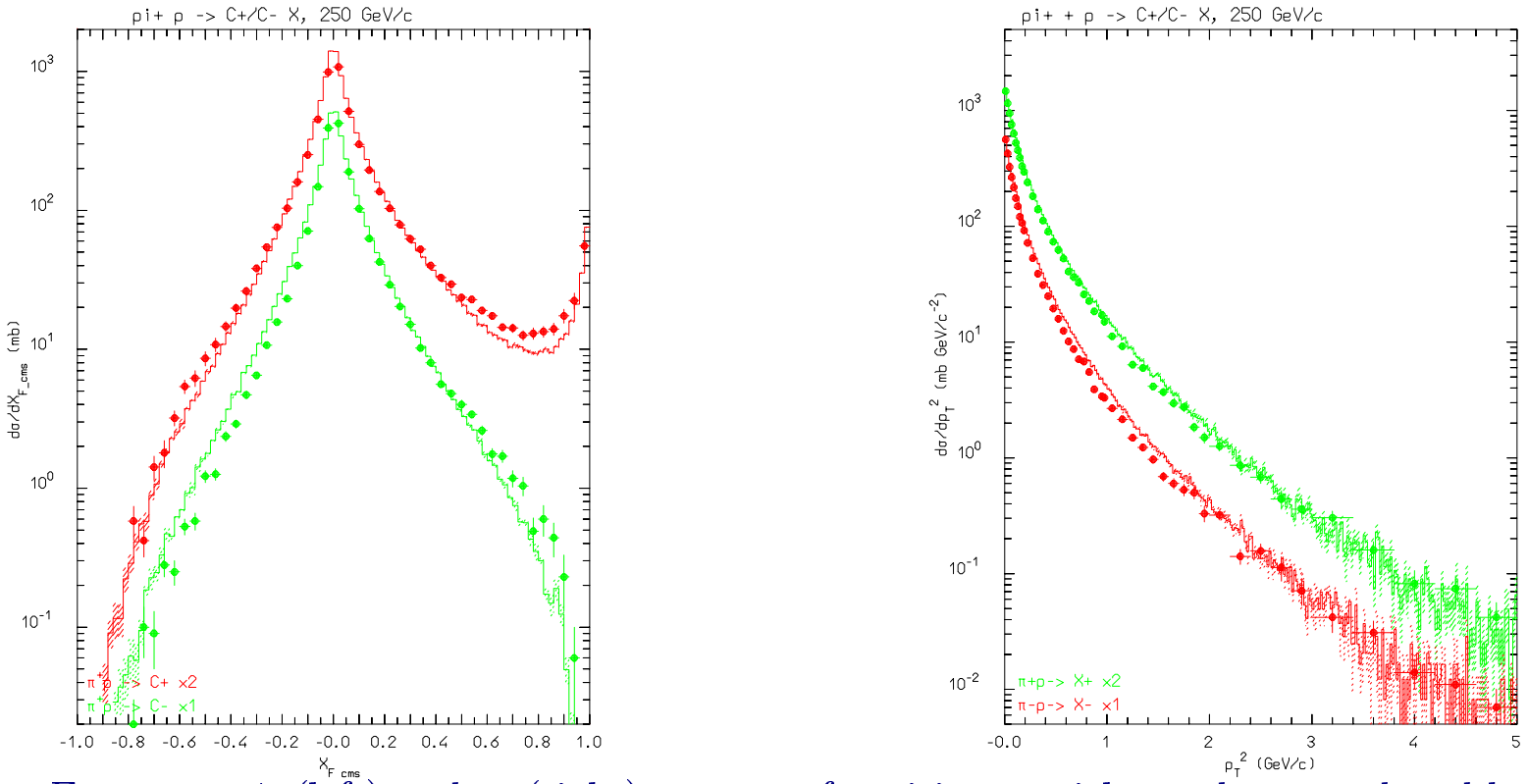

Feynman x_F^* (left) and p_t (right) spectra of positive particles and π^- produced by 250 GeV/c π^+ incident on an hydrogen target. Exp. data (symbols) have been taken from M. Adamus et al. ZPC39, 311 (1988).

hA at high energies: GLAUBER Cascade

Elastic, Quasi-elastic and Absorption hA cross sections derived from Free hadron-Nucleon cross section + Nuclear ground state ONLY .

Inelastic interaction $\equiv$ multiple interaction with ν target nucleons, with binomial distribution:

$$P_{r\ \nu}(b) \equiv \left(\begin{array}{c} A \\ \nu \end{array} \right) P_r^{\nu}(b) \left[1 - P_r(b)\right]^{A-\nu}$$

where $P_r(b) \equiv \sigma_{hN\ r} T_r(b)$, and $T_r(b)$=folding of nuclear density and scattering profiles along the path.

On average :

$$< \nu >= \frac{Z\sigma_{hp\ r} + N\sigma_{hn\ r}}{\sigma_{hA\ abs}}$$

$$\sigma_{hA\ abs}(s) = \int \mathrm{d}^2\vec{b} \left[1 - (1 - \sigma_{hN\ r}(s) T_r(b))^A\right]$$

h-A at high energies: Glauber-Gribov

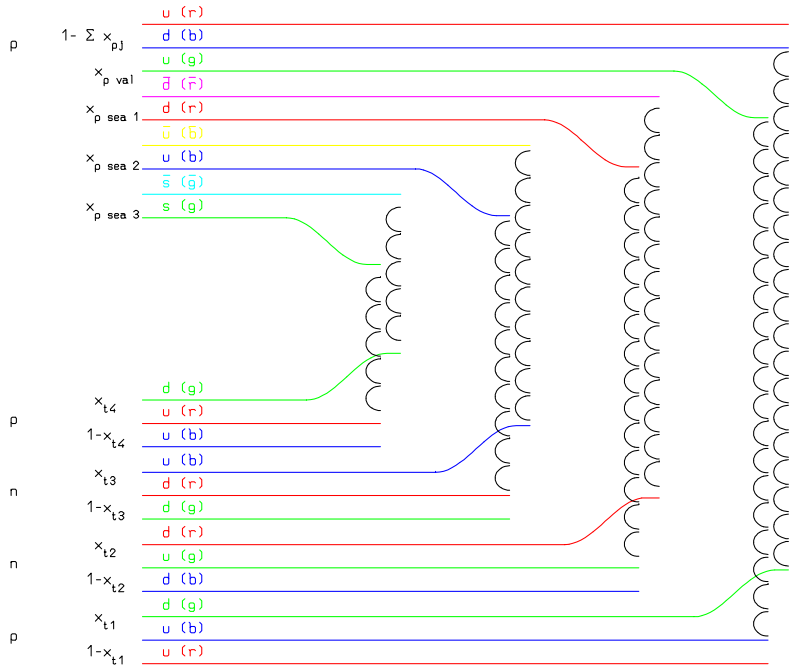

One of the possibilities for Glauber-Gribov scattering with 4 collisions

Gribov

$\Downarrow$

2ν chains

2 valence-valence chains

$2(\nu - 1)$ chains between projectile sea and target valence (di)quarks.

No freedom, except in mass effects at low energies.

Fermi motion included $\rightarrow$ smearing of E and p_T distributions

Nonelastic hA interactions at high energies: examples

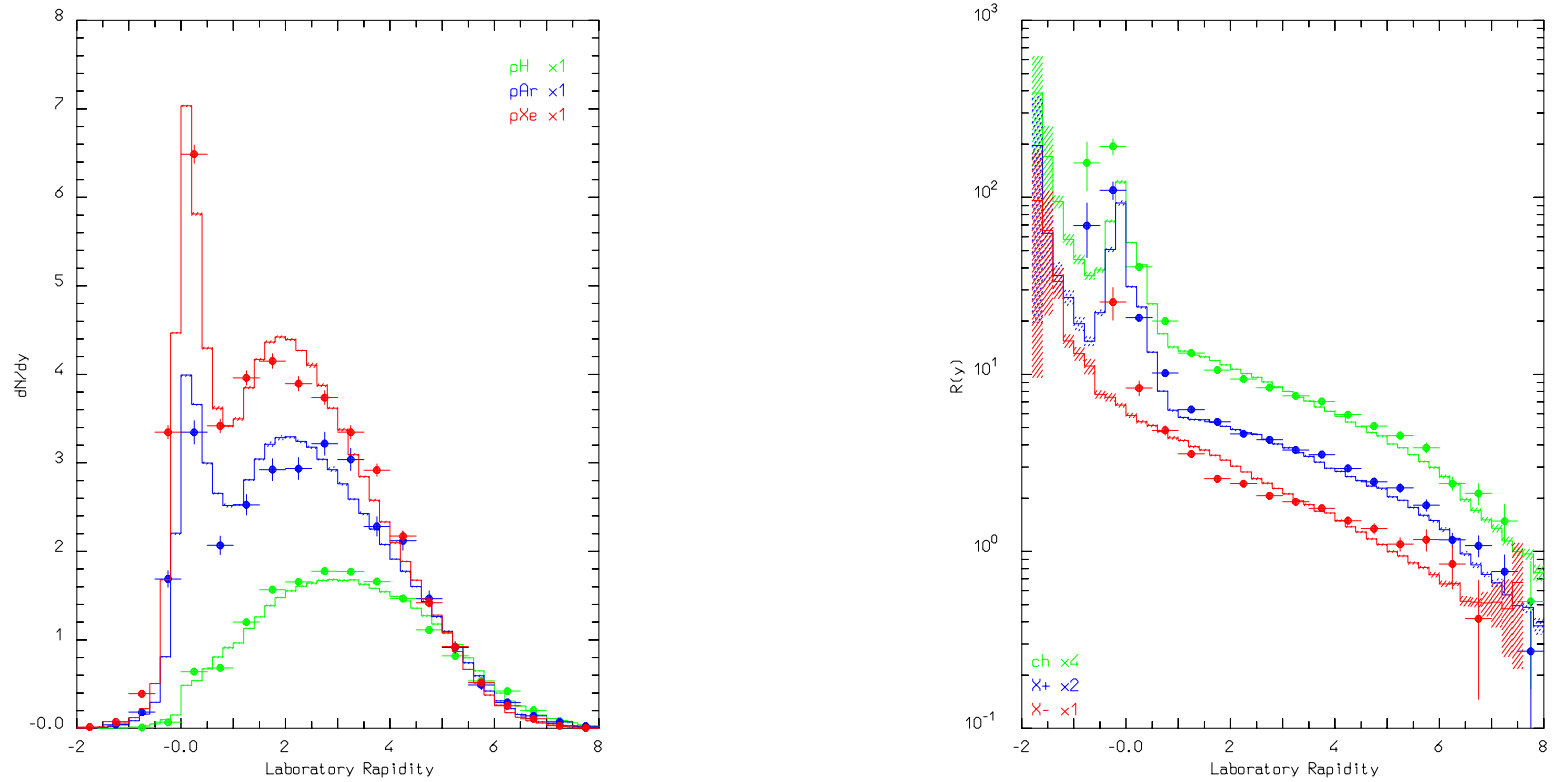

Rapidity distribution of charged particles produced in 200 GeV proton collisions on Hydrogen, Argon, and Xenon target (left) and ratio of rapidity distribution of charged, positive, and negative particles produced in 200 GeV proton collisions on Xenon and Hydrogen (right). Data from C. De Marzo et al., PRD26, 1019 (1982).

Nonelastic hA interactions at high energies: examples

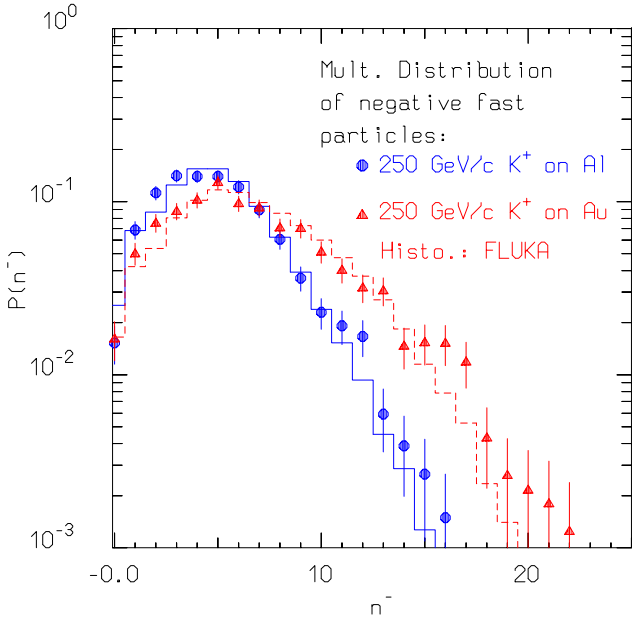

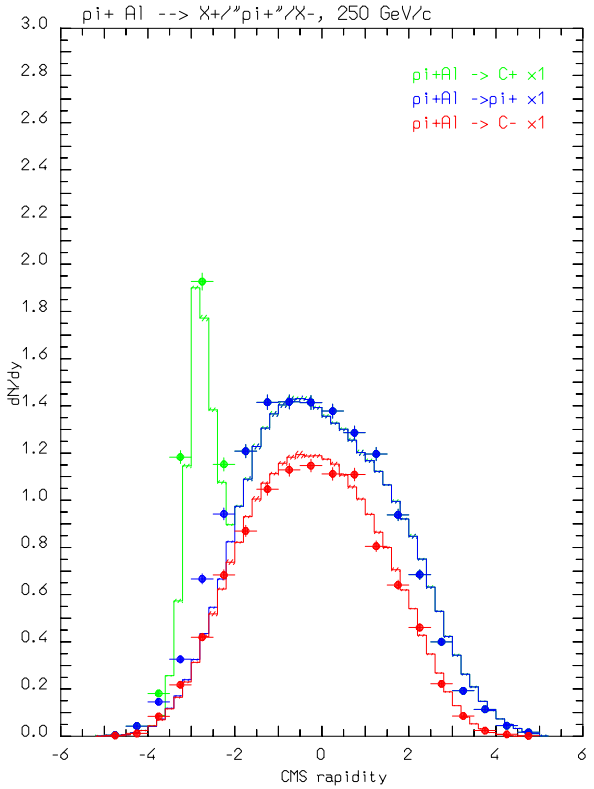

Multiplicity distribution of negative shower particles for 250 GeV/c K^+ on Aluminium and Gold targets (left), and rapidity distribution of positive, negative, and "π^+" particle for 250 GeV/c π^+ on Aluminium (right). Data from I.V. Ajinenko et al. ZPC42 377 (1989) and N.M. Agababyan et al. ZPC50 361 (1991).

Recent improvements in the high energy model

The DPM + Glauber model embedded into old FLUKA versions (and in *MCNPx*, *GEANT-FLUKA*) had important limitations:

- Glauber cascade described at an elementary level;
- all resonances assumed on mass shell;
- coarse chain hadronization, and no particular attention to threshold and finite mass effects;
- isospin conservation not enforced at each individual hadron production step;
- transverse motion reasonable but still far from satisfactory;
- simplified description of diffractive processes.

Recent improvements in the high energy model

All improved along the years:

Very old reference : FLUKA92 and GEANT-FLUKA

Many versions in between: most already done in 1995

Latest optimization: chain hadronization [1]

- *Threshold and finite mass effects checked against low energy data (chains with few had.)*
- *Fragmentation functions checked vs. 16-450 GeV h-N and h-A data*
- *Constraint: hadron multiplicity at 200 GeV*
- *Balanced optimization: better SPY agreement could be achieved, spoiling low energy data*

[1] (G. Collazuol, A. Ferrari, A. Guglielmi and P.R. Sala, NIM A 449 (2000), 609

Improvements: SPY II : forward yield

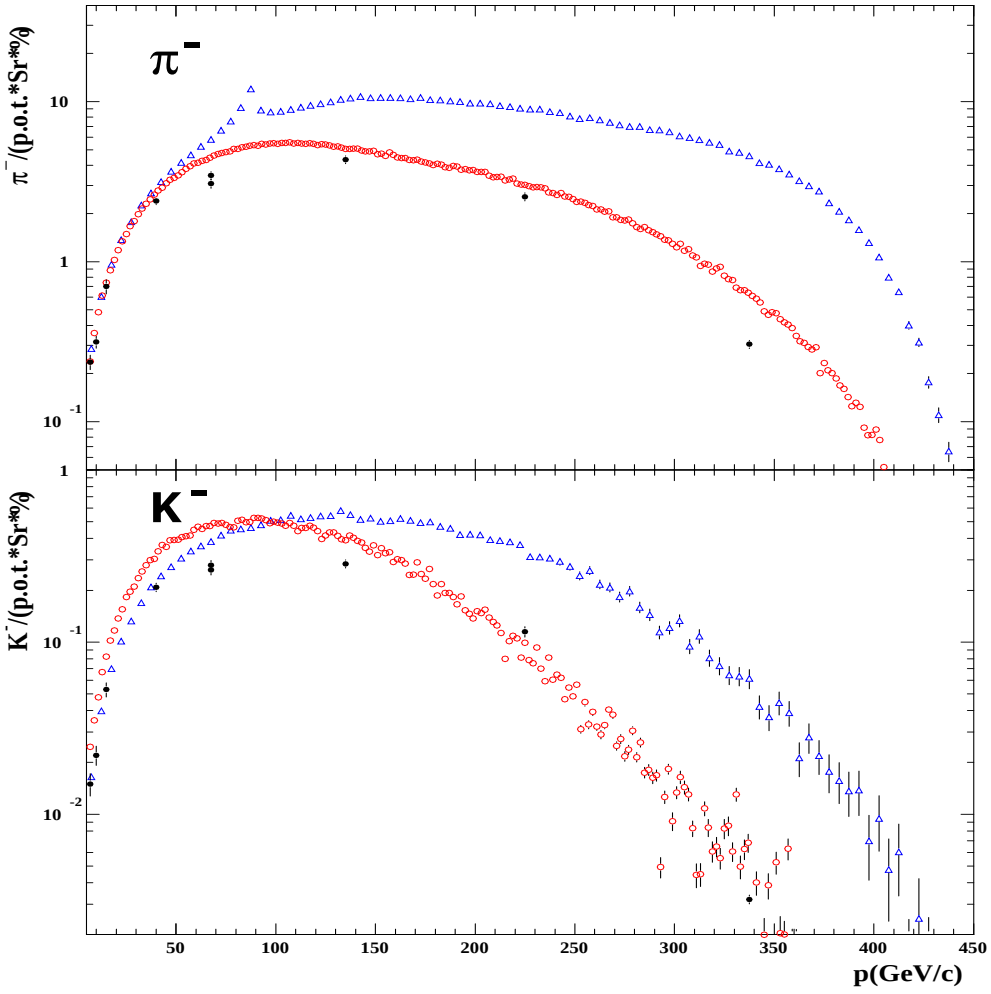

π^- and K^-

$d^2N\,/\,(dp/p\,d\Omega)$

100 mm Be target,

$\theta \leq 0.2$ mrad

SPY ($P \leq 135$ GeV/c, •)

and Atherton et al.

($P \geq 67.5$ GeV/c,)

compared with the

FLUKA and the

GEANT-FLUKA

predictions.

Comparison with SPY I

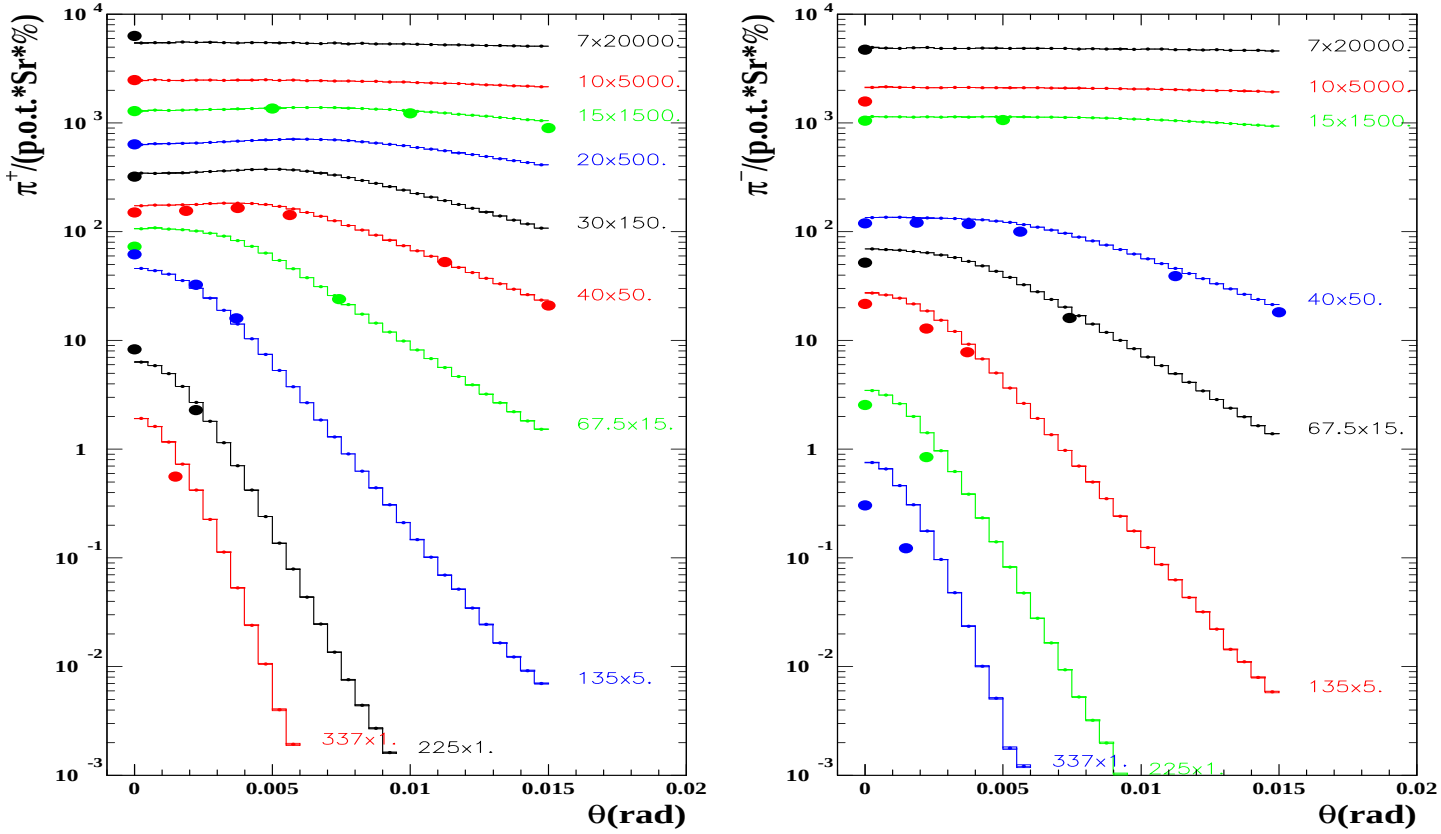

Double differential cross section for π^+ (left) and π^- (right) production for 450 GeV/c protons on a 10 cm thick Be target (data from H.W. Atherton CERN 80–07, G. Ambrosini et al. PL B425 208 (1998)).

Nonelastic hA interactions at high energies: examples IV

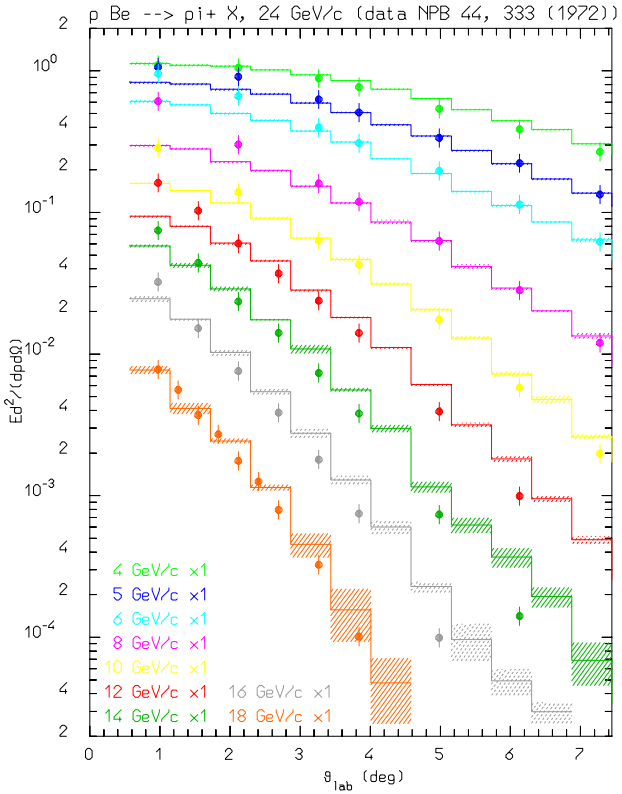

Invariant cross section distribution for π^+, 24 GeV/c protons on Be (T.Eichten et al. NPB 44, 333 (1972)).

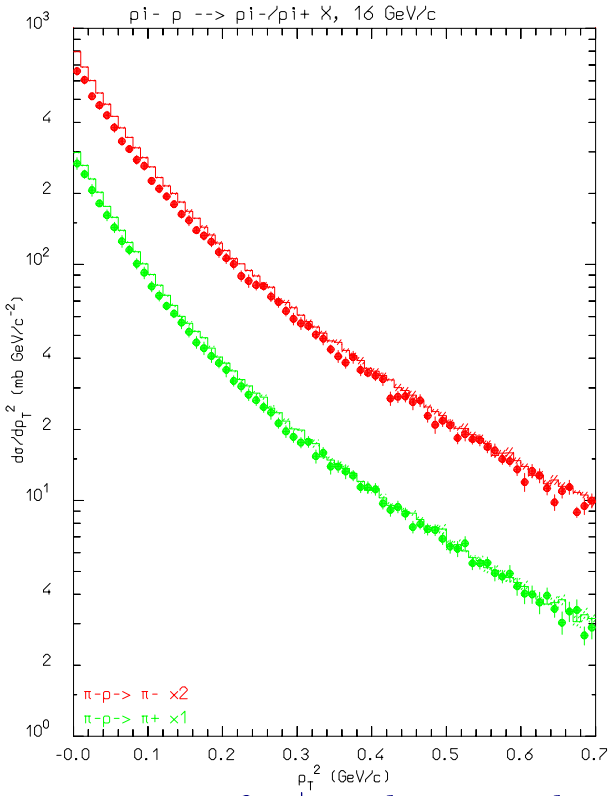

p_T spectra of π^+ and π^- produced by 16 GeV/c π^- on H. (M.E Law et al. LBL80 (1972)).

Improvements: effect on WANF

Intensity, mean energy and relative abundances for ν fluxes at NOMAD fiducial area as calculated with the FLUKA and GEANT-FLUKA generator.

	Neutrino	intensity $[\nu/pot]$	$< E_\nu >$ $[GeV]$	relative abb.
FLUKA	ν_μ	1.11×10^{-2}	23.5	1.0
	$\overline{\nu}_\mu$		19.2	0.0627
	ν_e		37.1	0.0094
	$\overline{\nu}_e$		31.3	0.0024
GEANT-FLUKA	ν_μ	1.25×10^{-2}	23.5	1.0
	$\overline{\nu}_\mu$		23.1	0.0702
	ν_e		36.7	0.0092
	$\overline{\nu}_e$		34.2	0.0025

CERN Neutrino to GranSasso

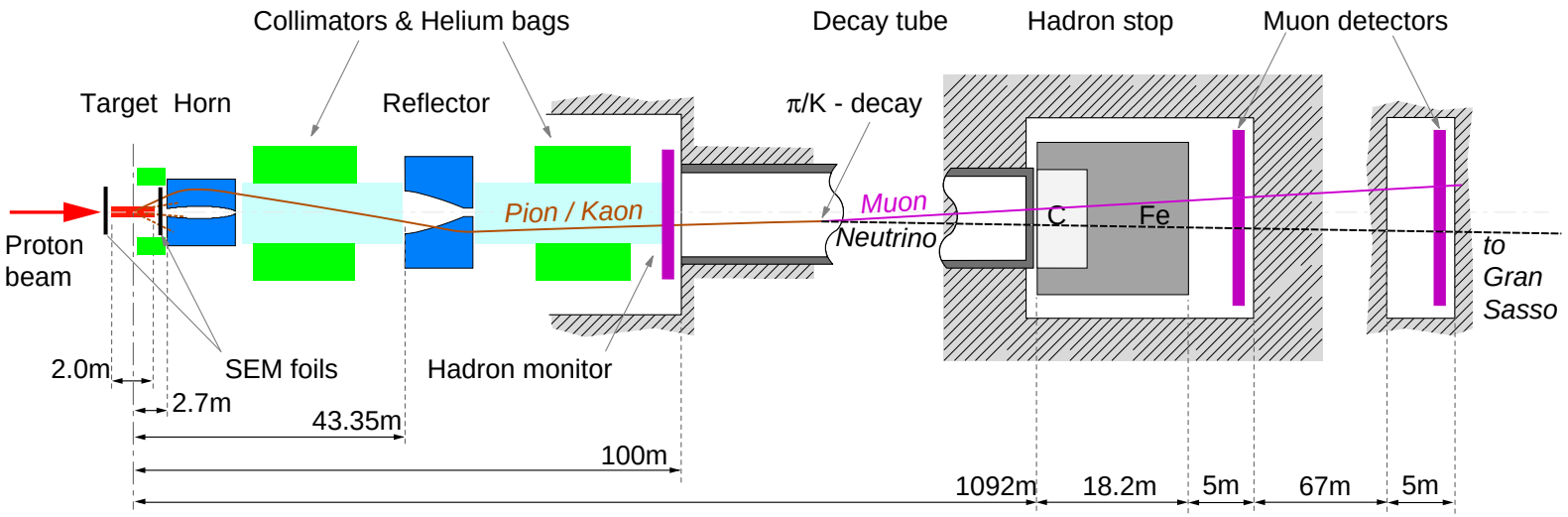

400 GeV/c protons, double fast extraction, $5\ 10^{13}$ protons every 6 s

Thin graphite target (⌀5/4 mm, 13 bars 100 mm each)

Two magnetic lenses focalize 35 and 50 GeV positive

1 Km decay tube

730 Km to Gran Sasso

Nice agreement with experiment → confidence in prediction for CNGS

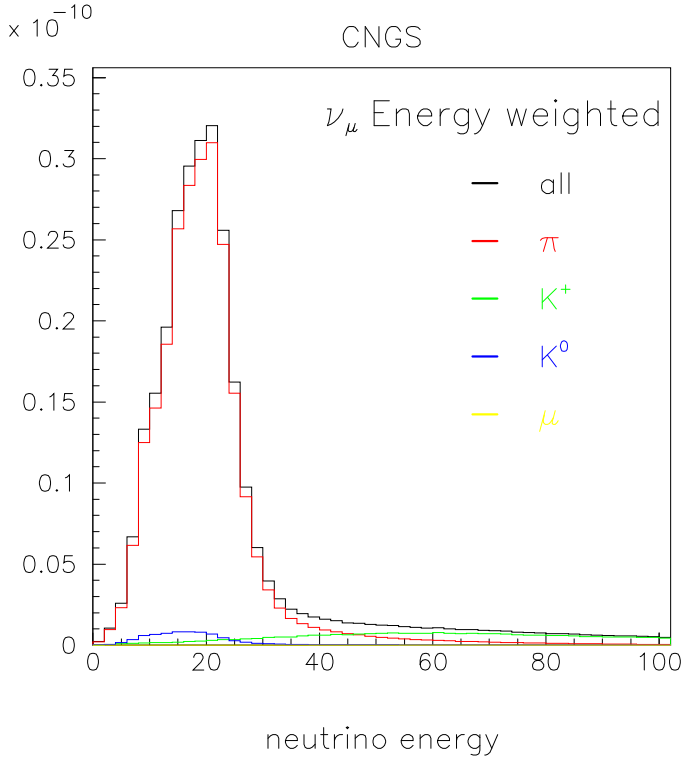

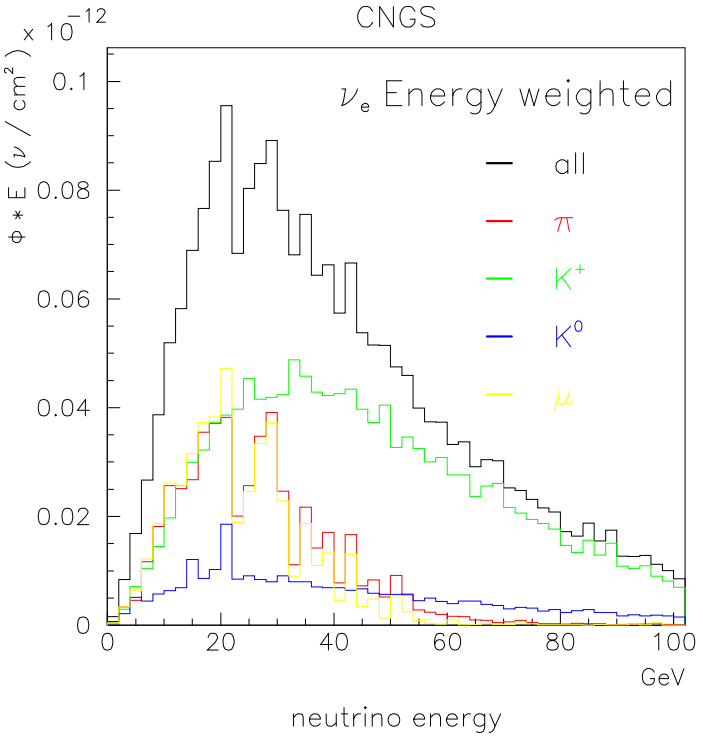

Baseline CNGS target : 13 Graphite rods, ⌀=5(x2) 4(x11) mm, total length 2000 mm, Carbon length 1280 mm

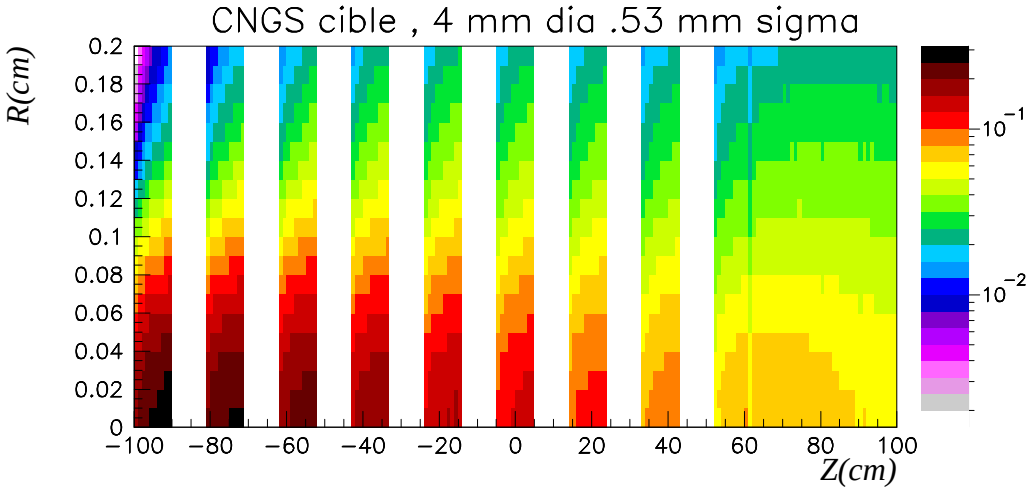

Energy deposition in the standard CNGS target, in GeV/cm^3/primary, for a 400 GeV proton beam with σ=0.53mm

(Generalized) IntraNuclear Cascade basic assumptions

1. Primary and secondary particles moving in the nuclear medium
2. *Target nucleons motion and nuclear well according to the Fermi gas model*
3. Interaction probability from σ_{free} + Fermi motion $\times$ $\rho(r)$ + exceptions (ex. π)
4. *Glauber cascade at high energies*
5. Classical trajectories $(+)$ nuclear mean potential (*resonant for π's!!*)
6. Curvature from nuclear potential $\rightarrow$ refraction and reflection.
7. Interactions are incoherent and uncorrelated
8. Interactions in projectile–target nucleon CMS $\rightarrow$ Lorentz boosts
9. *Multibody absorption for π, μ^-, K^-*
10. *Quantum effects (Pauli, formation zone, correlations...)*
11. *Exact conservation of energy, momenta and all additive quantum numbers,including nuclear recoil*

Formation Zone

Naively: "materialization" time. Qualitative estimate: in the frame where $p_{\|} = 0$

$$\bar{t} \;=\; \Delta t \approx \frac{\hbar}{E_T} = \frac{\hbar}{\sqrt{p_T^2 + M^2}}$$

particle proper time

$$\tau \;=\; \frac{M}{E_T}\bar{t} = \frac{\hbar M}{p_T^2 + M^2}$$

Going to lab system

$$t_{lab} \;=\; \frac{E_{lab}}{E_T}\bar{t} = \frac{E_{lab}}{M}\tau = \frac{\hbar E_{lab}}{p_T^2 + M^2}$$

As a function of particle rapidity y

$$t_{lab} = \bar{t}\cosh y = \frac{\hbar}{\sqrt{p_T^2 + M^2}}\cosh y$$

Condition for possible reinteraction inside a nucleus:

$$v \cdot t_{lab} \leq R_A \approx r_0 A^{\frac{1}{3}}$$

h-A at high energies: the invariance of the target fragmentation region

The Glauber cascade and the formation zone act together in reaching a regime where the "slow" part of the interaction is almost independent of the particle energy

This regime can be easily verified looking at charged particle average multiplicities and multiplicity distributions as a function of energy

- "Fast" tracks, coming from the projectile primary interactions, show the typical $\approx$ logarithmic increase observed for hN interactions
- "Gray" tracks, mostly due to intranuclear cascade reinteractions tend to saturate just above 10 GeV
- "Black" tracks, mostly due to evaporation charged particles saturate as well

Nonelastic hA interactions at high energies: examples

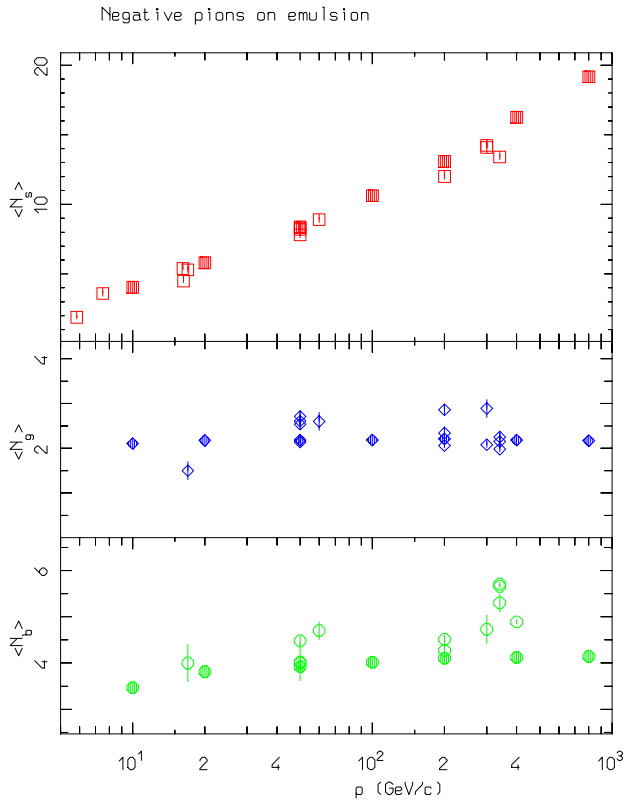

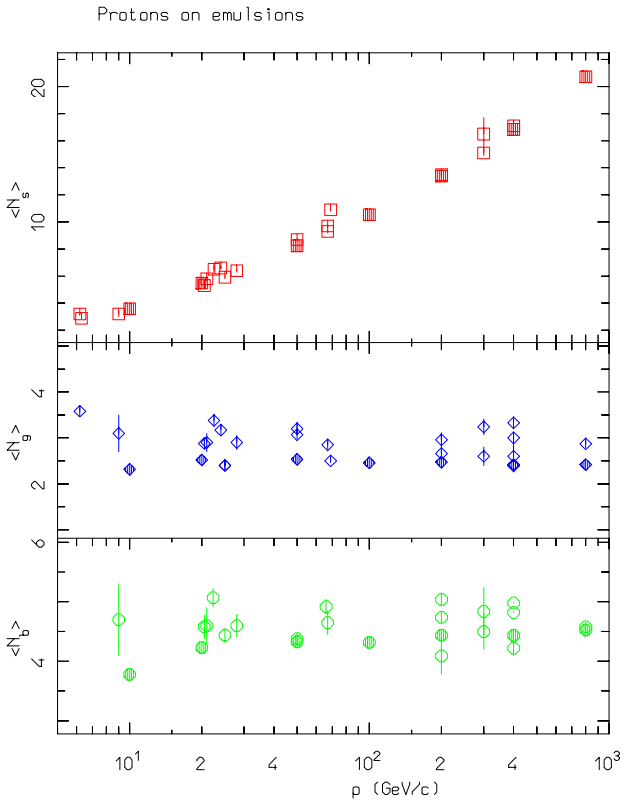

Shower, grey, and black tracks multiplicities for π^- (left) and protons (right) incident on emulsion, as a function of the projectile momentum. Open symbols are experimental data from various sources, full symbols are FLUKA results.

Nonelastic hA interactions at high energies: examples II

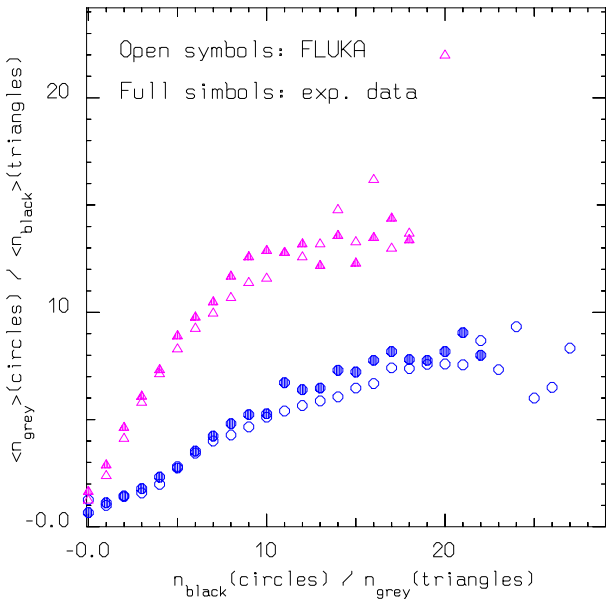

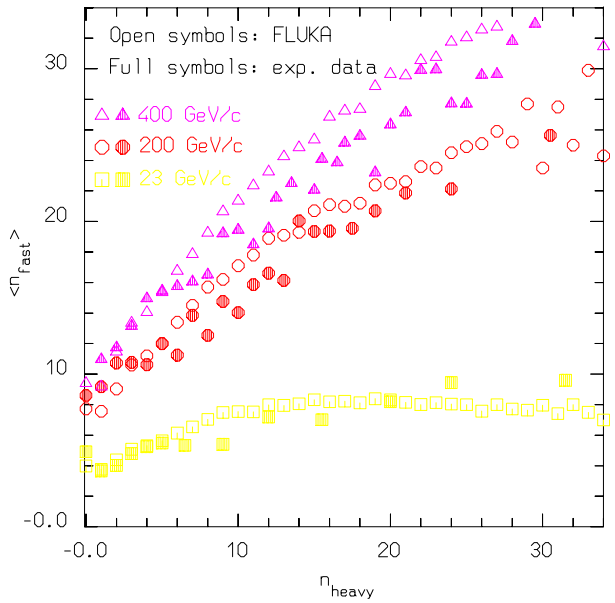

Correlation between the number of heavy prongs and fast particle multiplicity for protons on emulsion at various momenta, and mutual correlations ($< n_g >$ vs n_b and $< n_b >$ vs n_g) between black and grey charged tracks for 400 GeV/c p on emulsion. Open symbols are experimental data from various sources, full symbols are FLUKA results.

"Coherence length"

Coherence length $\equiv$ formation time for elastic or quasielastic interactions.

Given a two body interaction between with four-momentum transfer

$$q = p_{1i} - p_{1f}$$

the energy transfer seen in a frame where the particle 2 is at rest is given by

$$\Delta E_2 \; = \; \nu_2 = \frac{q \cdot p_{2i}}{m_2}$$

From the uncertainty principle this ΔE corresponds to a indetermination in proper time given by $\Delta\tau \cdot \Delta E_2 = \hbar$, that boosted to the lab frames gives a coherence length

$$\Delta x_{lab} \; = \; \frac{p_{2lab}}{m_2} \cdot \Delta\tau = \frac{p_{2lab}}{m_2} \frac{\hbar}{\nu_2}$$

And analogue for particle 1

Can be applied also to $\nu - h$ interactions

Nucleon Fermi Motion

Fermi gas model: Nucleons = Non-interacting Constrained Fermions

$$\text{Momentum distribution} \propto \frac{\mathrm{d}N}{dk} = \frac{|k|^2}{2\pi^2}$$

for k up to a (local) Fermi momentum $k_F(r)$ given by

$$k_F(r) = \left[3\pi^2 \rho_N(r)\right]^{\frac{1}{3}}, \quad \rho_N = \textit{neutron or proton density}$$

The Fermi energy ($k_F \approx 1.36\ fm$, $E_F \approx 260\ MeV$ at nuclear max. density) is customarily used in building a sefl-consistent Nuclear Potential

$$\Downarrow$$

Depth of the potential well $\equiv$ Fermi Energy + Nucleon binding Energy

Effect on hadron-nucleon interactions

Smearing of momentum distributions

Smearing of the center of mass energy

Origin of the residual nuclear excitation

Positive Kaons: A probe of Fermi distribution

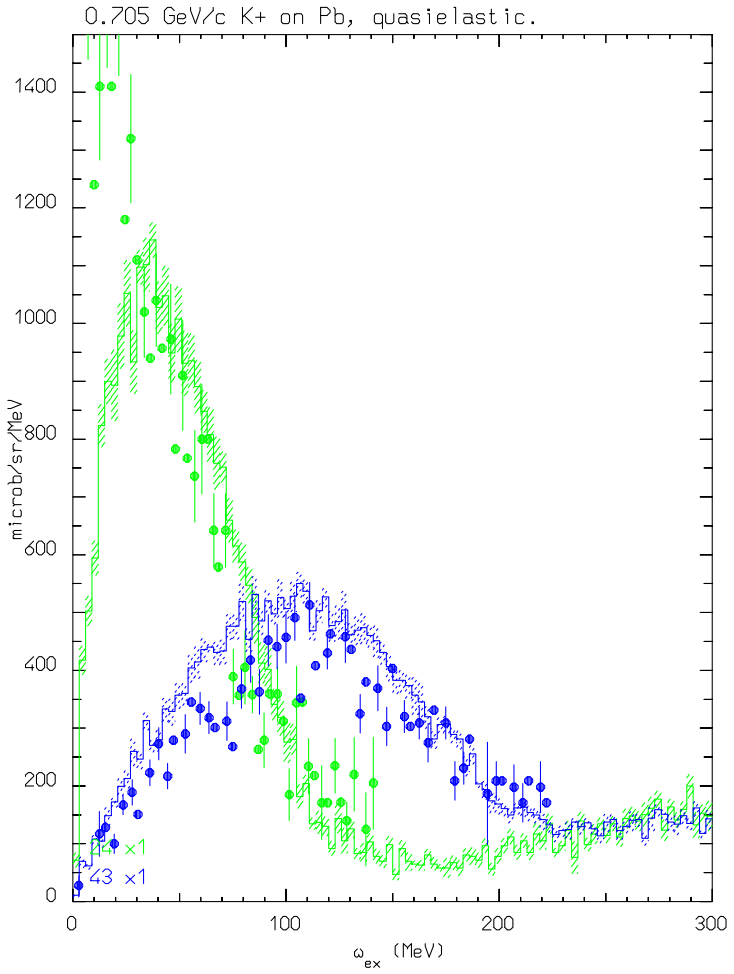

K^+ K^0

No low mass S=1 baryons $\rightarrow$

weak K^+N interaction

only elastic and ch. exch. up to ≈ 800 MeV/c

$(K^+, K^{+\prime})$ on Pb vs residual excitation, 705 MeV/c, at 24° and 43°.

Histo: FLUKA, dots: data (Phys. Rev. C51, 669 (1995))

On free nucleon: recoil energy :

43 MeV at 24° , 117 MeV at 43°.

Pions: nuclear medium effects

Pion-nucleon interactions: non-resonant channel and p-wave resonant formation of Δ's. In nuclear medium Δ's can either decay, resulting in elastic scattering or charge exchange, or interact with other nucleons, resulting in pion absorption $\rightarrow$ the width of the resonance is thus different from the free one and the free pion-nucleon cross section must be modified according to

Assuming a Breit-Wigner for the free resonant cross section with width Γ_F

$$\sigma_{res}^{Free} = \frac{8\pi}{p_{cm}^2} \frac{M_\Delta^2 \Gamma_F (p_{cm})^2}{\left(s - M_\Delta^2\right)^2 + M_\Delta^2 \Gamma_F (p_{cm})^2}$$

An "in medium" resonant cross section σ_{res}^A can be obtained adding to Γ_F the imaginary part of the (extra) width arising from nuclear medium effects:

$$\frac{1}{2}\Gamma_T = \frac{1}{2}\Gamma_F - \mathrm{Im}\Sigma_\Delta, \quad \Sigma_\Delta = \Sigma_{qe} + \Sigma_2 + \Sigma_3$$

(Σ_{qe}, Σ_2, Σ_3 = widths for quasielastic scattering, two and three body absorption)

The effective in-nucleus cross section is then obtained taking also into account a further two-body s-wave absorption cross section derived from the optical model

$$\sigma_t^A = \sigma_{res}^A + \sigma_t^{Free} - \sigma_{res}^{Free} + \sigma_s^A, \quad \sigma_s^A(\omega) = \frac{4\pi}{p}(1 + \frac{\omega}{2m})\mathrm{Im}B_0(\omega)\rho$$

Microscopic pion absorption cross sections

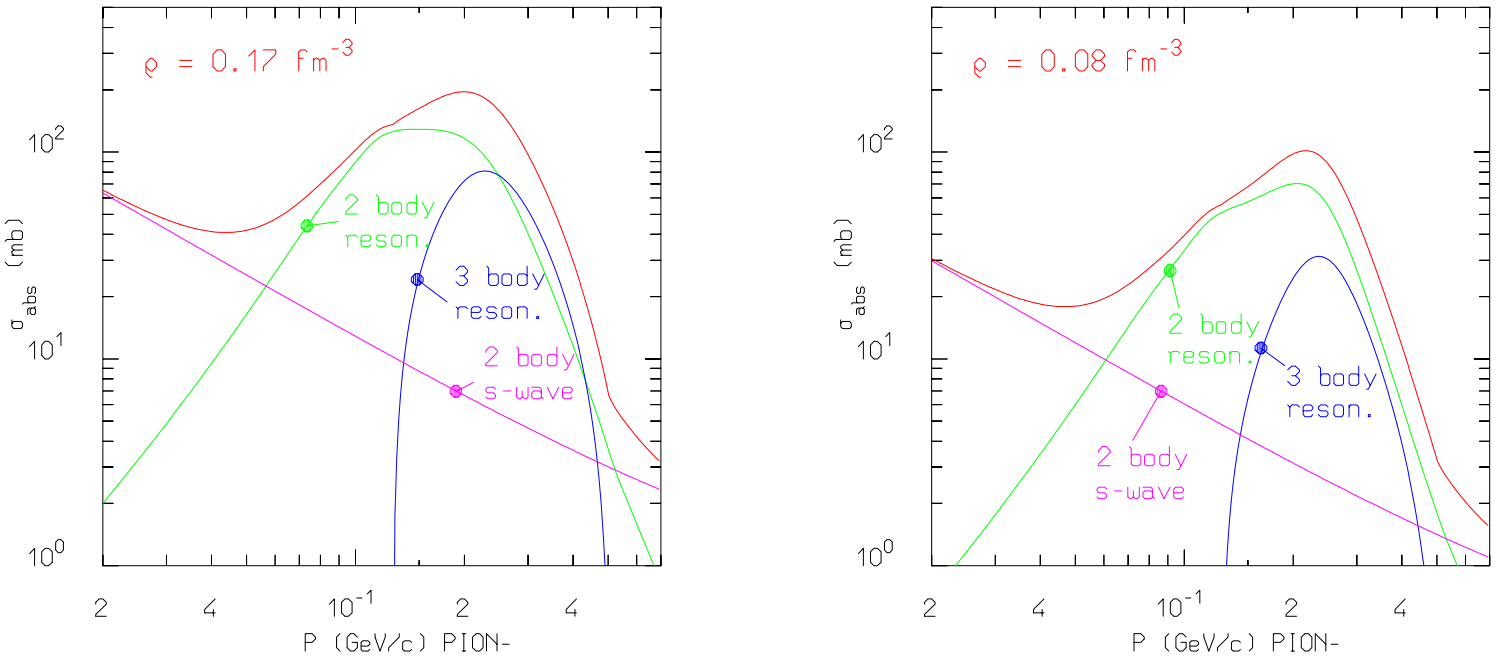

Charged pion absorption cross section for infinite symmetric nuclear matter at two different density values ($\lambda_{abs}^{-1} = \sigma_{abs} \cdot \frac{1}{2}\rho = \sigma_{abs} \cdot \rho_{pro} = \sigma_{abs} \cdot \rho_{neu}$)

Pions: optical potential

For pions, a complex nuclear potential can be defined out of the pion-nucleon scattering amplitude to be used in conjunction with the Klien-Gordon equation:

$$\left[(\omega - V_c)^2 - 2\omega U_{opt} - K^2\right]\Psi \;=\; m_\pi^2 \Psi$$

In coordinate space, this is written as (the upper/lower signs refer to π^+/π^-):

$$\begin{aligned}
2\omega U_{opt}(\omega, r) \;&=\; -\beta(\omega, r) + \frac{\omega}{2M}\nabla^2\alpha(\omega, r) - \nabla\cdot\frac{\alpha}{1+g\alpha(\omega, r)}\nabla \\
\beta \;&=\; 4\pi\left[\left(1+\frac{\omega}{M}\right)\left(b_0(\omega) \mp b_1(\omega)\frac{N-Z}{A}\right)\rho(r) + \left(1+\frac{\omega}{2M}\right)B_0(\omega)\rho^2(r)\right] \\
\alpha \;&=\; 4\pi\left[\frac{1}{1+\frac{\omega}{M}}\left(c_0(\omega) \mp c_1(\omega)\frac{N-Z}{A}\right)\rho(r) + \frac{1}{1+\frac{\omega}{2M}}C_0(\omega)\rho^2(r)\right]
\end{aligned}$$

Using standard methods to get rid of the non-locality, in momentum space

$$\begin{aligned}
2\omega U_{opt}(\omega, K) \;&=\; -\beta - K^2\frac{\alpha}{1+g\alpha} + \frac{\omega}{2M}\nabla^2\alpha \\
K^2 \;&=\; k_0^2 + V_c^2 - 2\omega V_c^2 - 2\omega U_{opt}(\omega, K) = \frac{k_0^2 + V_c^2 - 2\omega V_c^2 + \beta - \frac{\omega}{2M}\nabla^2\alpha}{1-\bar{\alpha}} \\
\bar{\alpha} \;&=\; \frac{\alpha}{1+g\alpha}
\end{aligned}$$

Pion optical potential examples

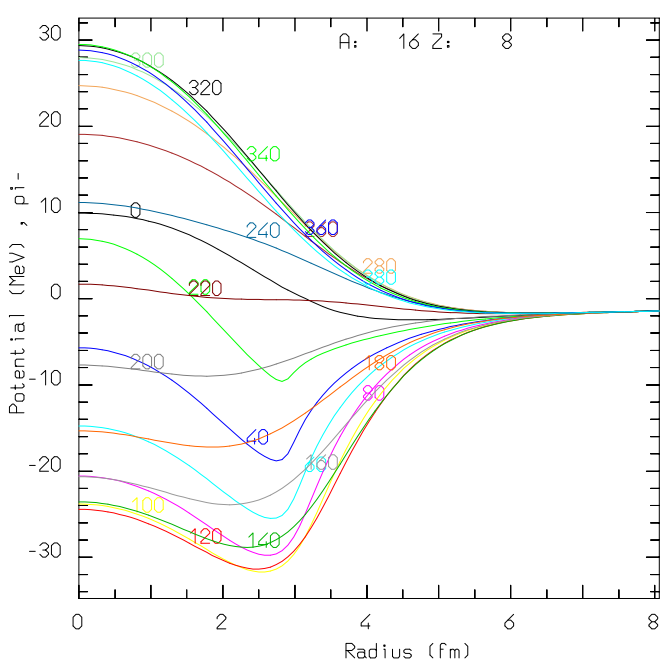

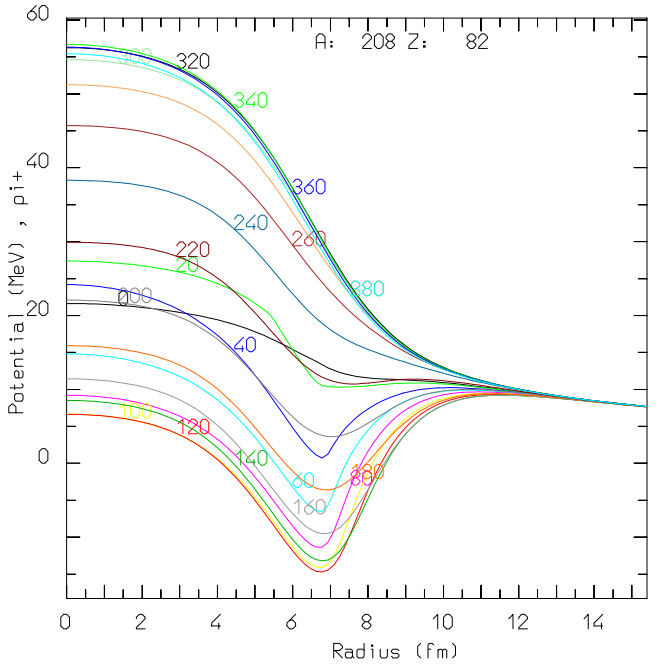

The real part of the pion optical potential for π^- on ^{16}O (left) and π^+ on ^{208}Pb (right) as a function of radius for various pion energies (MeV)

Pion absorption cross sections: examples

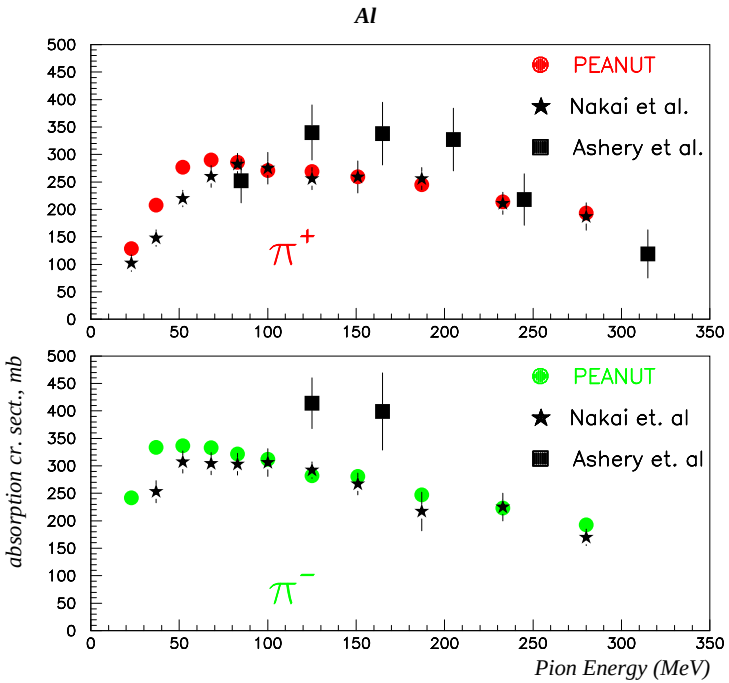

Computed and exp. pion absorption cross section on Aluminum as a function of energy

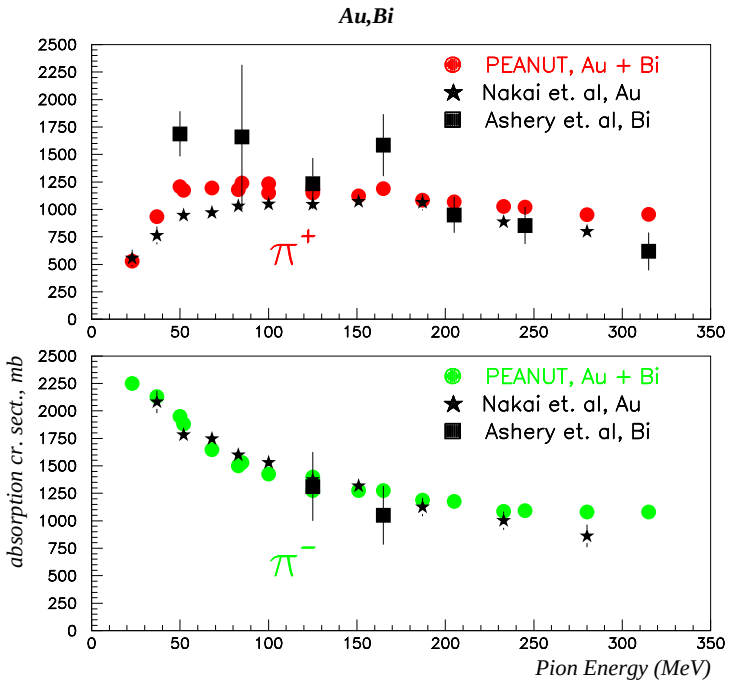

Computed and exp. pion absorption cross section on Gold or Bismuth as a function of energy

(Exp. data: D. Ashery et al., **PRC23**, (1981) 2173 and K. Nakai et. al., **PRL44**, (1979) 1446)

Pion-nucleus interactions: examples

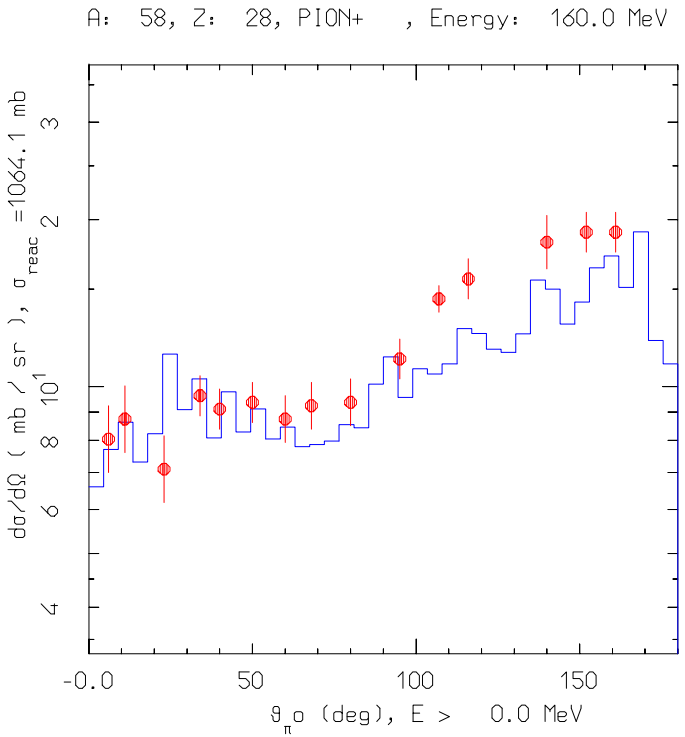

Computed and exp. pion charge exchange angular distribution for $^{58}Ni(\pi^+,\pi^0)$ *at 160 MeV*

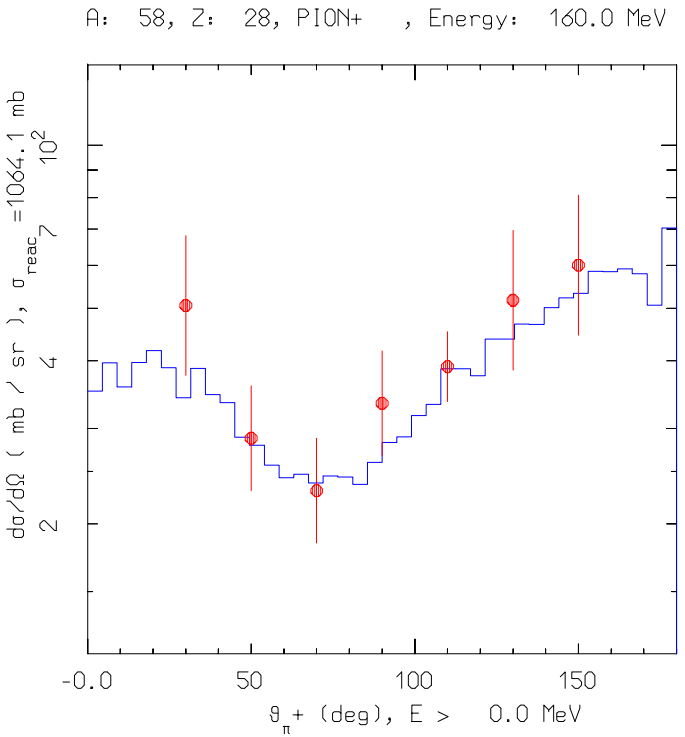

Computed and exp. pion inelastic angular distribution for $^{58}Ni(\pi^+,\pi^{+\prime})$ *at 160 MeV*

(Exp. data: W.J. Burger et al., **PRC41**, *(1990) 2215 and R.D. McKeown et al.,***PRC24**, *(1981) 211)*

K^- $\bar{K}^0$ -nucleon interactions at medium-low energies

Plenty of S=1 baryonic resonances at low energies

$\Lambda\pi$ and $\Sigma\pi$ channels already open at rest

$\rightarrow$ Strong K^-N interaction

Multichannel analisys needed

Many partial waves contribute

Kaon nuclear potential non-negligible

Hyperons can be bound in nuclei

In PEANUT: in progress

Multichannel partial wave expansion

s wave at low momenta [2];

$0 < l < 5$ up to 1.8 GeV/c [3]

Isospin relations to link different charge states

Mass differences taken into account (charge exchange)

[2] A.D. Martin, Nuc.Phys. B179 (1981) 33

[3] G.P. Gopal et al., Nuc. Phys. B119(1977),362

Kaon-nucleon interactions examples

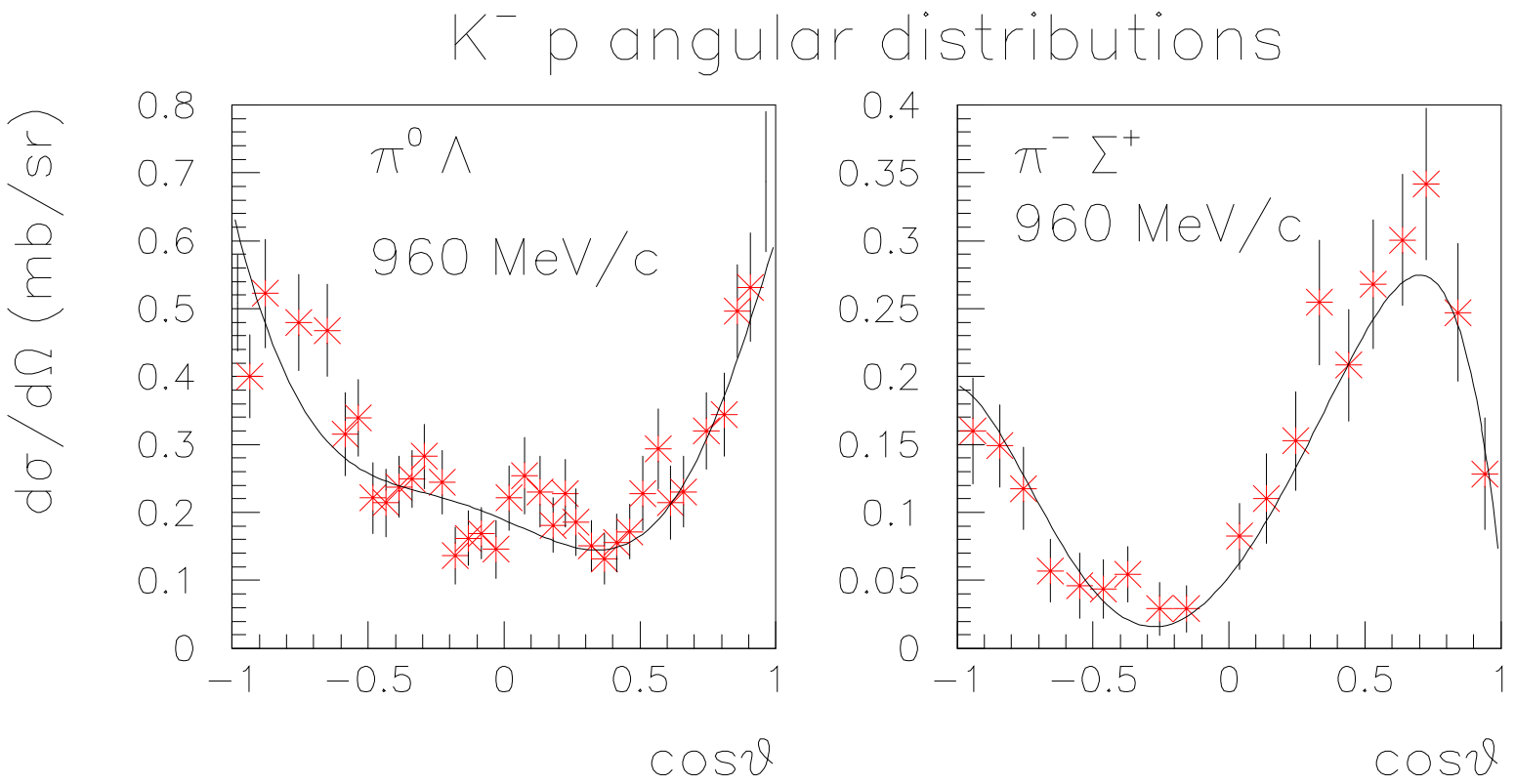

Line: FLUKA, partial wave expansion, symbols: exp. data from B.R. Martin and M.K. Pidkok, Nucl. Phys. B126 (1977) 266

Preequilibrium

For E $>$ π production threshold $\rightarrow$ only (G)INC models

At lower energies$\rightarrow$ a variety of preequilibrium models

Two leading approaches

the quantum-mechanical multistep model	the exciton model
Very good theoretical background	statistical assumptions
complex, difficulties for multiple emission	simple and fast

Exciton model: chain of steps, each (n_{th}) step corresponding to N_n

"excitons" == either a particle above or a hole below the Fermi surface

Statistical assumption: any partition of the excitation energy E among N, $N = N_h + N_p$, excitons has the same probability to occur

Step: nucleon-nucleon collision with $N_{n+1} = N_n + 2$ ("never come back" approximation)

Chain end = equilibrium = N_n sufficiently high or excitation energy below threshold

N_1 depends on the reaction type and on the cascade history

Preequilibrium : GDH

Preequilibrium emission probability:

$$P_{x,n}(\epsilon)d\epsilon = \sum n_{p_x} \frac{\rho_n(U,\epsilon) g d\epsilon}{\rho_n(E)} \frac{r_c(\epsilon)}{r_c(\epsilon) + r_+(\epsilon)}$$

where the density (MeV^{-1}) of exciton states is given by:

$$\rho_n(E) = \frac{g(gE)^{n-1}}{n!(n-1)!}$$

the emission rate in the continuum:

$$r_c = \sigma_{inv} \frac{\epsilon}{g_x} \frac{(2s+1)\, 8\pi m}{h^3}$$

and the reinteraction rate:

$$r_+(\epsilon) = f_{Pauli}(\epsilon, E_F) \left[\rho_p \sigma_{xp} + \rho_n \sigma_{xn}\right] \left[\frac{2(\epsilon + V)}{m}\right]^{1/2}$$

$$(or\ from\ optical\ potential)$$

GDH: ρ,E_F are "local" averages on the trajectory and constrained exciton state densities are used for the lowest lying exciton configurations.

Preequilibrium: modified GDH in PEANUT

- σ_{inv} from systematics
- Correlation/formation zone / hardcore effect on reinteractions:

$$\frac{r_c(\epsilon)}{r_c(\epsilon)+r_+(\epsilon)} \rightarrow P_c^{(h\tau)} + P_c^{(co)} + P_c^{(std)}$$

$$\begin{aligned}
P_c^{(h\tau)} &= escape\ prob.\ in\ zone\ = max(\tau, hardcore) \equiv h\tau \\
P_c^{(co)} &= escape/total\ prob.\ in\ zone\ = (correlation\ -\ h\tau) \\
&\quad (here\ reinteraction\ only\ on\ \mathrm{non}-correlated\ nucleon\ specie\ ) \\
P_c^{(std)} &= \text{"}standard\text{"}\ escape/total\ in\ remaining\ zone.
\end{aligned}$$

- Constrained exciton state densities configurations 1p-1h, 2p-1h, 1p-2h, 2p-2h, 3p-1h and 3p-2h
- Energy dependent form for g_x

Preequilibrium: modified GDH in PEANUT II

- Position dependent parameters = point like values :
  - first step : n_h holes generated in the INC step at positions $\vec{x}_i$:

$$\rho^{loc}_{n_h} = \frac{\Sigma_{i=1}^{n_h} \rho(\vec{x}_i)}{n_h} \qquad E^{loc}_{F\ n_h} = \frac{\Sigma_{i=1}^{n_h} E_F(\vec{x}_i)}{n_h}$$

  - When looking at reinteraction: consider neighborhood:

$$\rho^{nei}_{n_h} = \frac{n_h \rho^{loc}_{n_h} + \rho^{ave}}{n_h + 1} \qquad E^{nei}_{F\ n_h} = \frac{n_h E^{loc}_{F\ n_h} + E^{ave}_F}{n_h + 1}$$

  - Subsequent steps: go towards *ave*rage quantities

$$\rho^{loc}_{n_h+1} = \rho^{nei}_{n_h} \qquad E^{loc}_{F\ n_h+1} = E^{nei}_{F\ n_h}$$

Preequilibrium/(G)INC transition

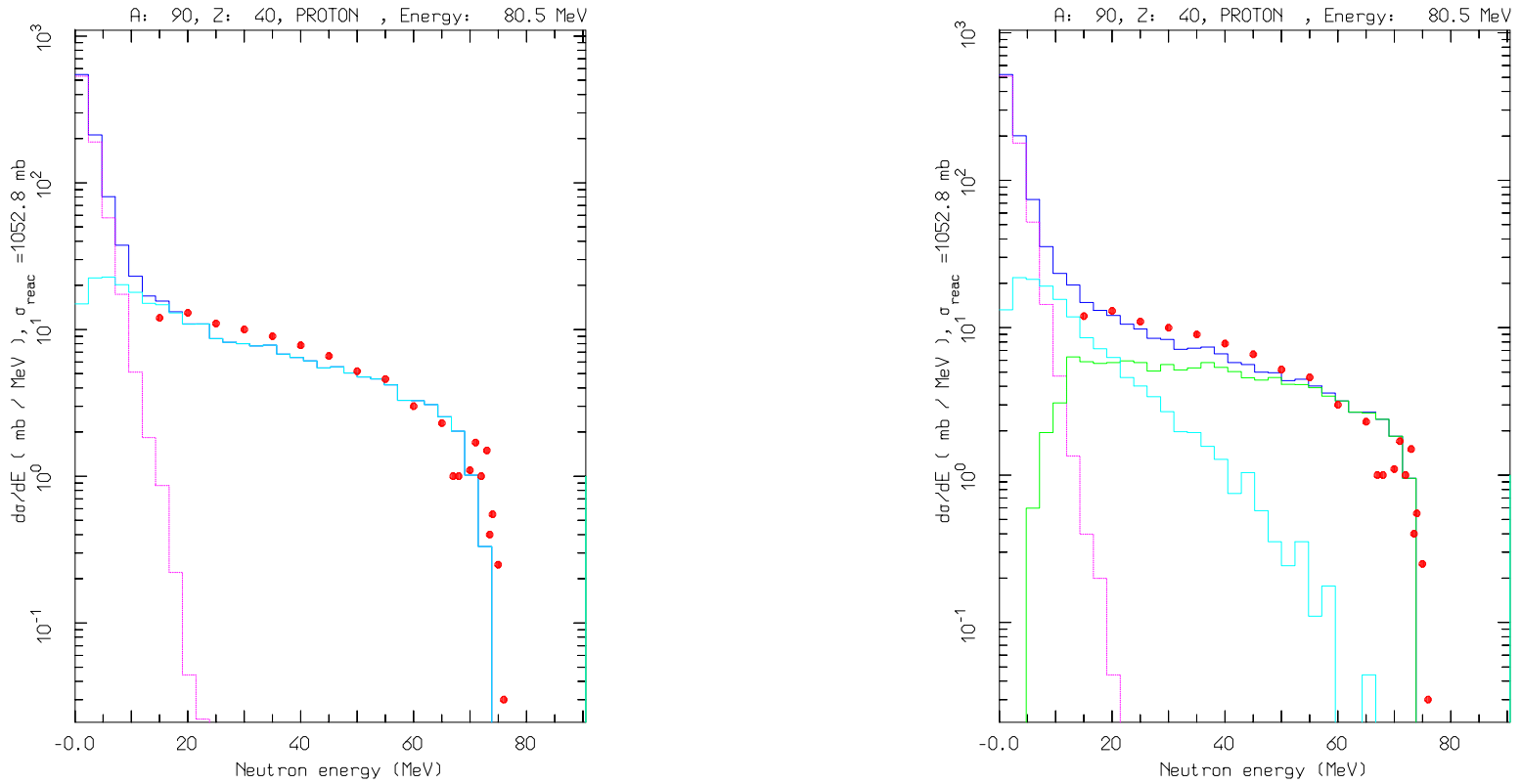

Example of angle integrated ^{90}Zr(p,xn) at 80.5 MeV calculations with the full algorithm (right), and without the INC stage (left). The various lines show the total, INC, preeq. and evaporation contributions, the exp. data have been taken from M.Trabandt et al. **PRC39** (1989) 452

Nonelastic interactions at intermediate energies: examples

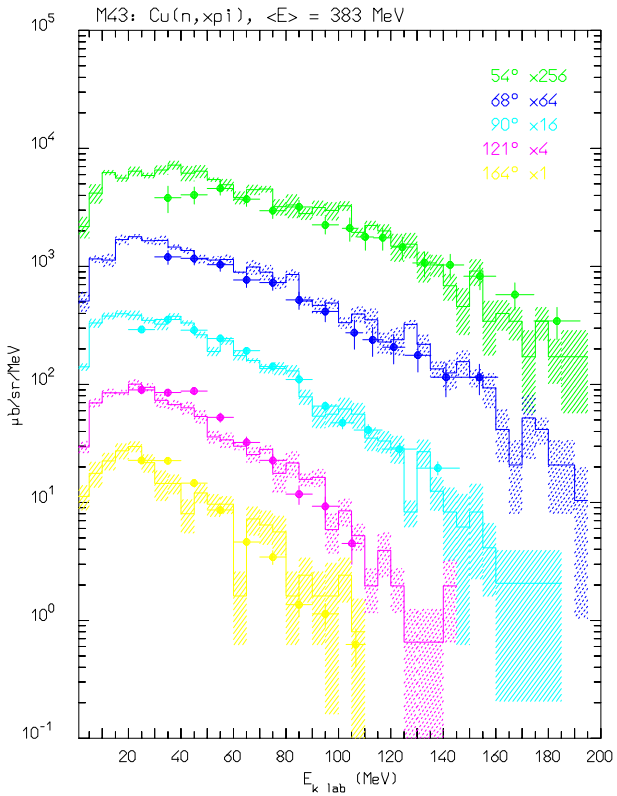

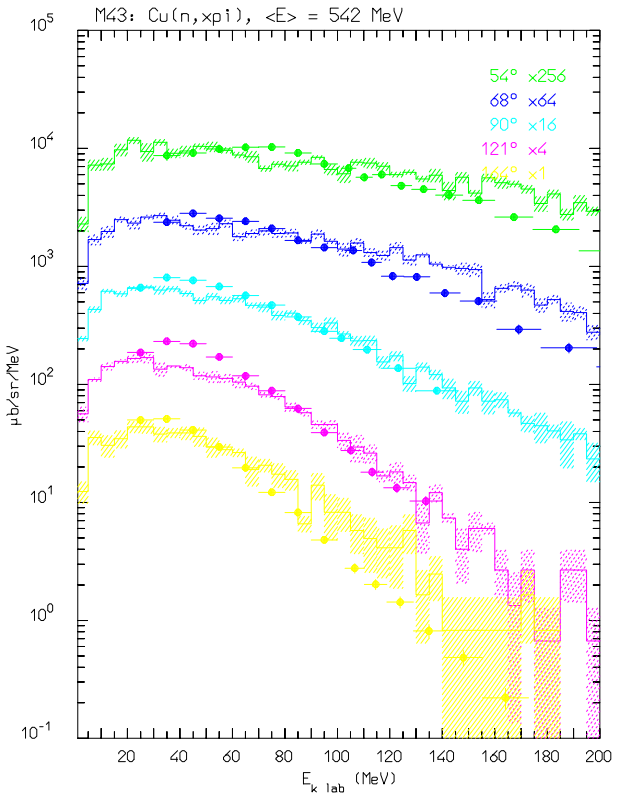

Double differential distributions of charged pions produced by neutrons of $< E_n >$=383 (left) and 542 MeV (right). Exp. data have been taken from Buchle et al. **NPA515**, (1990) 541

Nonelastic interactions at intermediate energies: examples II

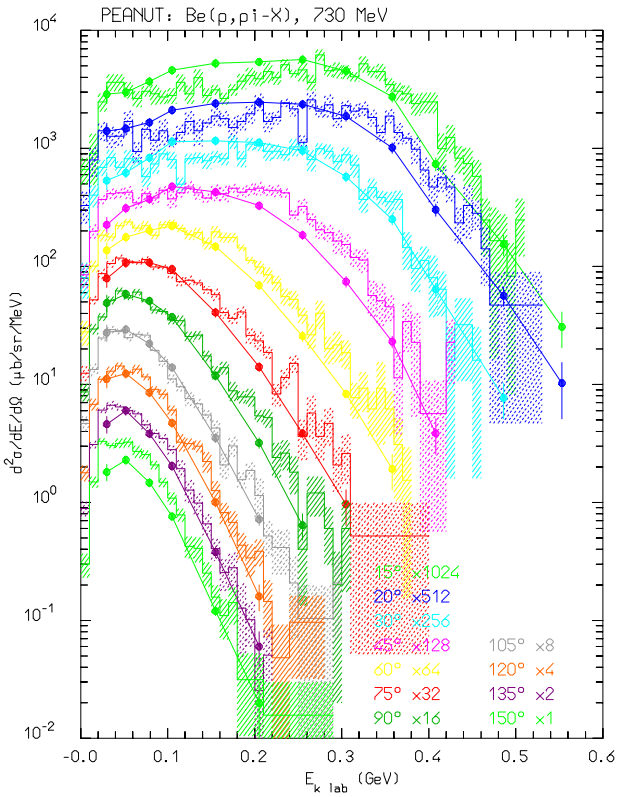

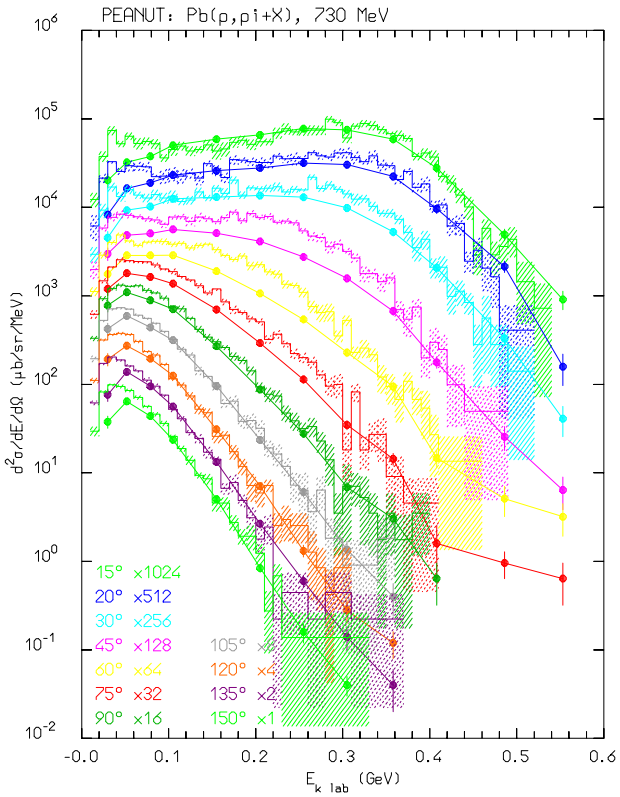

Double differential distributions of pions produced by 730 MeV protons. π^-'s from Be (left) and π^+ frpm Pb (right). Exp. data (symbols) have been taken from D.R.F. Cochran et al., **PRD6**, (1972)

Nonelastic interactions at intermediate energies: examples III

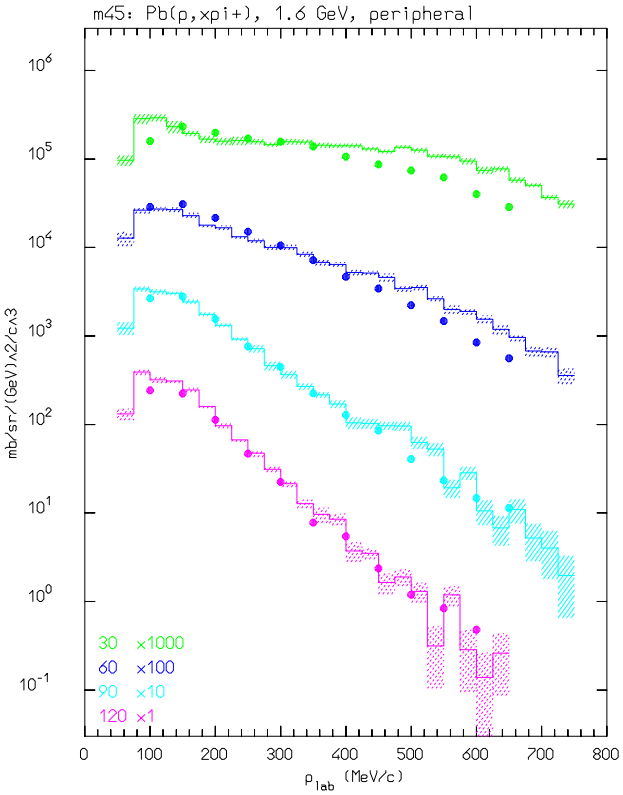

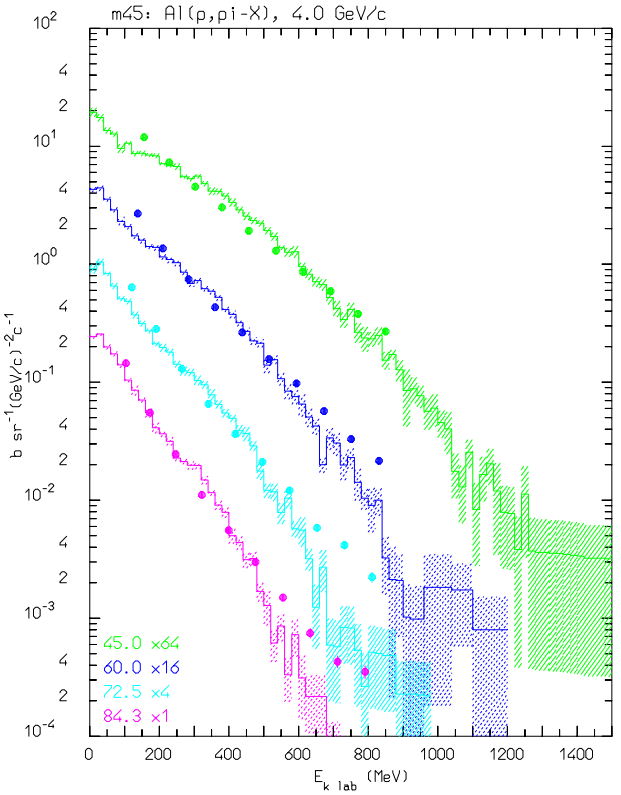

Double differential distributions of π^+'s produced by 1.6 GeV protons on Pb (left, exp. data from M.C.Lemaire et. al., CEA-N-2670) and π^- produced by 4 GeV/c protons on Al (right, exp data from H. En'yo et al, PL 159B, 1 (1985)).

Nucleon emission: thin target examples I

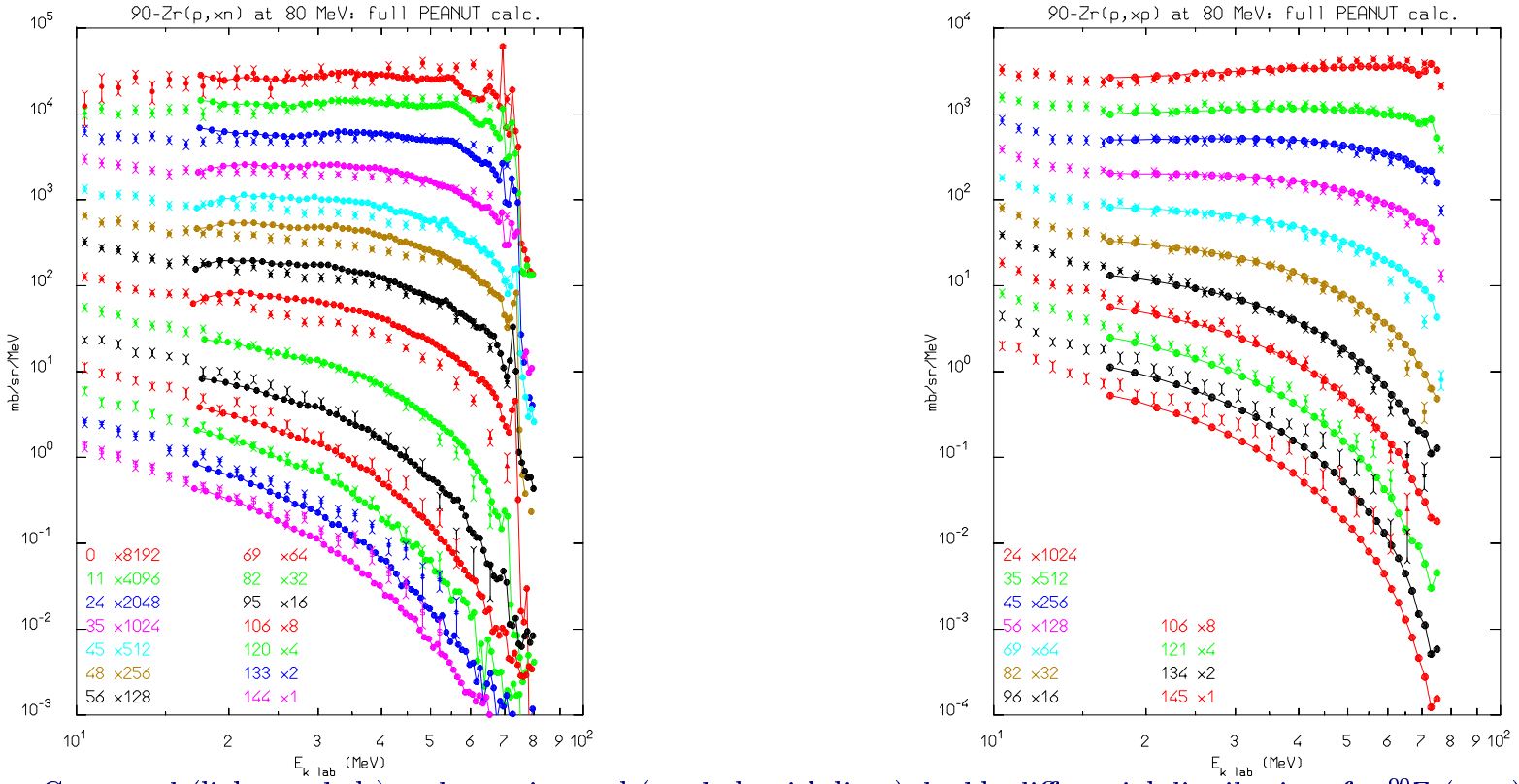

Computed (light symbols) and experimental (symbols with lines) double differential distributions for ^{90}Zr(p,xn) (left) and ^{90}Zr(p,xp) at 80.5 MeV. The exp. data have been taken from M.Trabandt et al. **PRC39** (1989) 452 and A.A. Cowley et al., **PRC43**, (1991) 678

Nucleon emission: thin target examples I

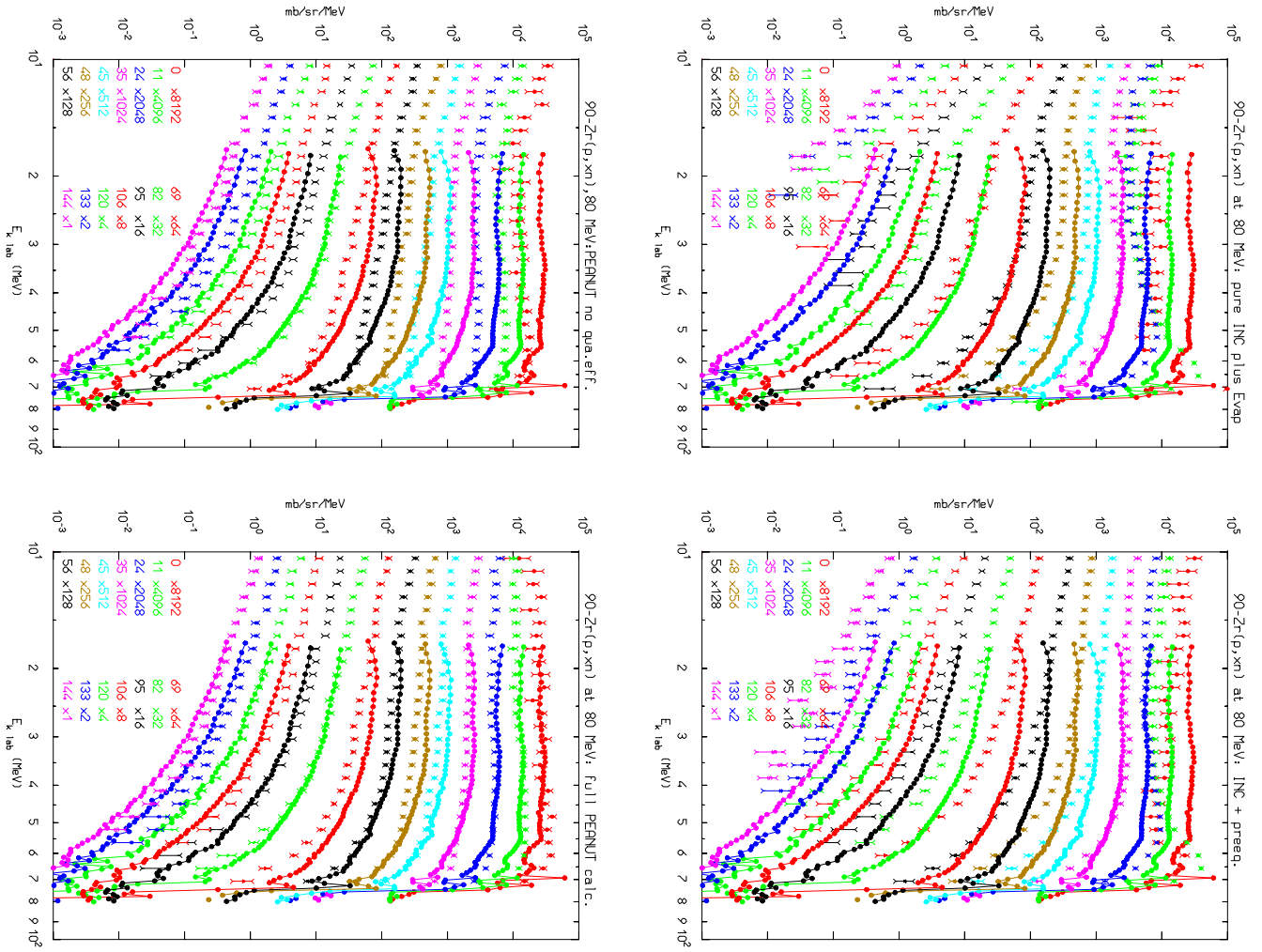

Nucleon emission: thin target examples I

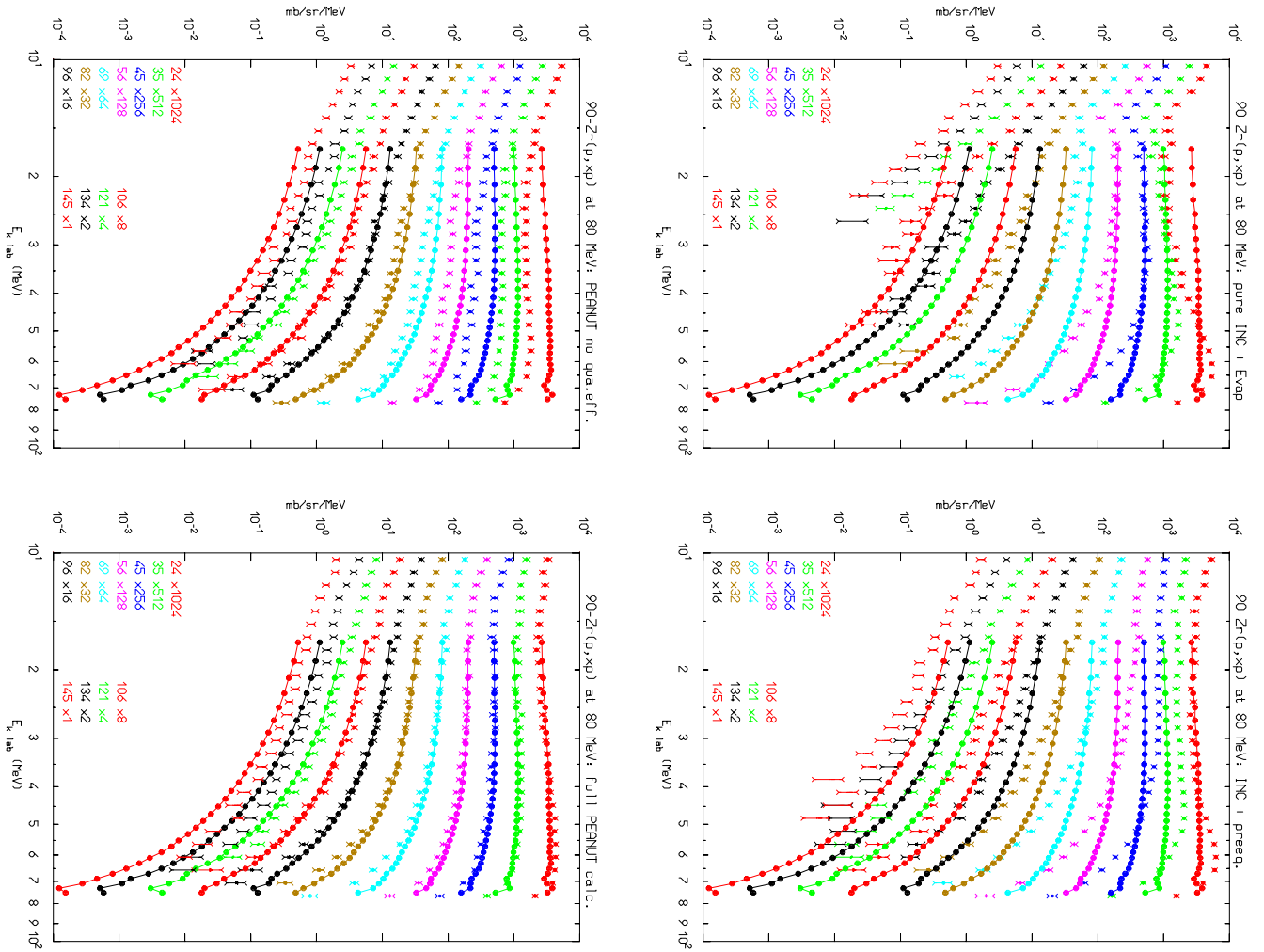

Nucleon emission: thin target examples II

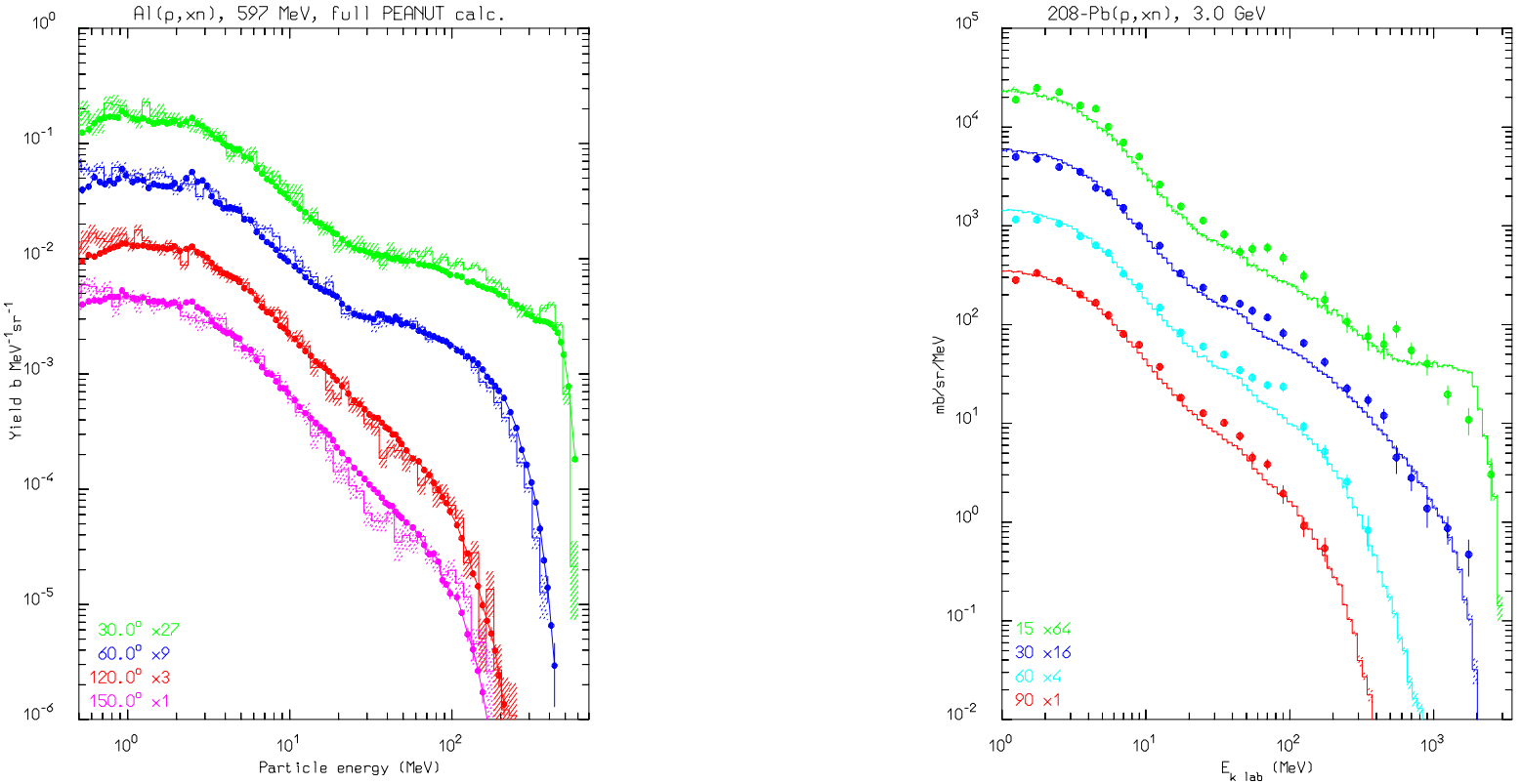

Computed (histograms) and experimental (symbols) double differential neutron distributions for Al(p,xn) (left) at 597 MeV and Pb(p,xn) at 3 GeV. The exp. data have been taken from W.B. Amian et al., Nucl. Sci. Eng. **115**, (1993) 1, and K. Ishibashi et al, Nucl. Sci. Technol. **32** (1995) 827.

Evaporation, fission and nuclear break-up

The evaporation probability for a particle of type j , mass m_j, spin $S_j \cdot \hbar$ and kinetic energy E and the total fission probability are given by

(i for initial nucleus, f for final, F at fission saddle point)

$$P_j = \frac{(2S_j+1)m_j}{\pi^2\hbar^3}\int_{V_j}^{U_i-Q_j-\Delta_f}\sigma_{\text{inv}}\frac{\rho_f(U_f)}{\rho_i(U_i)}EdE$$

$$P_F = \frac{1}{2\pi\hbar}\frac{1}{\rho_i(U_i)}\int_0^{(U_i-B_F)}\rho_F(U_i-B_F-E)dE$$

- ρ's: nuclear level densities,
- U: excitation energy,
- V_j: (possible) Coulomb barrier for emitting a particle of type j
- Q_j: reaction Q for emitting a particle of type j,
- σ_{inv}: cross section for the inverse process

For low mass residuals: Fermi break-up: statistical phase-space production of multiple (excited) fragments

Excitation energy AFTER evaporation $\rightarrow \gamma$ emission

Latest Improvements to evaporation

- Improved state density $\rho = \exp\left(2\sqrt{aU}\right)/U^{\frac{5}{4}}$
- No Maxwellian approximation for energy sampling
- γ competition in progress

- Sub-barrier emission:

$$\sigma_{inv}^{x} = (R+\bar{\lambda})^2 \frac{\hbar\omega_x}{2E} \ln\left[1 + e^{\frac{2\pi(E-V_C)}{\hbar\omega_x}}\right]$$

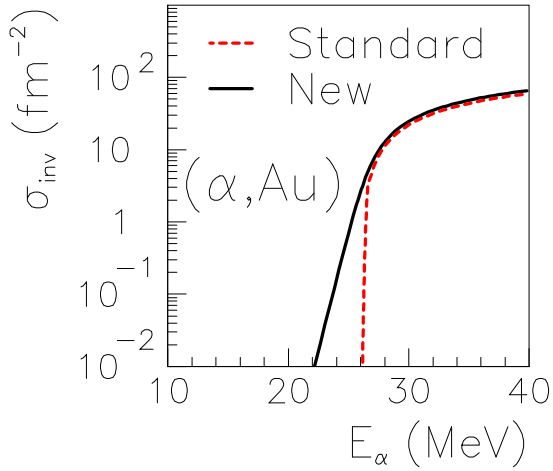

Residual nuclei predictions: "new" vs "old" evap.

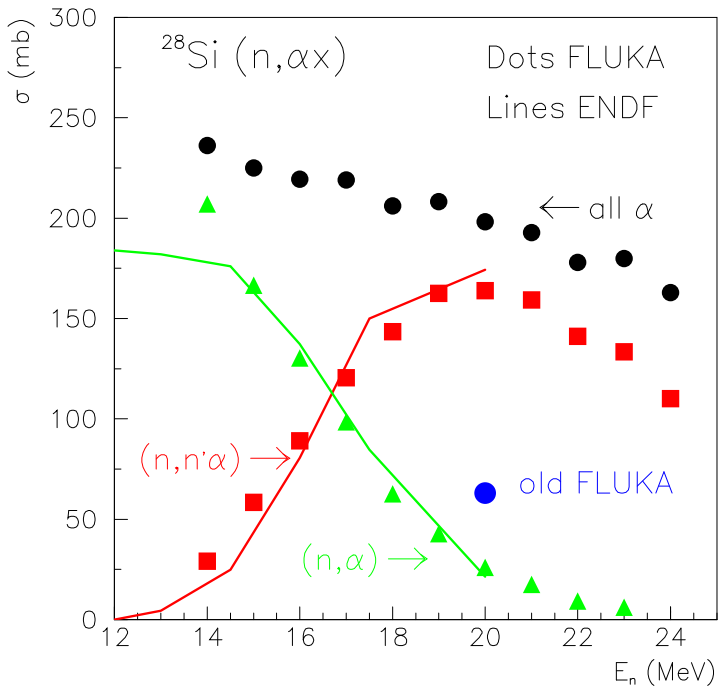

A practical case:
Si damage
α production by neutrons
compared to ENDF data

Residual nuclei

The production of residuals is the result of the last step of the nuclear reaction, thus it is influenced by ALL the previous stages

Residual mass distributions are very well reproduced

Residuals near to the compound mass are usually well reproduced

However, the production of specific isotopes may be influenced by additional problems which have little or no impact on the emitted particle spectra

- Extreme sensitivity to details of evaporation
- Nuclear structure effects
- Lack of spin-parity dependent calculations in most MonteCarlo models
- Difficulty to model fragmentation processes, that populate A<20-30 for medium/heavy target nuclei.
- Isomer production: an open question
- Interesting cross section values typically spans *four* order of magnitudes

Residual nuclei predictions: a look at the isotope table

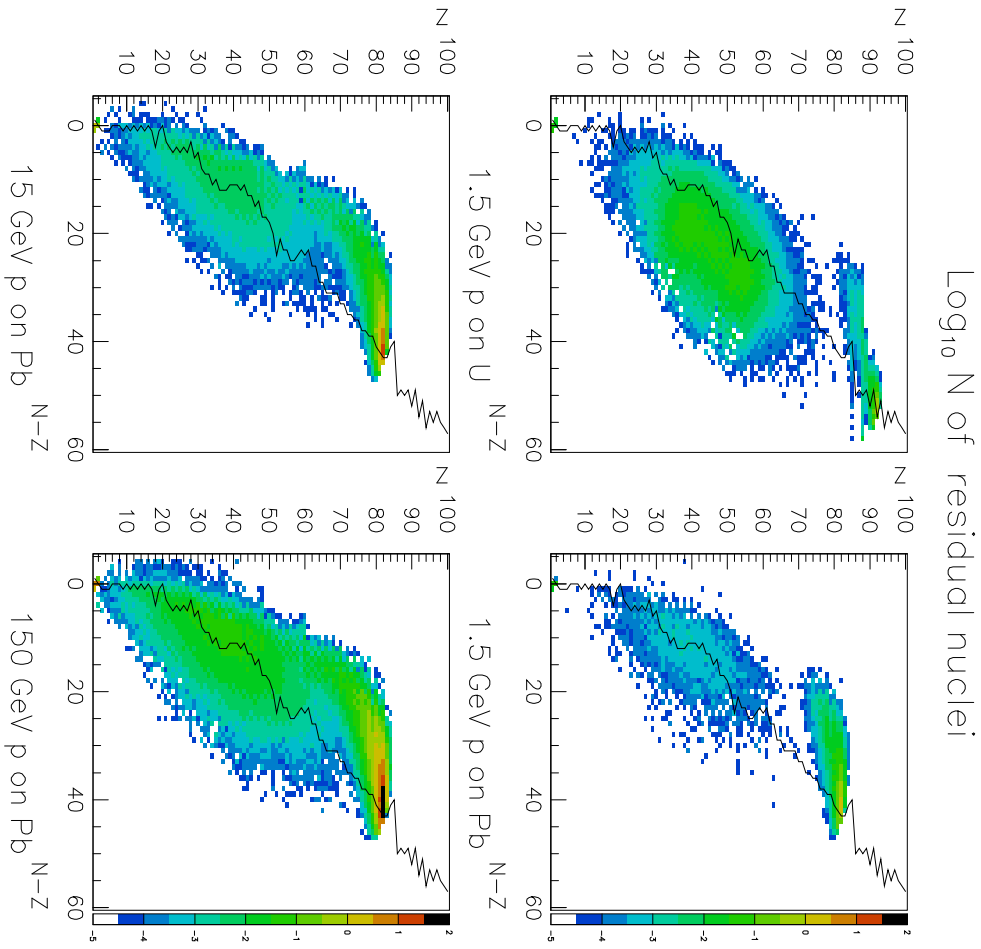

Residual nuclei: the mass distribution at high energies

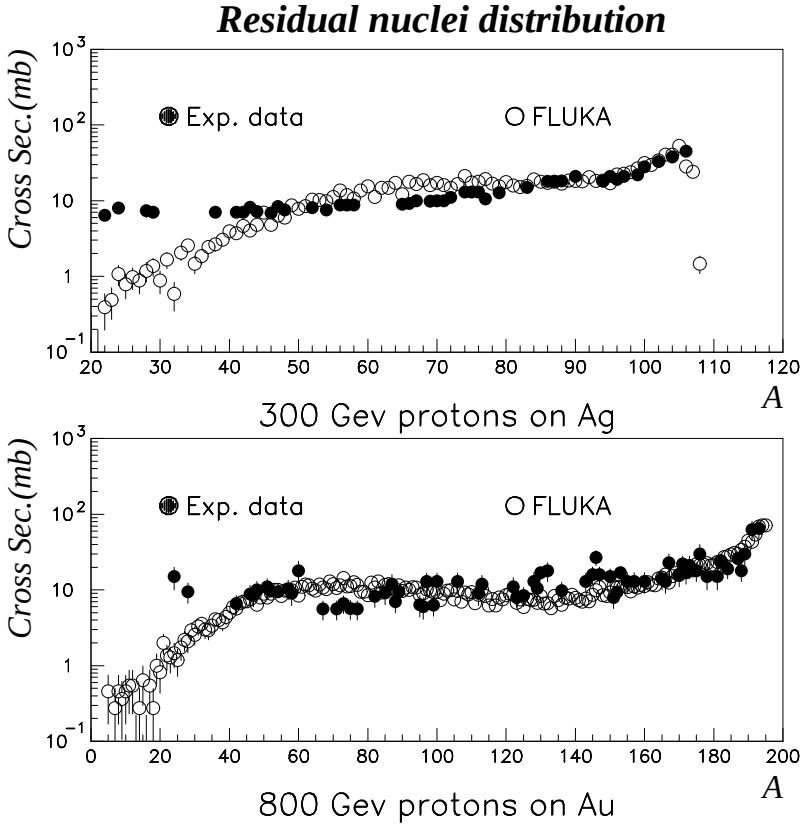

Experimental and computed residual nuclei mass distribution following for Ag(p,x)X at 300 GeV (top) and Au(p,x)X at 800 GeV (bottom).

Residual nuclei predictions: examples

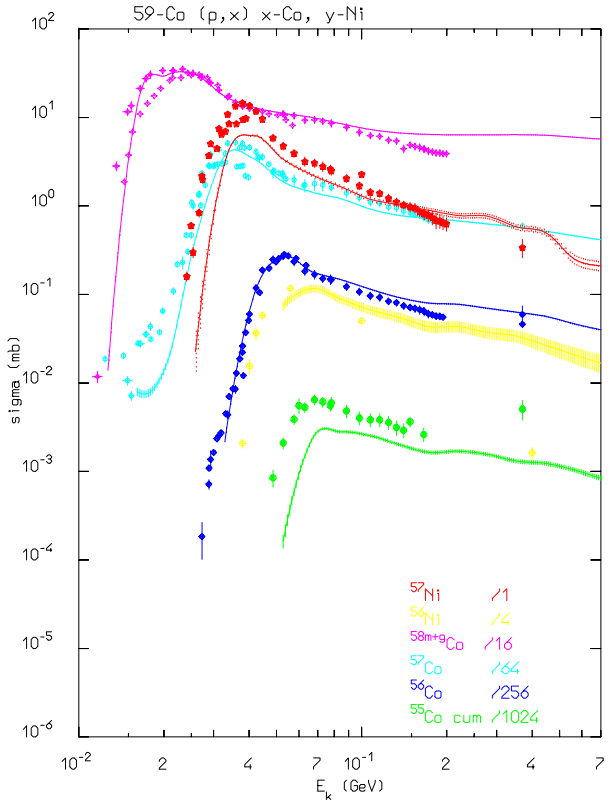

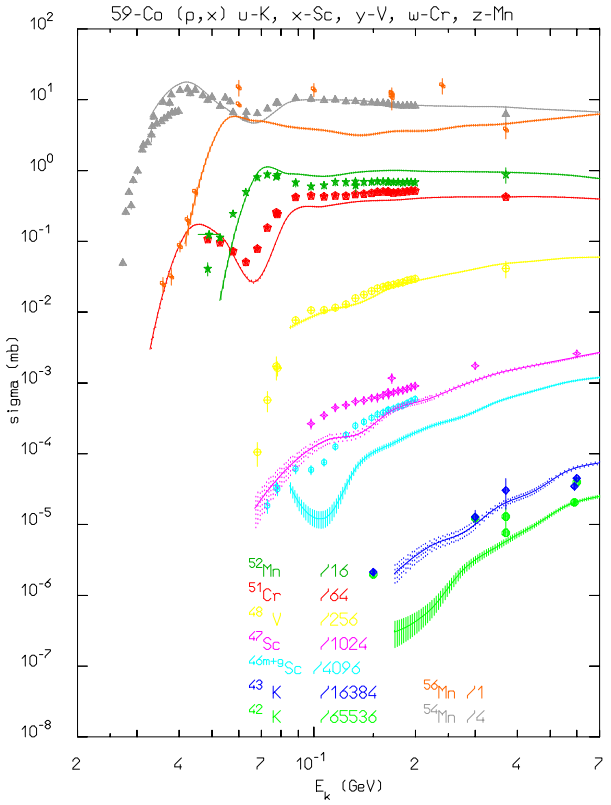

Comparison between computed and measured (A.S. Iljinov et al., Landolt-Börnstein, **Vol. 13a** (1991)) isotope production by protons on natural Cobalt

Residual nuclei predictions: "new" vs "old" evap.

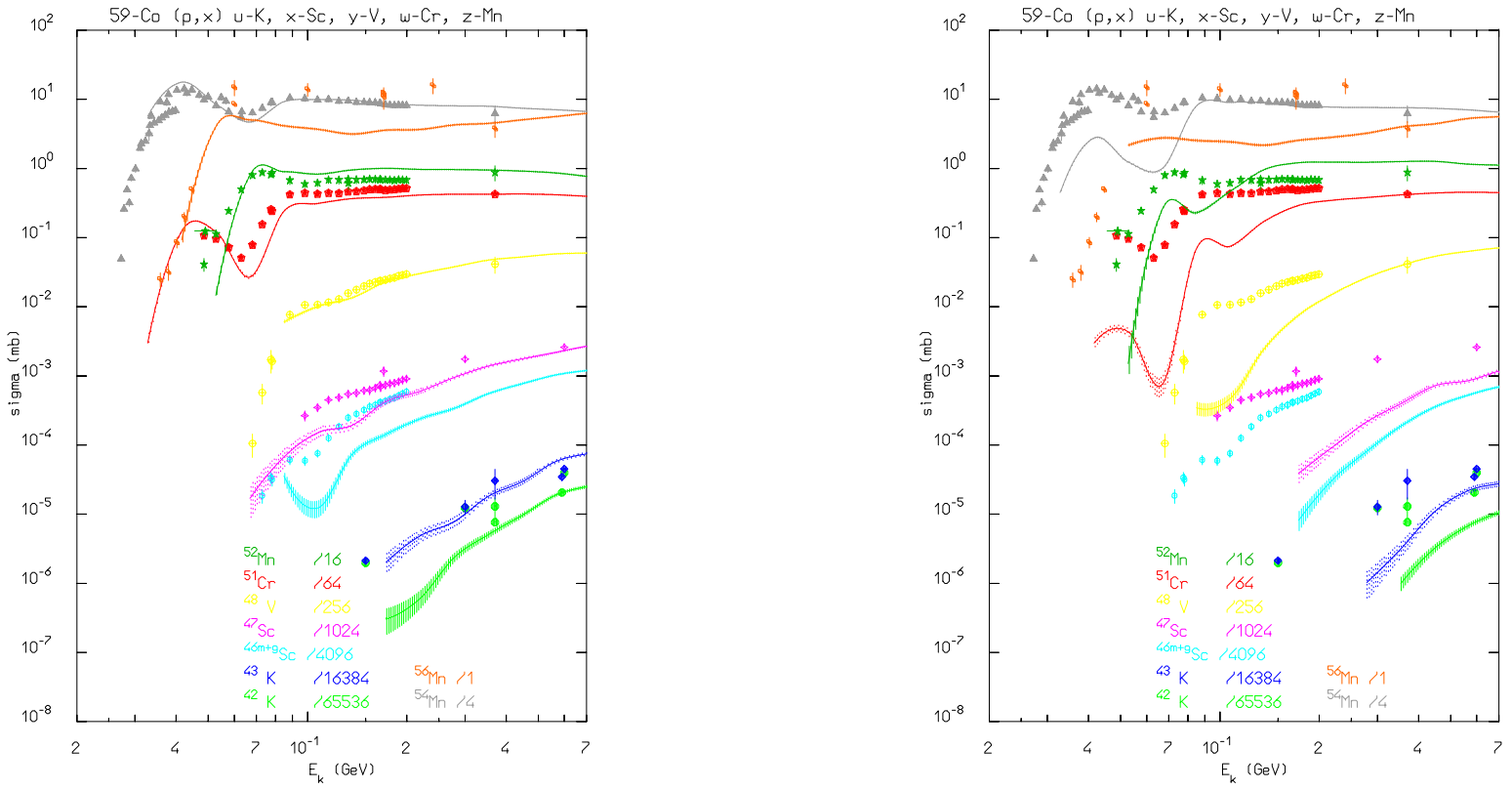

Comparison between isotope yields computed with the new (left) and (right) evaporation model in FLUKA

Neutron transport below 20 MeV

- ENEA multigroup cross-sections: 72 groups, ≈100 elements/isotopes
- Gamma-ray generation, different temperatures, Doppler broadening, self-shielding
- Transport: standard multigroup transport with photon and fission neutron generation
- Detailed kinematics and recoil transport for elastic and inelastic scattering on hydrogen and for $^{14}N(n,p)$, $^{10}B(n,\alpha)$ and $^{6}Li(n,x)$
- Correlated capture gamma generation for selected isotopes
- Photons transported with EMF
- Kerma factors to calculate energy deposition
- Residual nuclei production

An example of calculated cooldown curve

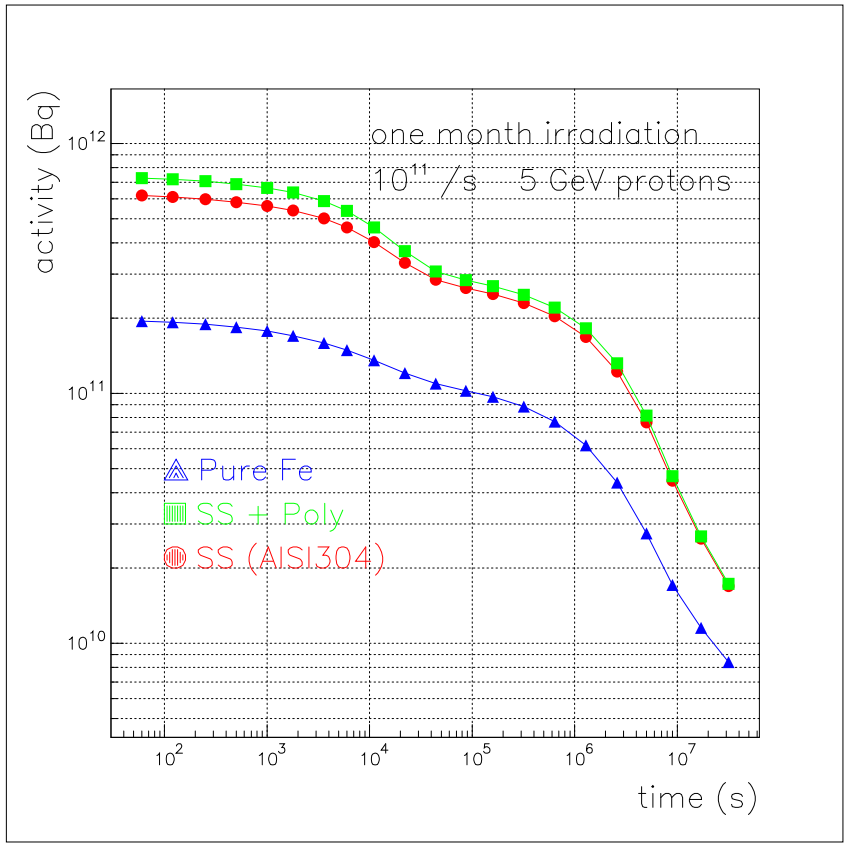

Cooling curves for residual activity for a Stainless Steel, Stainless Steel+CH_2 or Iron target (40 cm radius, 100 cm long) irradiated by 10^{11} 5 GeV protons s^{-1} for one month

Evolution of residual nuclei: SS/Iron target

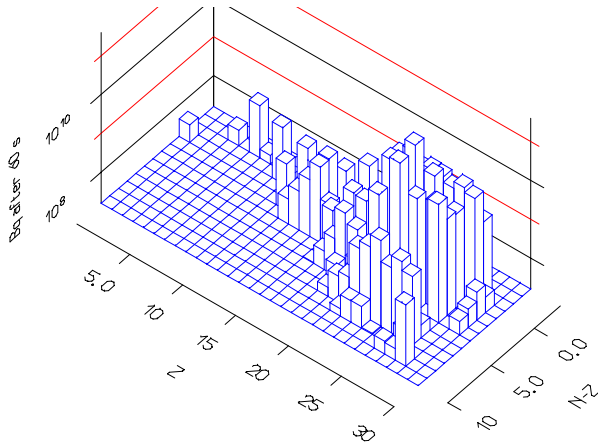

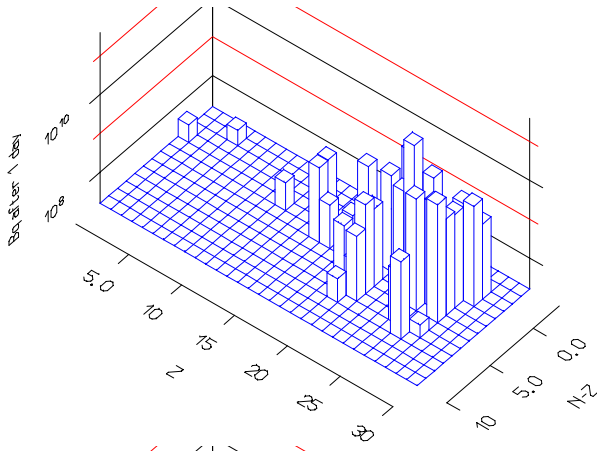

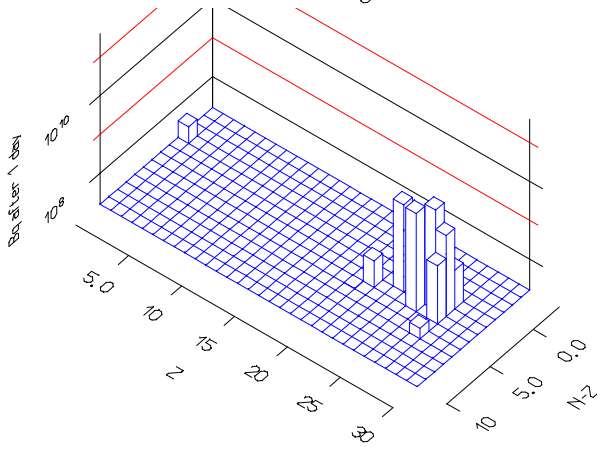

Computed residual activities (Bq) as a function of the isotope atomic number Z and neutron excess N-Z for an AISI304 target (40 cm radius and 100 cm long) irradiated by 10^{11} 5 GeV protons s^{-1} for one month: after 60 s (top left), 1 day (top right) and after 1 year (right)

Neutron production examples: thick targets

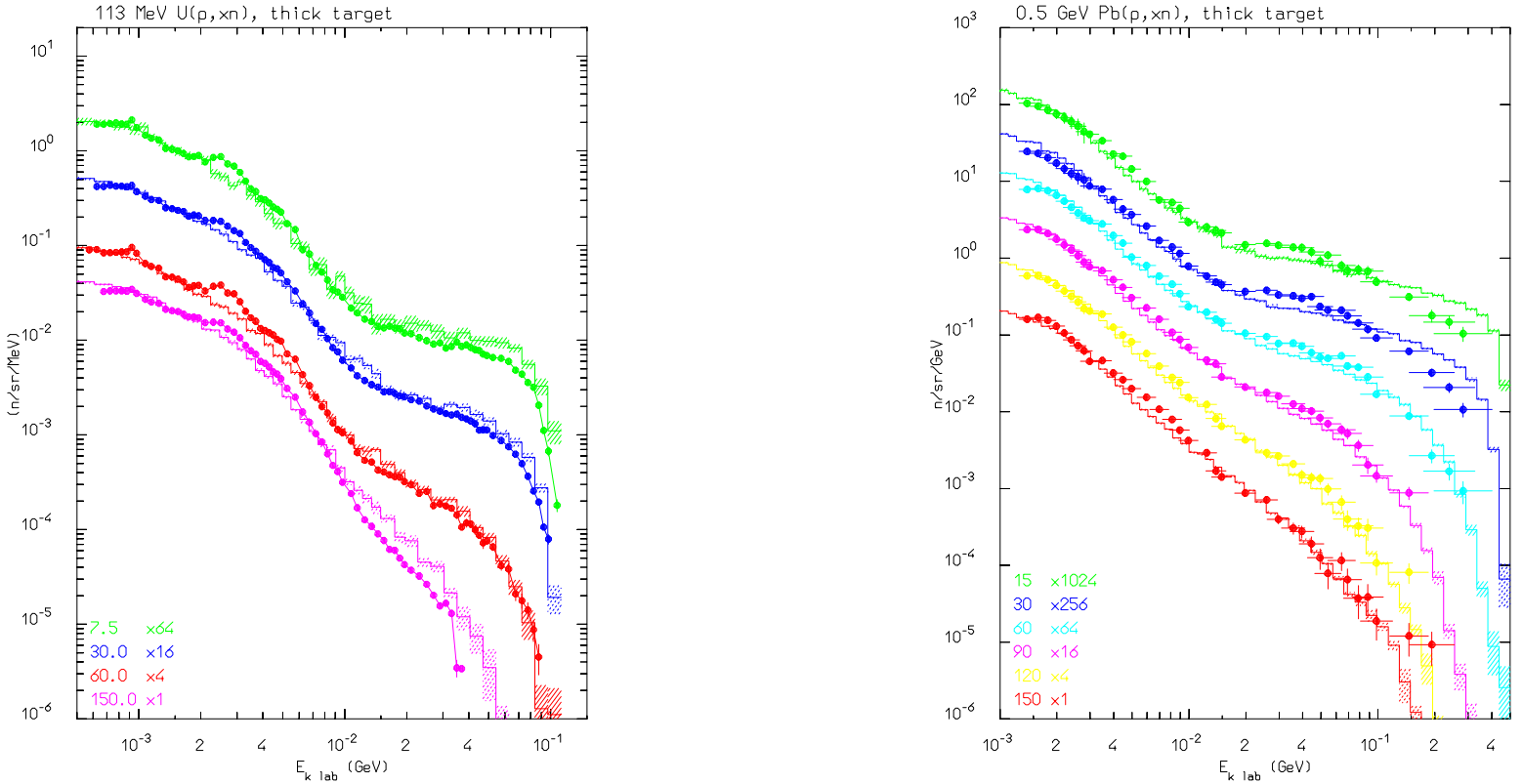

Simulated (dashed histogram) and experimental (symbols) neutron double differential distributions out of stopping length targets for 113 MeV protons on U (left, data from M.M. Meier et al., Nucl. Sci. Eng. **110**, (1992) 299) and 500 MeV protons on Pb and 256 MeV protons on uranium (right, S. Meigo et al., JAERI-Conf 95-008, (1995), 213)

EMF : ElectroMagnetic Fluka

Photoelectric : fluorescence,angular distribution,Auger , polarization

Compton and Rayleigh: atomic bonds,polarization

Pair production correlated angular and energy distribution; also for μ

Photonuclear see later; also for μ

Bremsstrahlung : LPM, angular distribution, finite at tip, ... also for μ

Bhabha and Møller scattering

Positron annihilation at rest and in flight

μ^- capture at rest

Optical photon (Čerenkov) production and transport

LEP dismantling: a calculational nightmare

Request : demonstrate that ALL activities are below 1/10 of the 1996 European Directive limits (around 10 Bq/g) after 10 year operation

An almost unaffordable task for a MC:
Starting from an electron beam,
simulate the extremely rare photon induced nuclear interactions
with such an accuracy as to determine the residual nuclei.

EXPERIMENT: samples of different materials on LEP beam dumps.

- Irradiation time: 5 months, at about 20 cm from the beam axis
- Specific activity of the radionuclides detected in the samples were compared with FLUKA calculations
- The measured activities are so low (few Bq/g) that even the experimental measurement is difficult

Photonuclear Interactions

- Giant Resonance interaction
- Quasi-Deuteron effect
- interaction in the Delta Resonance energy region
- Vector Meson Dominance in the high energy region
- INC, preequilibrium and evaporation via the PEANUT model
- Possibility to bias the photon nuclear inelastic interaction length to enhance interaction probability

In not many other existing transport codes photonuclear reactions are simulated over the whole energy range

Photonuclear Interactions

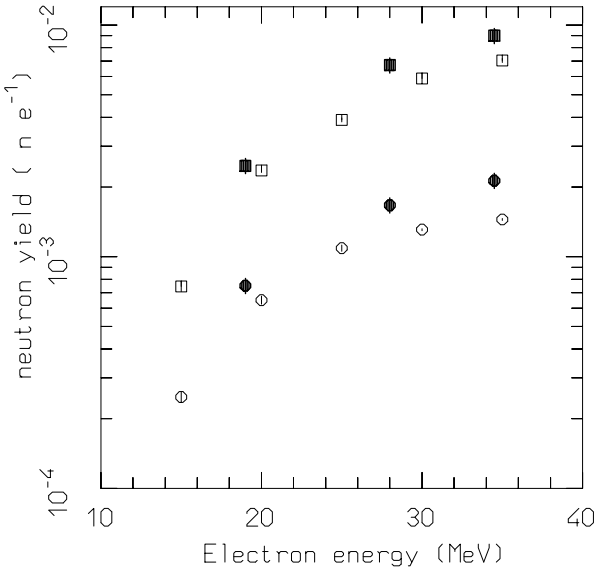

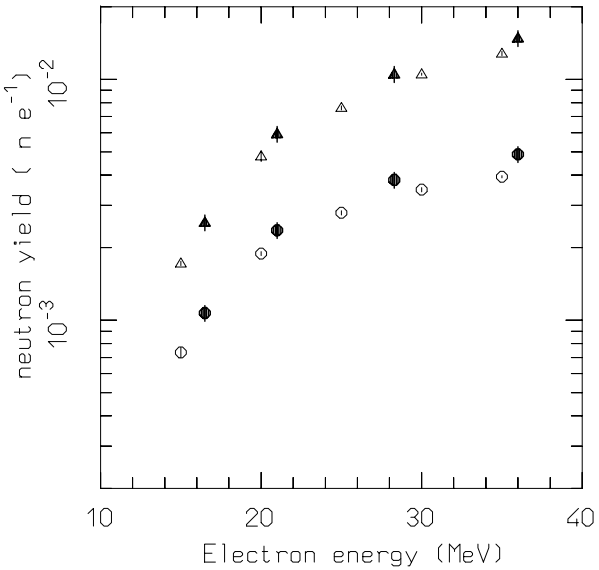

Yield of neutrons per incident electron as a function of initial electron energy. Open symbols: FLUKA, closed symbols: exp. data. Left: Pb, 1.01 (lower points) and 5.93 (upper) X_0 Right: U, 1.14 and 3.46 X_0

Pb(γ,xn) (exp. data NPA367, 237 (1981), NPA390, 221 (1982))

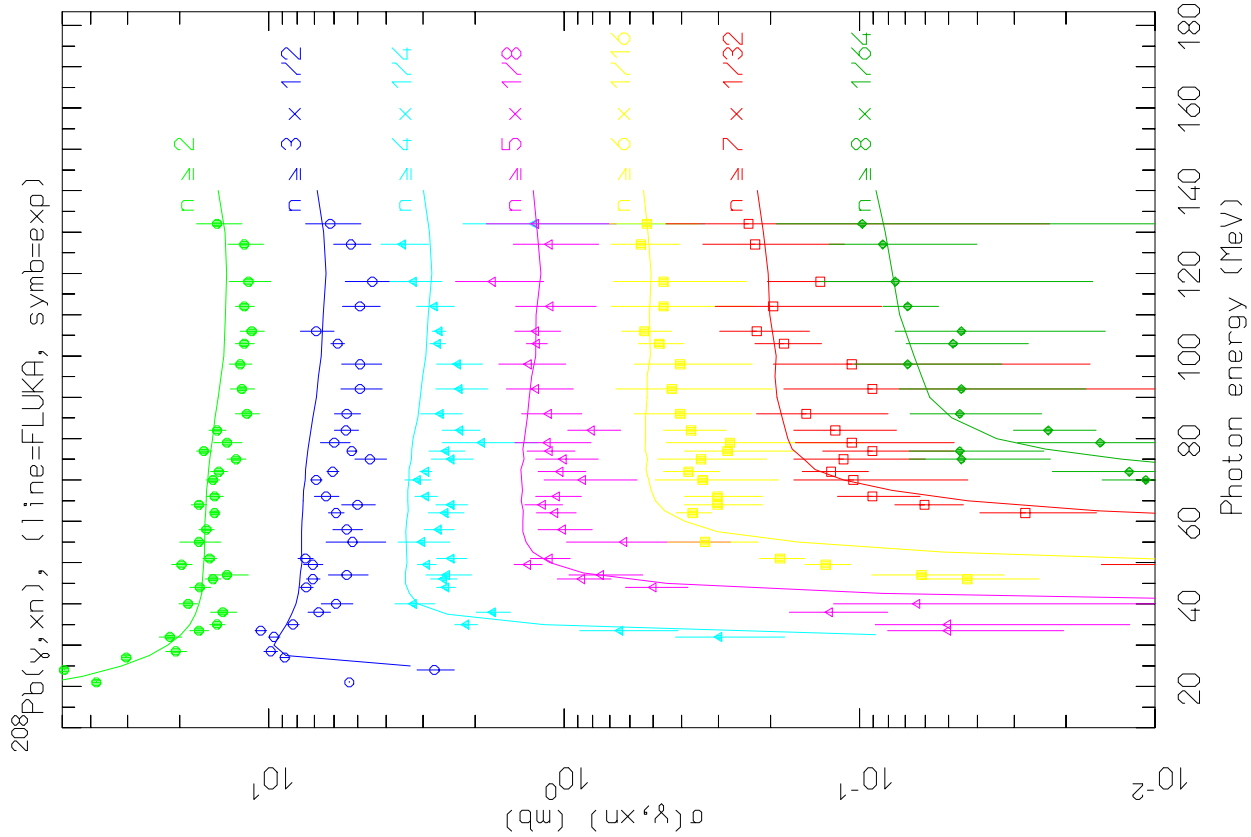

LEP activation: some experimental results

Radio nuclide	$T_{1/2}$	Specific Activity (Bq/g)			Ratio
		Exp.	FLUKA	(%)	F/E
^{46}Sc	83.8 d	0.13	0.065	12	0.5
^{48}V	15.97 d	0.31	0.52	7	1.7
^{51}Cr	27.7 d	4.12	2.7	5	0.65
^{52}Mn	5.6 d	0.17	0.74	6	4.3
^{54}Mn	312.2 d	3.54	2.9	2	0.82
^{59}Fe	44.5 d	0.028	0.0088	27	0.31
^{56}Co	77.7 d	0.29	0.46	7	1.6
^{57}Co	271.8 d	1.3	1.1	4	0.85
^{58}Co	70.9 d	2.65	1.4	3	0.52
^{60}Co	5.27 y	0.18	0.085	21	0.47
^{95}Nb	34.9 d	0.038	0.013	27	0.34

Stainless Steel sample on the LEP electron dump. The exp. points have a systematic error of ≈20%(A.Fassò et al. CERN-TIS-99-011-RP-CF/SLAC-PUB-8214 and CERN-TIS-99-012-RP-CF/SLAC-PUB-8215)

Charged particle transport

Ionization energy losses (below δ threshold)

Latest recommended values of ionization potential and density effect parameters implemented (Sternheimer, Berger & Seltzer) (can be overridden on user's request)
Special treatment of positron dE/dx (Kim et al. 1986)
a new general approach to ionization fluctuations *(see later)*

Multiple coulomb scattering

path length correction, lateral displacement, angle correlation
Soft approach to boundaries
Single scattering available, automatic if needed
Screening and spin-relativistic correction
Fully coupled to magnetic field transport

Ionization Fluctuations

The FLUKA approach:

- based on general statistical properties of the cumulants of a distribution (in this case a Poisson distribution convoluted with $\mathbf{d}\boldsymbol{\sigma}/\mathbf{d}\boldsymbol{E}$)
- integrals can be calculated analytically and exactly *a priori* $\Longrightarrow$ minimal CPU time
- applicable to any kind of charged particle , taking into account the proper (spin-dependent) cross section for $\boldsymbol{\delta}$ ray production
- the first 6 moments of the energy loss distribution are reproduced ($k_n =< (x - < x >)^n >$)

Ionization Energy losses

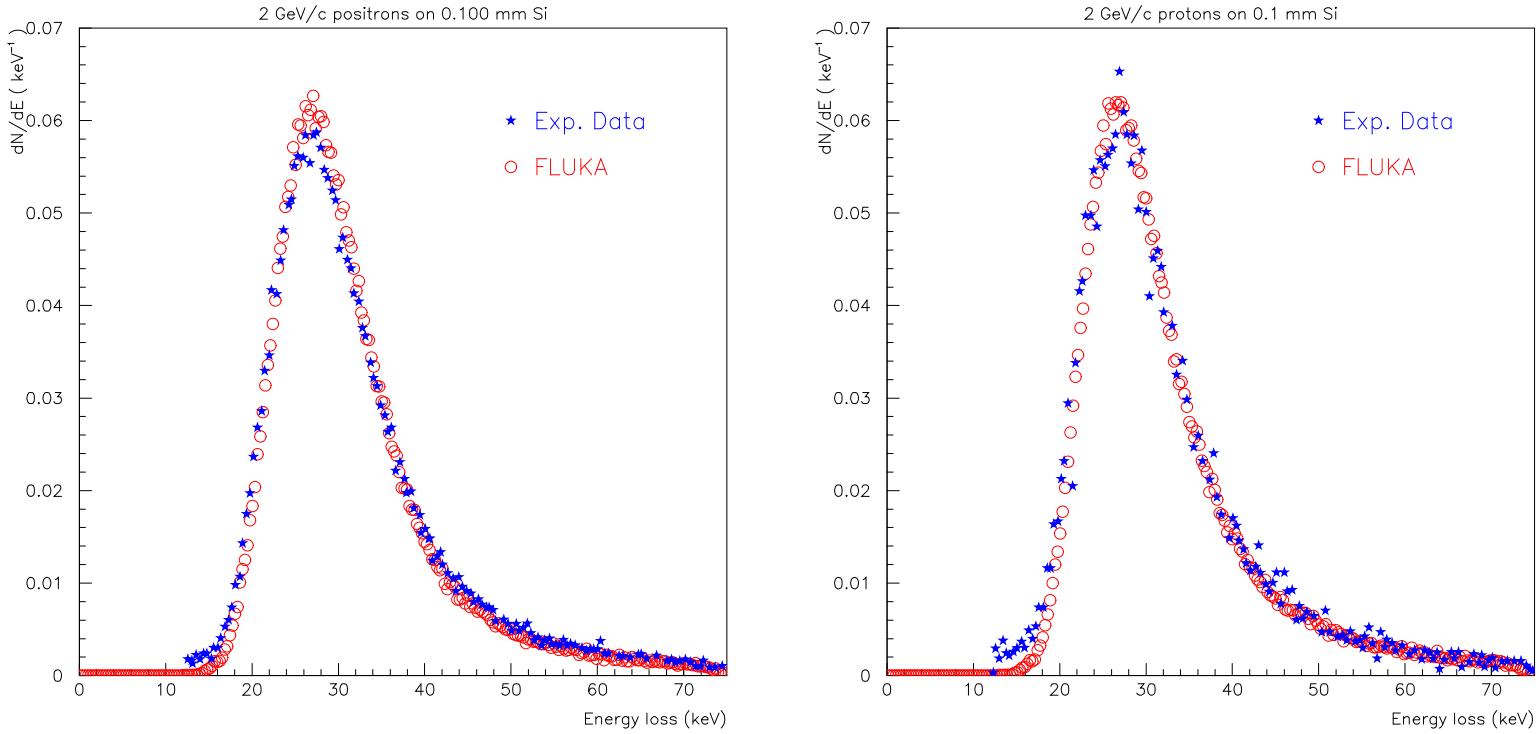

Experimental [4] and calculated energy loss distributions for 2 GeV/c positrons (left) and protons (right) traversing 100μm of Si

[4] J.Bak et al. NPB288, 681 (1987)

"New algorithm" additions: (work in progress)

- Position angle, η, randomly sampled around the "correct" Molière distribution trying to correlate correctly with the scattering angle
- Azimuthal angle between the position and velocity vectors randomly sampled
- "Polygonal" step path in order to maximize energy deposition accuracy and to help in getting correct boundary effects

Graphical example

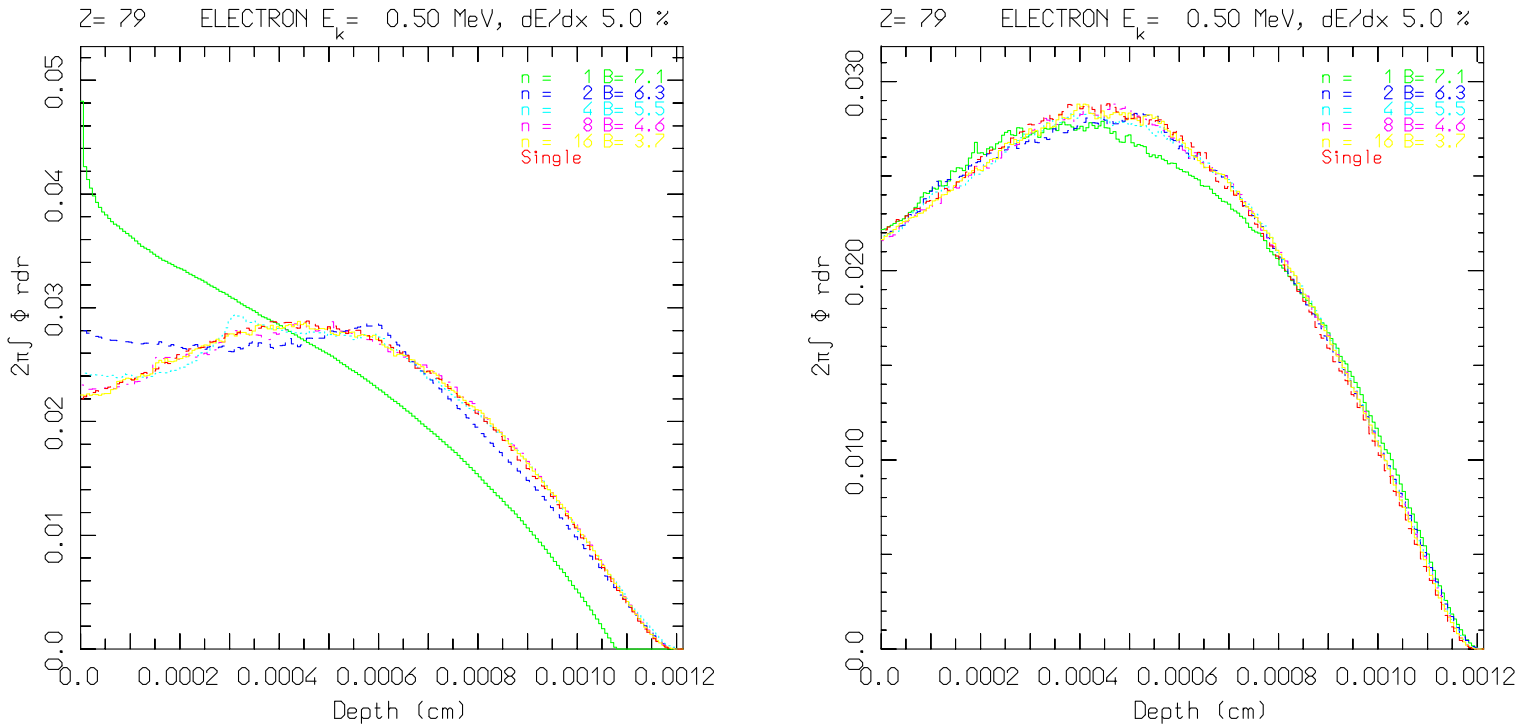

Tracklength vs depth distribution for 0.5 MeV e^- on Au, 5% step, for N=1,...,16 substeps and single scattering for the "old" (left) and "new" (right, with polygonal approach) algorithms

Heavy ions

Heavy ion transport and interactions are presently under development in FLUKA:

- Ionization energy losses already implemented
  - Up-to-date effective charge parametrizations
  - Energy loss straggling according to:
    * "normal" first Born approximation
    * Charge exchange effects (dominant at low energies, ad-hoc model developed for FLUKA)
    * Mott cross section and nuclear form factors (high energies)(in progress)
- Multiple scattering already implemented
- High energy A-A interactions ($E > 5 - 10\ GeV/u$): interface to DPMJET *test phase*
- Low energy A-A interactions: extension of the PEANUT model *almost ready for tests with* $\alpha's$

dE/dx and straggling of heavy ions

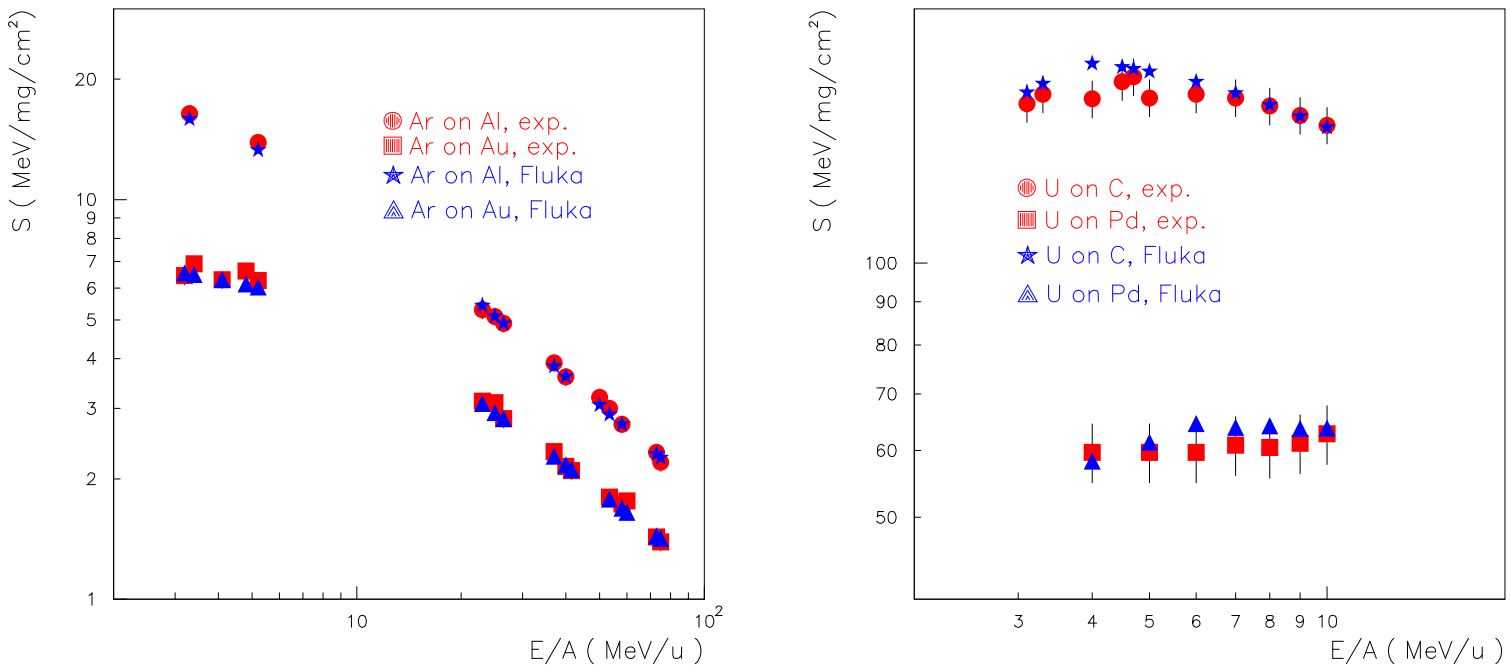

Experimental (red) (R.Bimbot, NIM**B69** (1992) 1) and FLUKA (blue) stopping powers of Argon and Uranium ions in different materials and at different energies.

dE/dx and straggling of heavy ions

Projectile	Target	thickness (mg/cm^2)	FWHM (keV) Exp		FLUKA
^{12}C	Al	0.217	74.5	± 3	90
^{16}O	Al	0.110	92	± 2	94
^{16}O	Al	0.246	147	± 3	144
^{16}O	Al	0.457	202	± 2	198
^{32}S	Al	0.315	290	± 30	356
^{32}S	Al	0.990	521	± 20	638
^{32}S	Au	0.053	98	± 20	140
^{32}S	Au	3.492	820	± 20	1092
^{127}I	Al	0.321	780	± 40	735
^{127}I	Al	0.530	1000	± 35	949
^{127}I	Al	0.990	1375	± 50	1297
^{127}I	Au	0.053	250	± 10	275
^{127}I	Au	1.186	1200	± 50	1255
^{127}I	Au	3.800	2250	± 90	1932

Measured (S. Ouichaoui et al. NIM B164-165 (2000) 259) and computed (FLUKA) straggling for 2 MeV/amu ^{12}C,^{16}O , ^{32}S ions and 1.467 MeV/amu ^{127}I ions

DPMJET

Authors: **R. Engel[†], J. Ranft[*], and S. Roesler[&]**
[†] Bartol, [*] Siegen University, [&] CERN

Nucleus-Nucleus interaction code [5] for collisions from ≈5-10 GeV/n till the highest cosmic ray energies ($10^{18} - 10^{20}$ eV)

Applications of DPMJET

- Predictions for heavy ion experiments at present and future accelerators (i.e. ALICE at LHC)
- Simulations of Cosmic Ray cascades in the HEMAS-DPM code used by the MACRO Collaboration
- Simulations of Cosmic Ray cascades in the CORSIKA code (Karlsruhe)

[5] PRD 51 (1995) 64; Gran Sasso INFN/AE-97/45 (1997); hep-ph/9911232; hep-ph/9911213; hep-ph/0002137

DPMJET: examples of performances

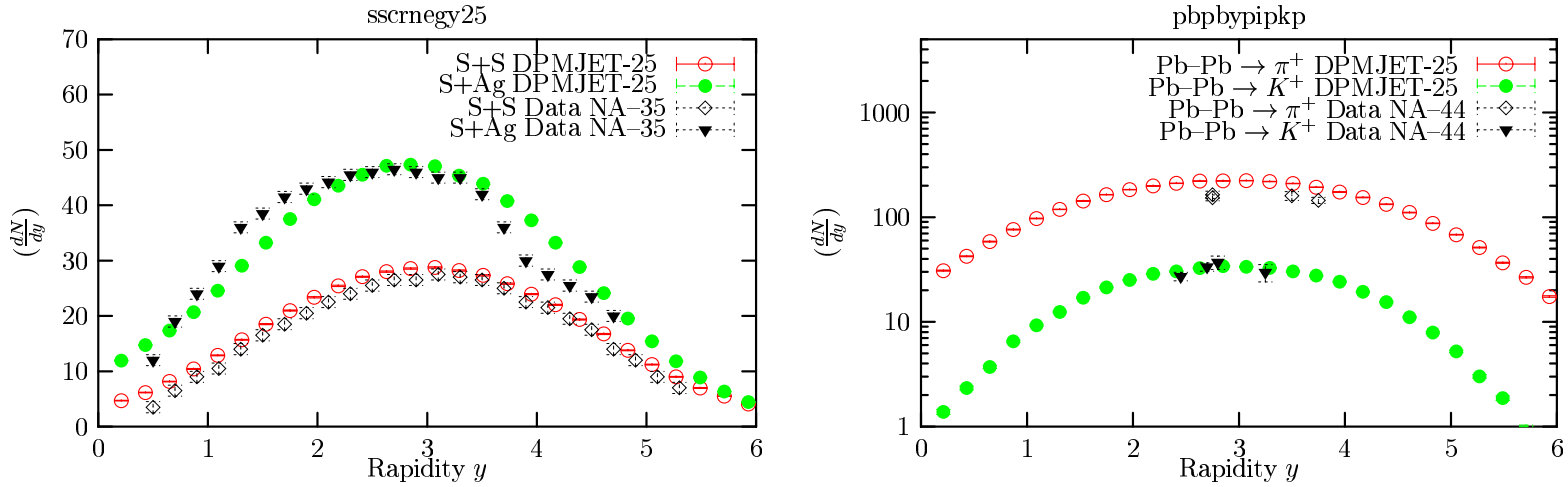

Rapidity distribution of negative particles for 158 AGeV/c S-S and S-Ag collisions (left) and of positive pions and kaons for 158 AGeV/c Pb-Pb collisions (right). Experimental data from the NA-35 and NA-44 collaborations are compared with DPMJET predictions.

Cascading/evaporation in A-A collisions (from ZPC71, 75 (1996))

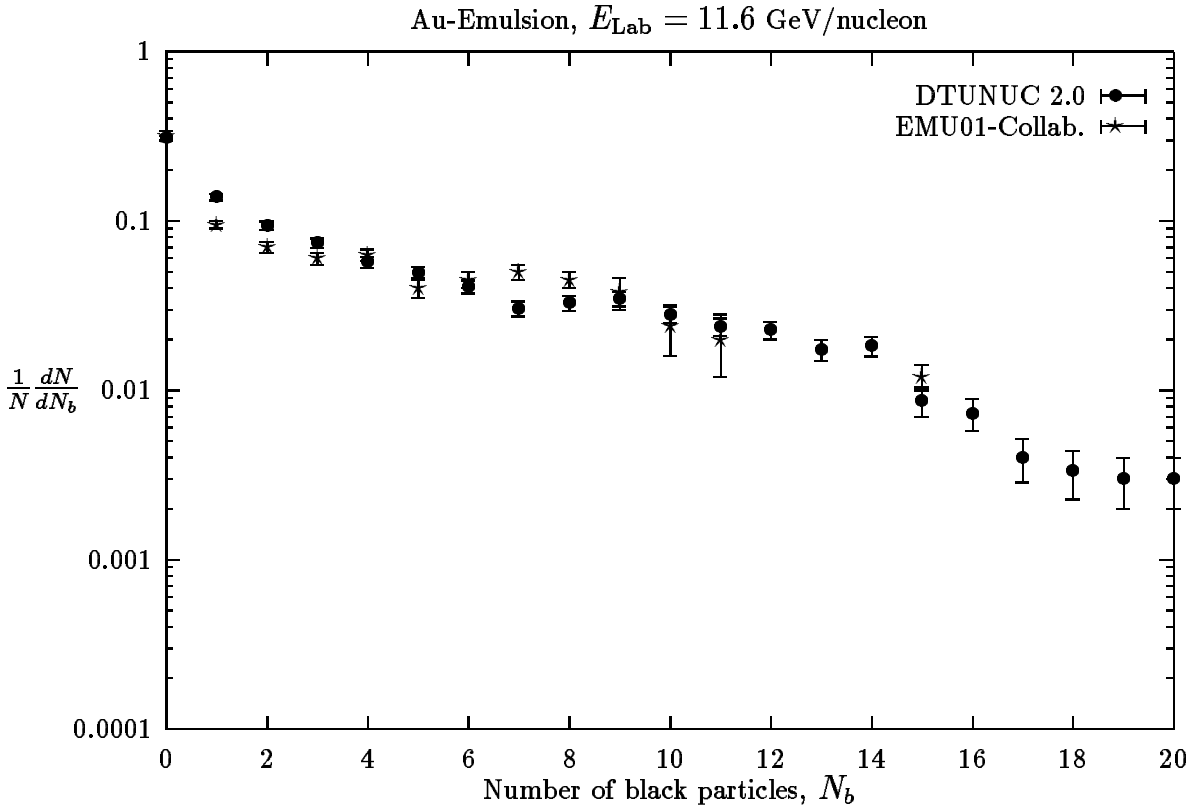

Black particle multiplicity distributions in gold-emulsion interactions compared with exp. data (ZPC65, 421 (1995))

Cascading/evaporation in A-A collisions (from ZPC71, 75 (1996))

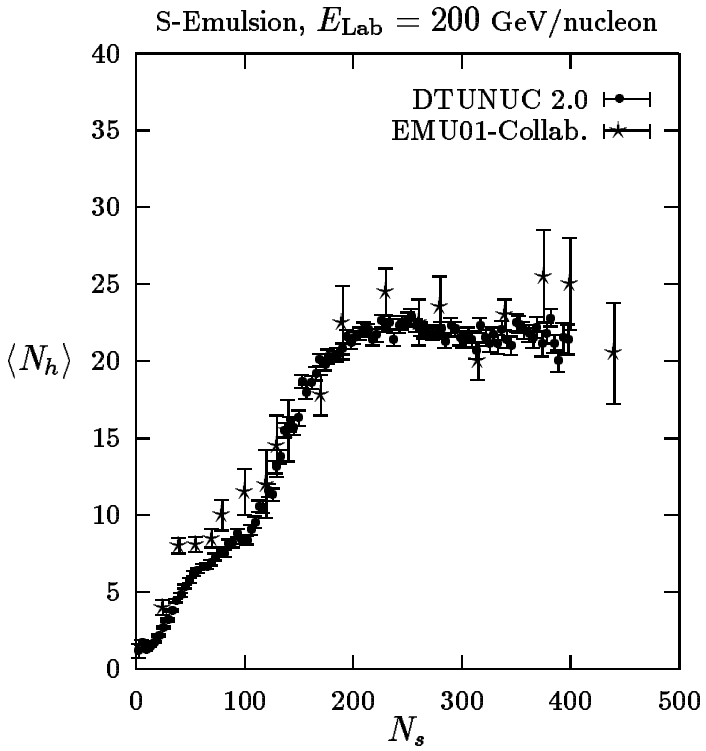

Correlations between shower (N_s) and heavy (N_h) particle multiplicities in sulfur-emulsion interactions, compared with exp. data (ZPC65, 421 (1995))

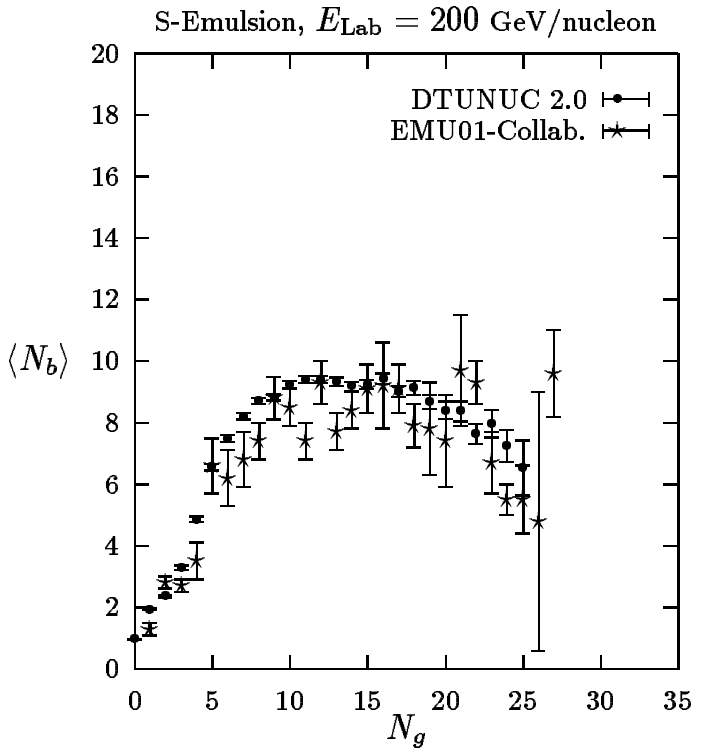

Correlations between gray (N_g) and black (N_b) particle multiplicities in sulfur-emulsion interactions, compared with exp. data (ZPC65, 421 (1995))

the FLUKA-DPMJET interface

Presently : DPMJET-II.53 , upgrade to DPMJET-3 in progress

Initialization

Cross sections pre-computed by DPMJET, tabulation is used by FLUKA
Glauber impact parameter distributions have been pre-computed for a complete matrix of projectile-target combinations up to A=246 over the entire available energy range (3 A GeV$-1.5 \cdot 10^6$A GeV in N-N cms).

Interface call at begin and end of single interactions
Reaction products given back to be transported by FLUKA
Residual nuclei deexcitation is performed in FLUKA

FLUKA-DPMJET: initialization

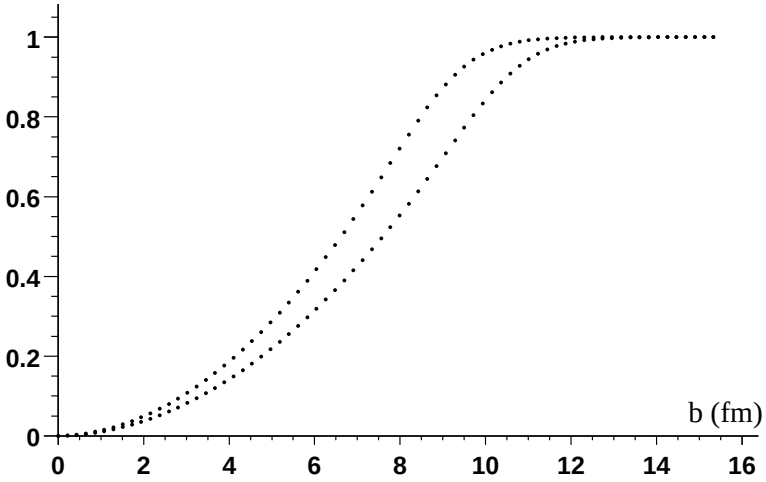

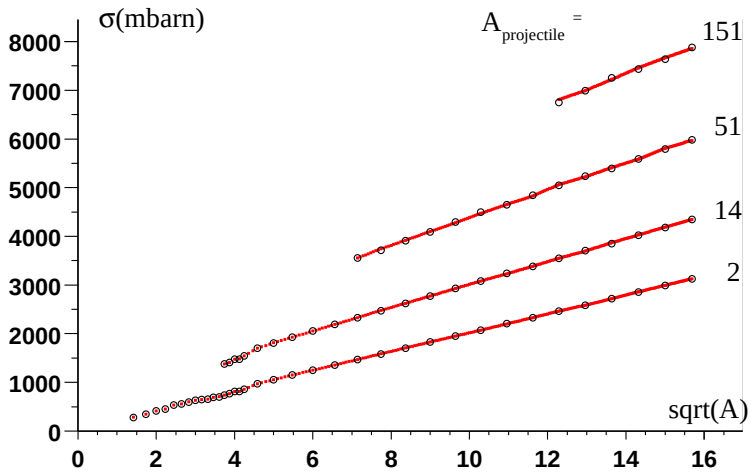

Integral Glauber impact parameter distributions for the extreme energy bins and one projectile-target combination.

DPMJET cross sections at $E_{lab} = 6.3 \cdot 10^6$ ATeV.
Symbols: computed values
lines:interpolation used by FLUKA

Muon Capture

An exotic source of neutron background *(See background at nTOF)*

Basic weak process : $\mu^- + p \rightarrow \nu_\mu + n$

μ^- at rest + atom $\rightarrow$ excited muonic atom $\rightarrow$ x-rays+g.s muonic atom

Competition between μ decay and μ capture by the nucleus.

In FLUKA: Goulard-Primakoff formula

$\Lambda_c \propto Z_{eff}^4$, calculated Z_{eff}, Pauli blocking from fit to data.

$\frac{\Lambda_c}{\Lambda_d} = 9.2 \cdot 10^{-4}$ for H, 3.1 for Ar, 25.7 for Pb

Nuclear environment (Fermi motion, reinteractions, deexcitation..) from the FLUKA intermediate-energy module PEANUT

Slow projectile, low energy transfer (neutron E=5 MeV on free p)

Experimentally: high energy tails in n-spectra

Beyond the simple one-body absorption

Good results from addition of two-nucleon absorption

Muon Capture-II

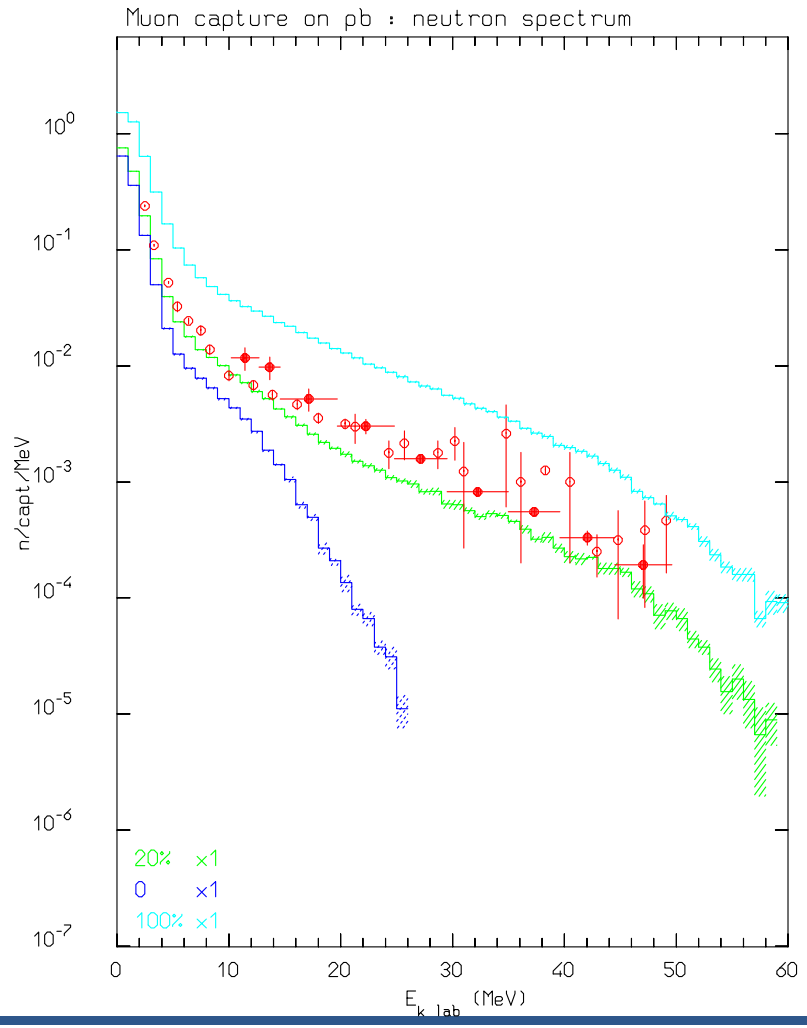

Neutron spectra following muon capture on Lead

Dots: experimental data

histograms: FLUKA calculations

The three curves correspond to a percentage of 2-body absorption of 0, 20%, and 100% .

Emitted:

1.7 neutrons/capture

0.002 protons/capture

Muon Capture-III

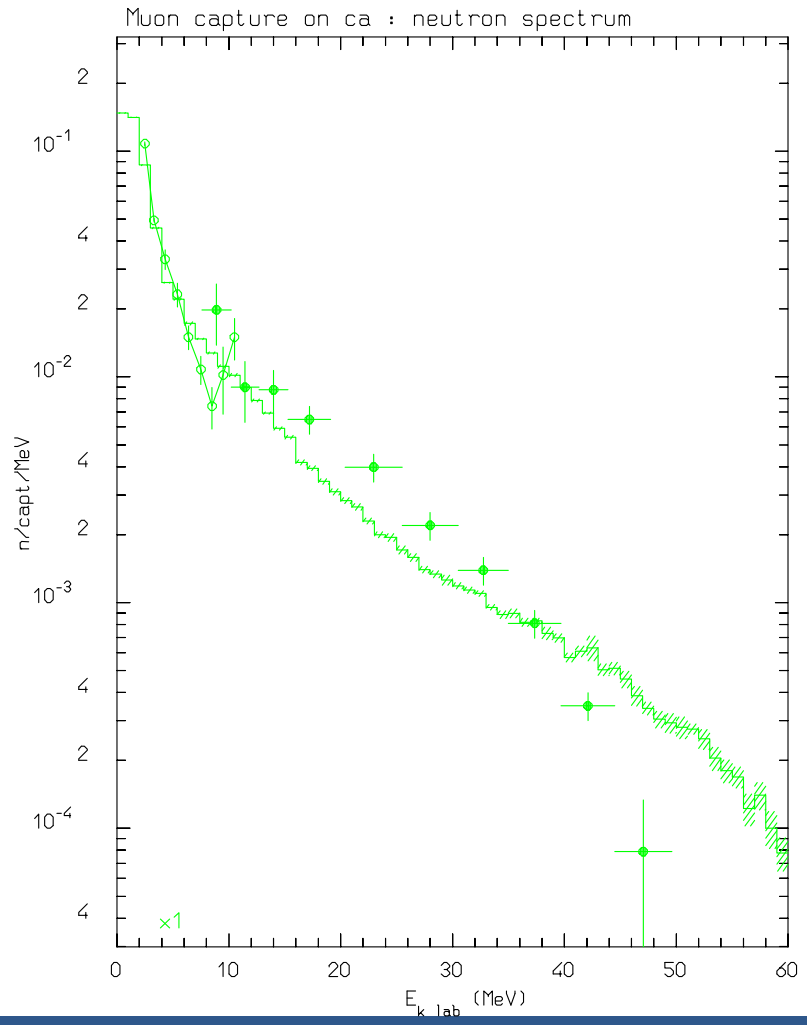

Neutron spectra following muon capture on Calcium

Dots: experimental data (Columbia Univ. rep. NEVIS-172 (1969), Phys. ReV. C7, 1037 (1973), Yad. Fiz. 14, 624 (1972))

histograms: FLUKA calculations

Emitted:

0.62 neutrons/capture

0.27 protons/capture

the nTOF facility

- High flux -high resolution spallation neutron source
  - Wide energy range: thermal up to GeV
  - High flux: $\approx\ 6 \times 10^5 n/cm^2/7 \cdot 10^{12} pr$ @ 200 m
  - Resolution: $\Delta E/E 2 \times 10^{-4}$ @ 1 keV, 2×10^{-3} @ 1 MeV
  - Low (expected) background: 10^{-6}
- Proton Beam
  - CERN-PS: 20 GeV/c, I_p= 4 bunches x $7 \times 10^{12}\ pr/14.4\ s$
- Measurements of neutron induced cross sections
  - ADS applications
  - Astrophysics

June 2001: first measurements facing a background > 50 times more than expected! → trying to understand (A.Ferrari, C.Rubbia, V.Vlachoudis, SL-EET 2001-036)

nTOF background: Simulation setup

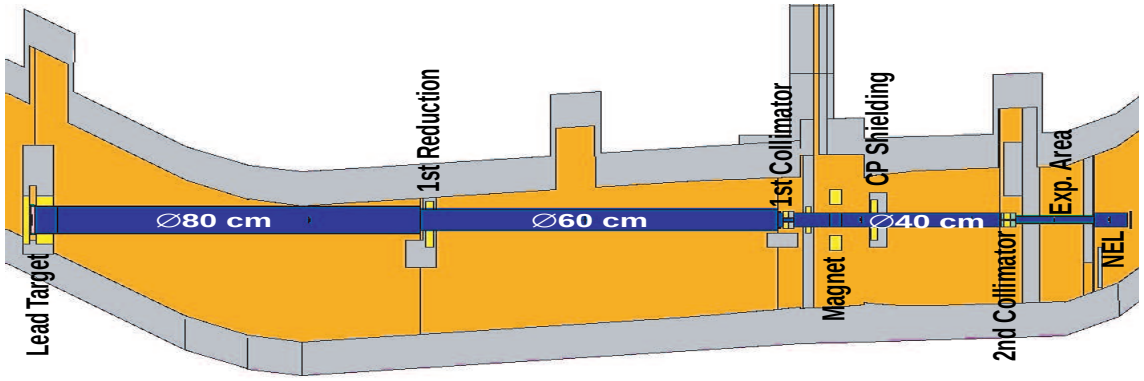

(a)

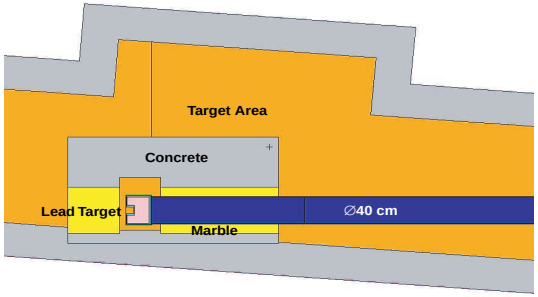

(b)

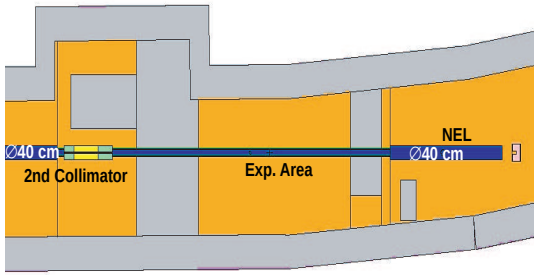

(c)

Top view of TT2A Tunnel Geometry used in the simulations **(a)**; zoom in target area **(b)**; and experimental area **(c)**.

nTOF Simulated muon fluence

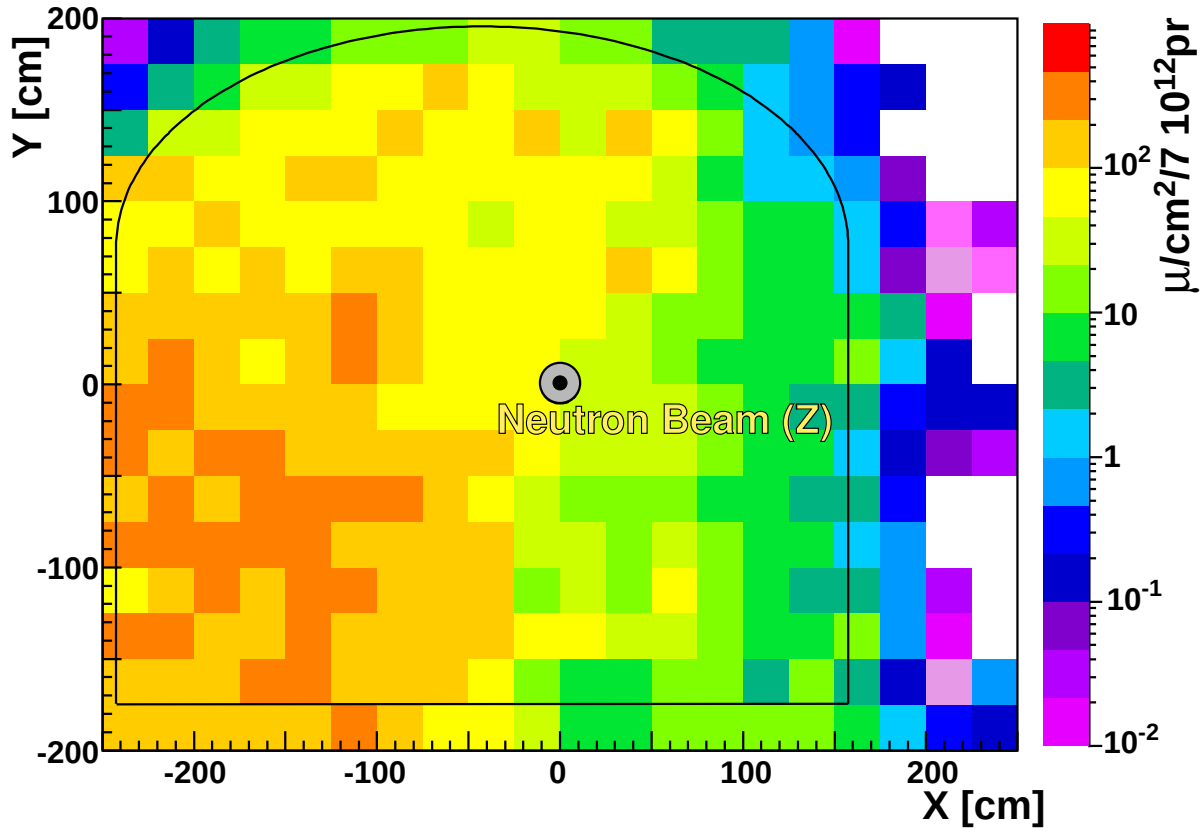

Simulated muon fluence at the entrance of the exp. station per 7 10^{12} protons

nTOF Simulated muon spectrum

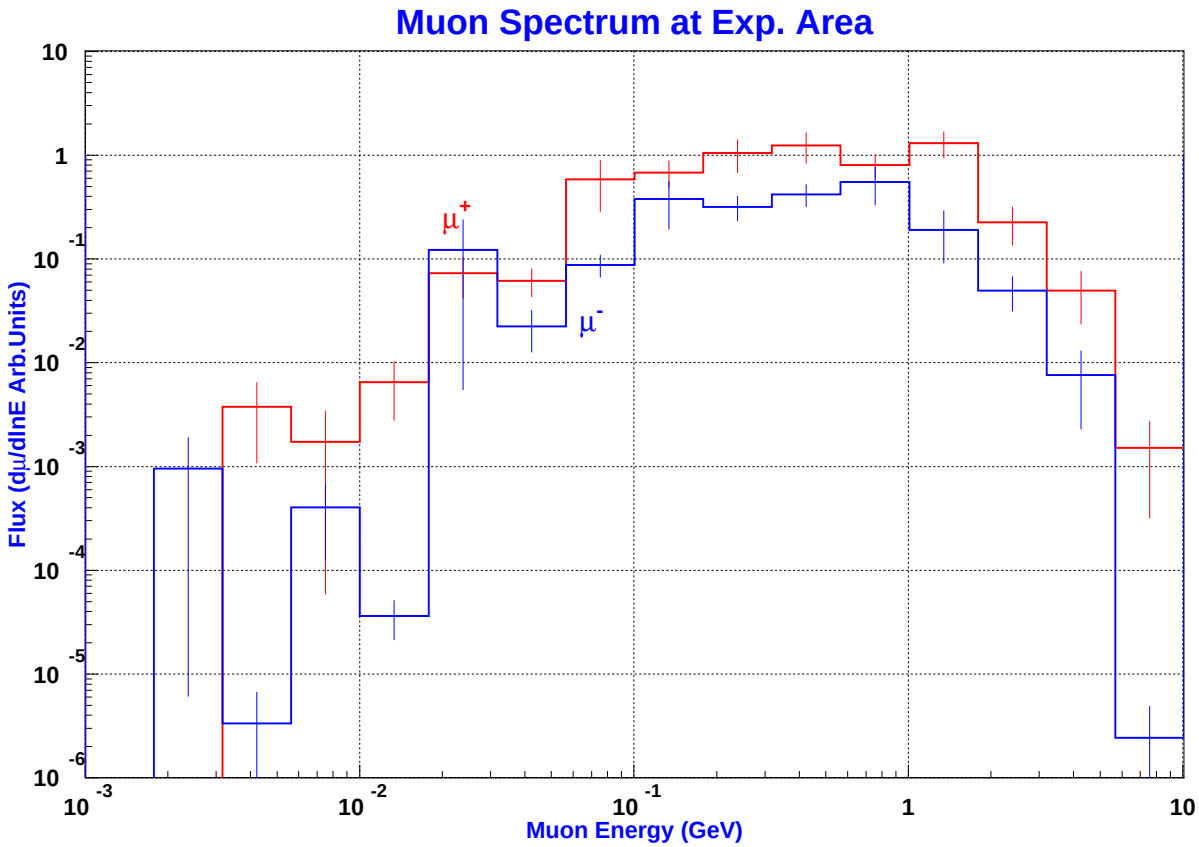

Energy spectrum (dn/dln(E)) of the muons entering the experimental area

nTOF Simulated neutron fluence

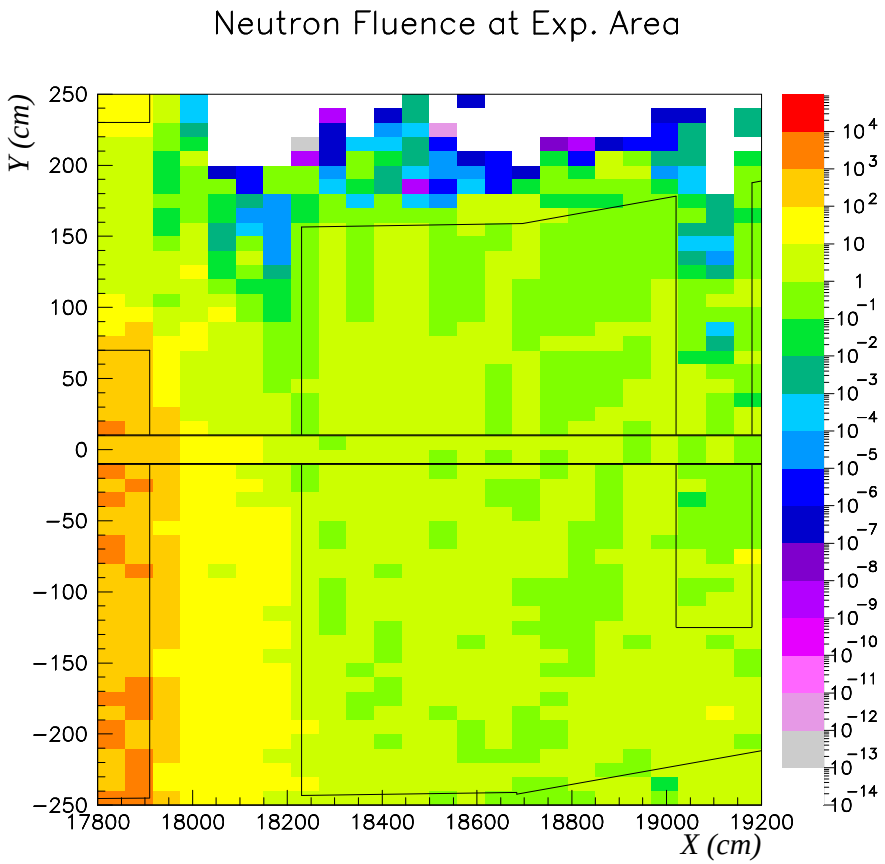

Computed neutron fluence (n/cm^2) inside the experimental area (from the top) for a standard pulse of 7×10^{12} protons

nTOF Simulated neutron energy spectrum

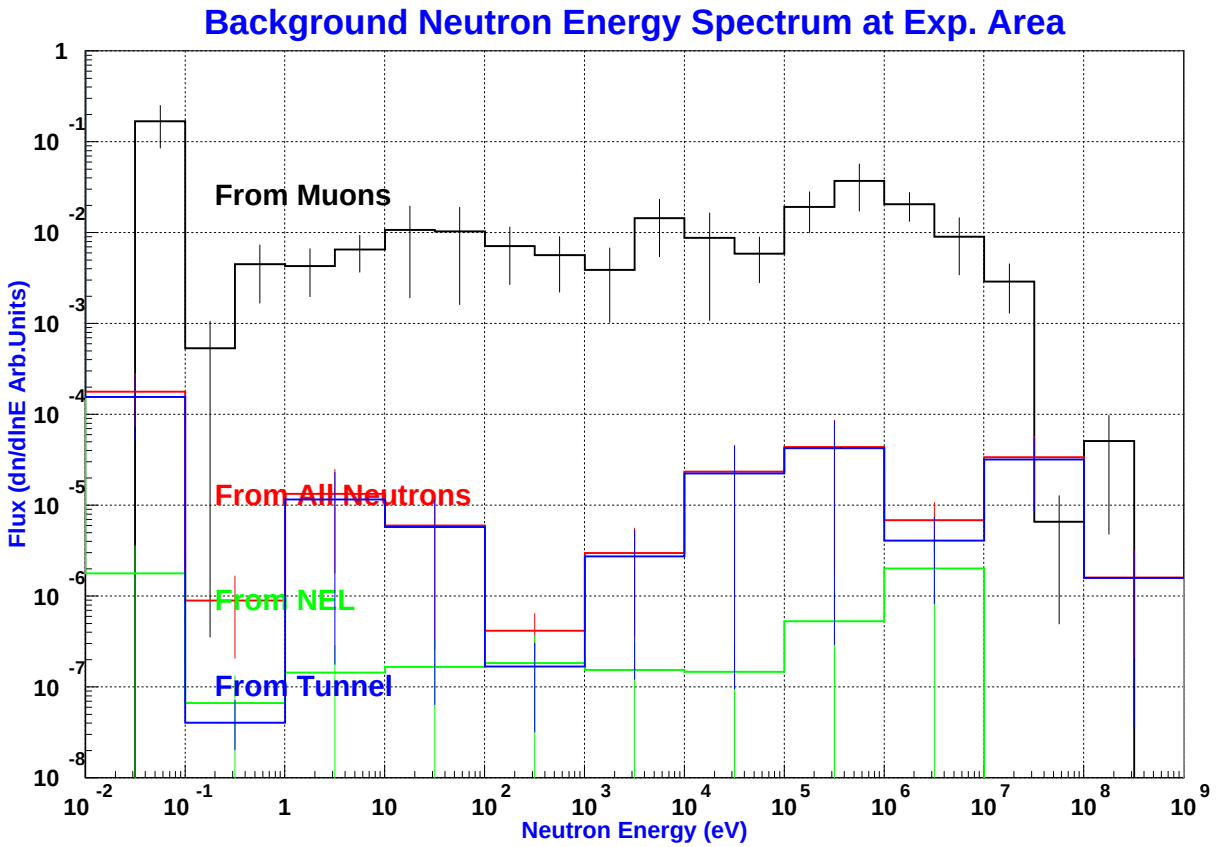

Background neutron entries split into different sources

nTOF Simulated neutron time distribution

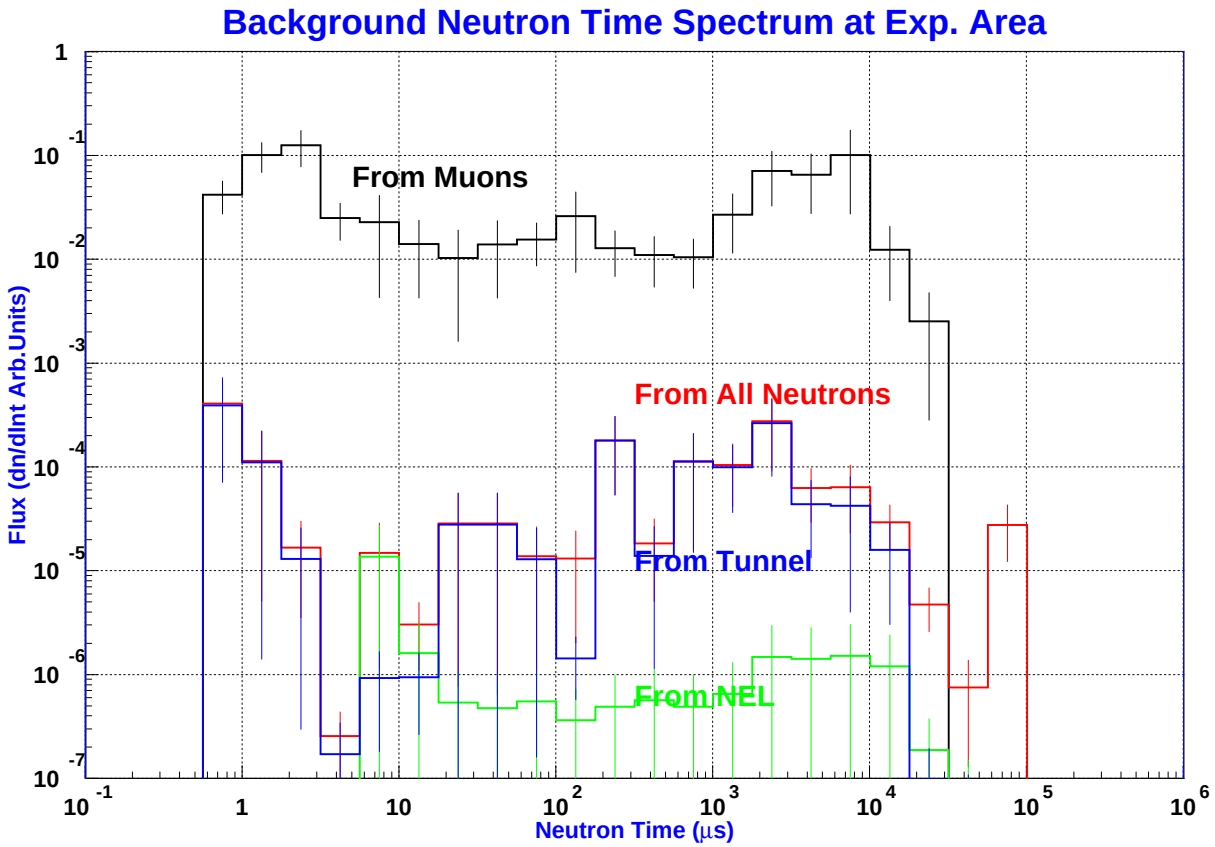

Background neutron time distribution divided into the different components

nTOF Simulated muon wall effectiveness

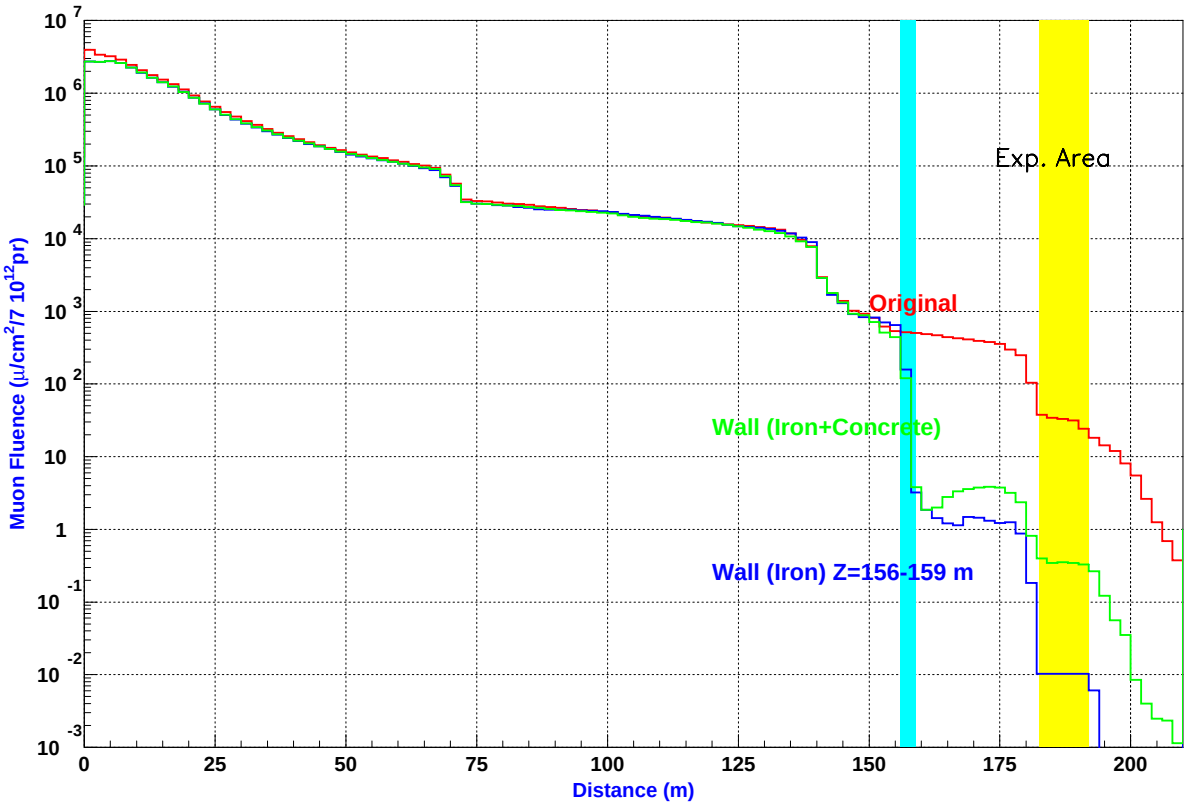

Computed muon fluence (μ/cm^2) along the n_TOF tunnel for a standard pulse of 7×10^{12} protons with and without the extra iron shield, and with the shield with a 1 m thick concrete basement. This is an average over the $\pm$ 1 m around the tube position

nTOF Provisional (october 2001) muon wall layout: picture

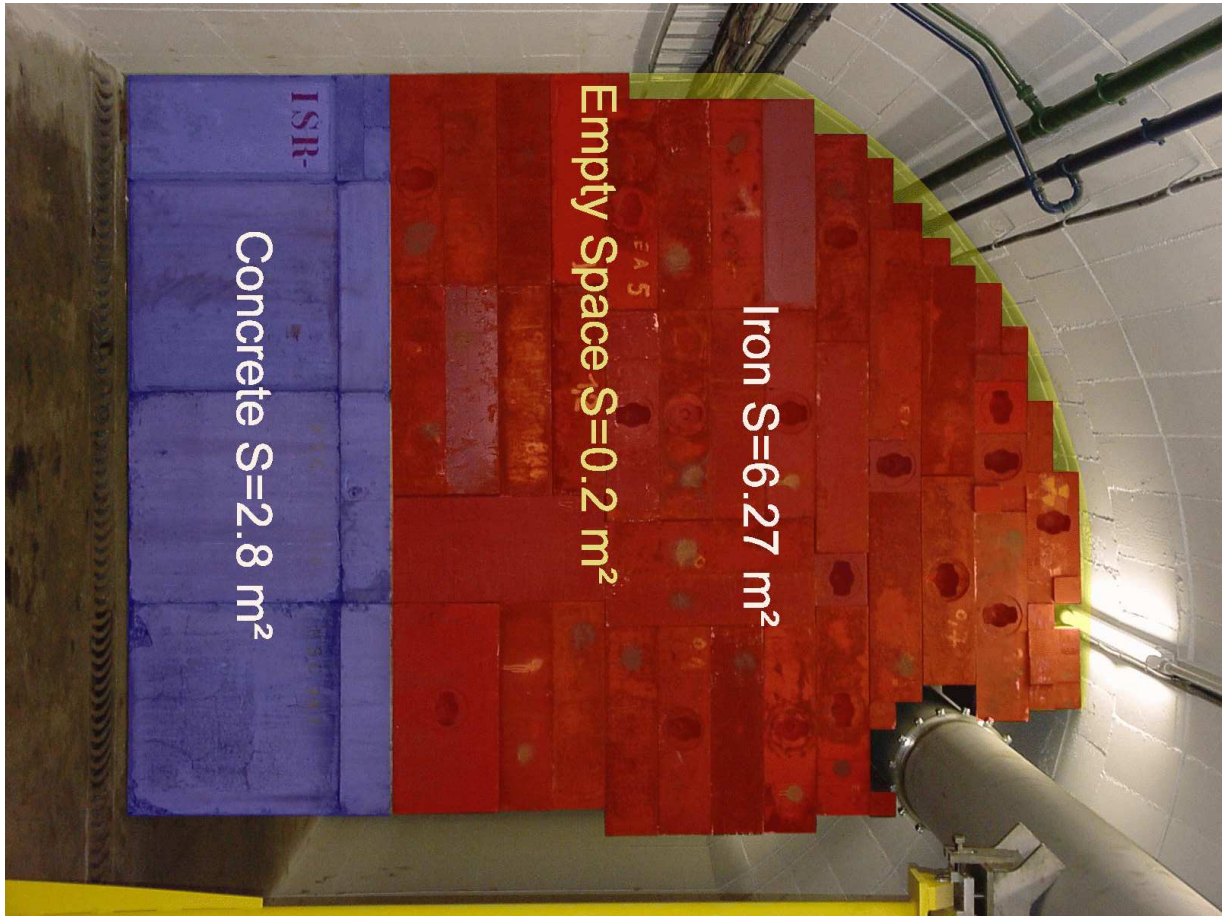

nTOF C6D6 Gold measurements: october vs may cont.

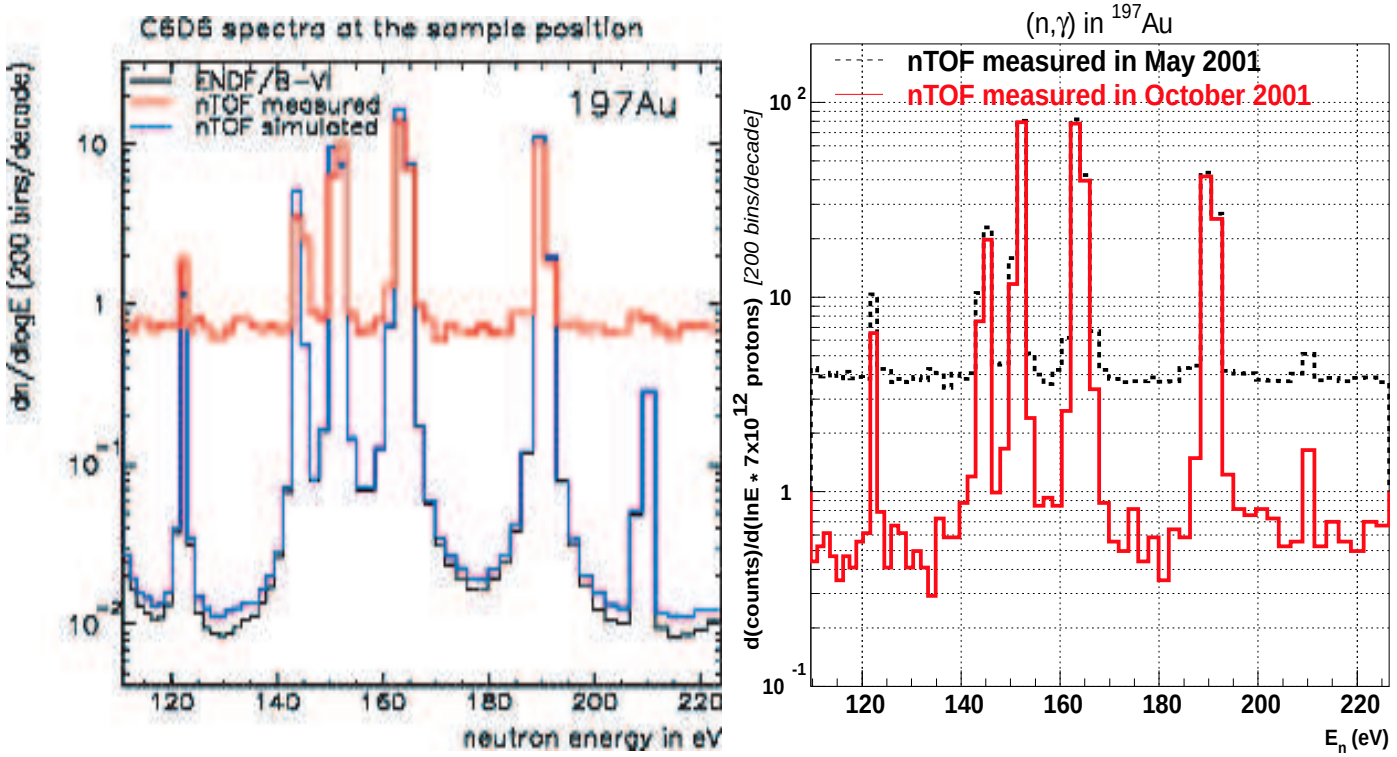

C6D6 spectra with a ^{197}Au sample: may 2001 (left), and october 2001 (right)

nTOF ^{3}He: measured vs simulated time spectra

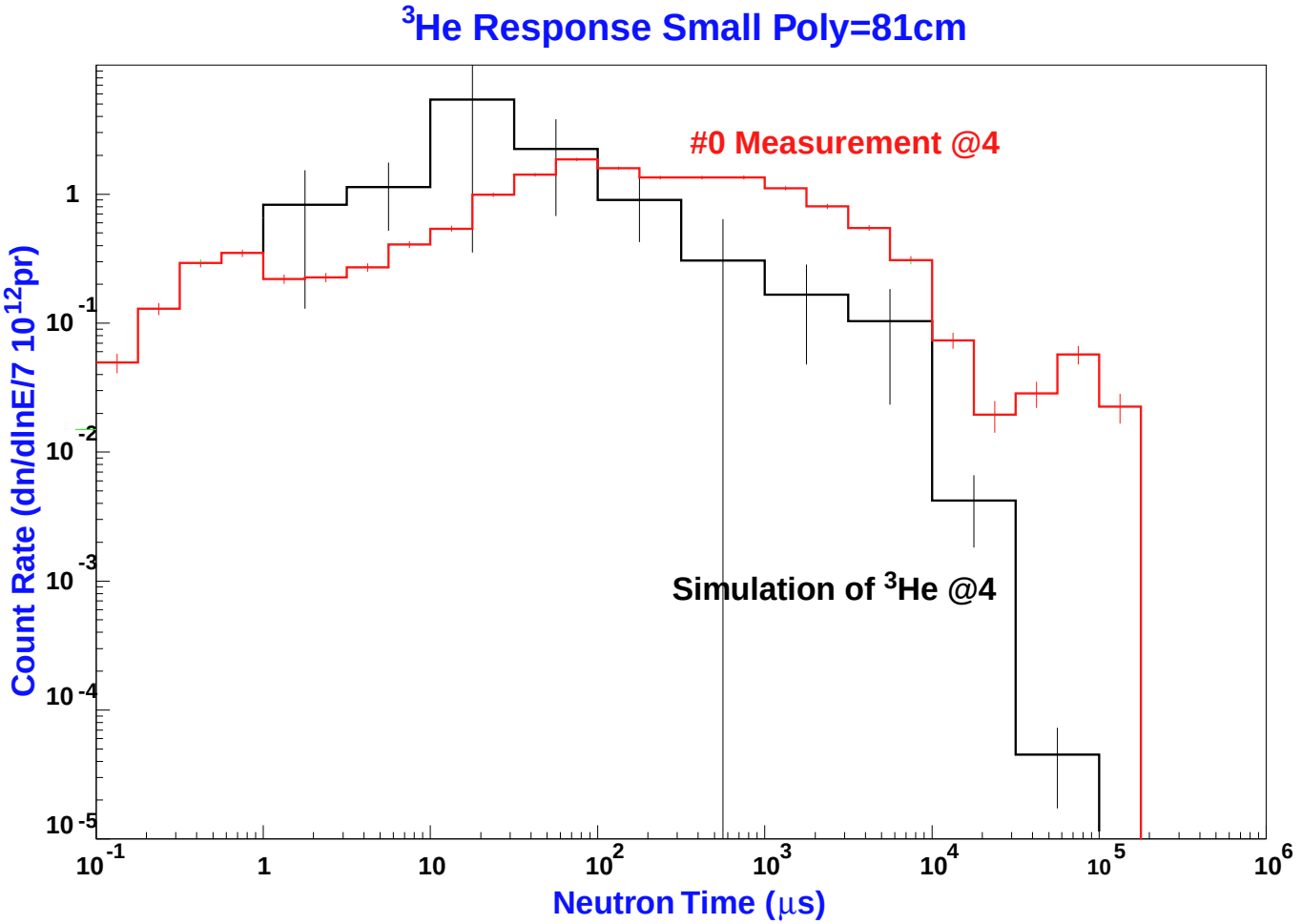

Measured (red) versus computed (black) ^{3}He + poly. 81 mm time spectra. The comparison is absolute

Different Applications

The FLUKA development, its accuracy and versatility originated to a great deal from the needs of the author experiments, and new applications arise from new code capabilities, with a continuous interplay which is always physics driven. Examples are given below.

- Neutrino physics and Cosmic Ray studies: initiated within ICARUS
  - Neutrino physics: ICARUS, CNGS, NOMAD, CHORUS
  - Cosmic Rays: First 3D ν flux simulation, Bartol, MACRO, Notre-Dame, AMS
- Accelerators and shielding : the very first FLUKA application field
  - Beam-machine interactions: CERN, NLC, LCLS
  - Radiation Protection: CERN, INFN, SLAC, Rossendorf
  - Waste Management and environment: LEP dismantling, SLAC
- Background and radiation damage in experiments: Pioneering work for ATLAS
  - all LHC experiments, NLC

Different Applications

- Dosimetry, radiobiology and therapy :
  - Dose to Commercial Flights: E.U., NASA
  - Dosimetry: INFN, ENEA, GSF, NASA
  - Radiotherapy: Already applied to real situations (Optis at PSI, Clatterbridge)
  - Dose and radiation damage to Space flights: NASA, ASI
- Calorimetry:
  - ATLAS test beams
  - ICARUS
- ADS, spallation sources (FLUKA+EA-MC, C.Rubbia et al.)
  - Energy Amplifier
  - Waste trasmutation with hybrid systems
  - Pivotal experiments on ADS (TARC, FEAT)
  - nTOF

ICARUS liquid argon imaging TPC (I)

- The LAr TPC technique is based on the fact that ionization electrons can drift over large distances (meters) in a volume of purified liquid Argon under a strong electric field. If a proper readout system is realized (i.e. a set of fine pitch wire grids) it is possible to realize a massive "electronic bubble chamber", with superb 3-D imaging.

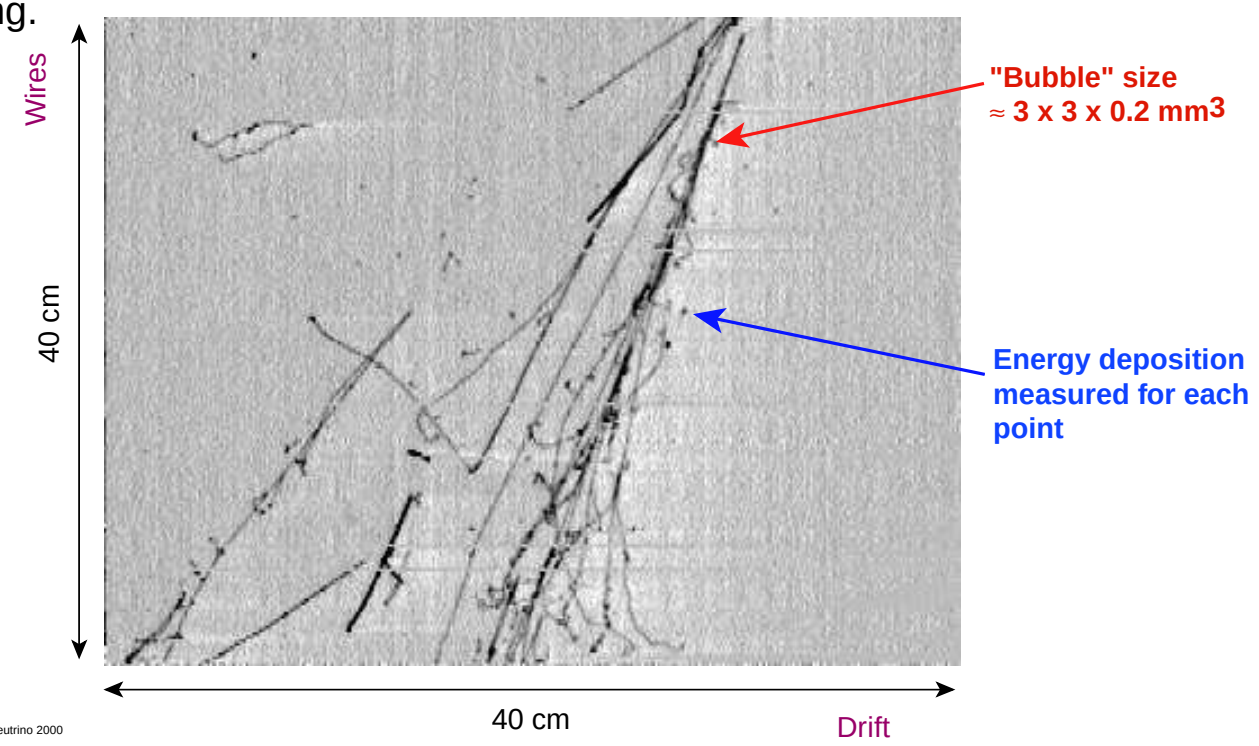

André Rubbia, ETH/Zürich, 21/6/00, Neutrino 2000

Calorimetry in imaging, fully sensitive liquid Argon

Liquid argon is a non-compensating medium. When used in a time projection chamber like ICARUS the effect is exacerbated by the relatively low electric field ($\approx$ 300–500 V/cm)

However, the medium appears as a *completely homogeneous volume with very high readout granularity*

$\Downarrow$

From the event visualisation and from the local charge deposition density, it is possible both to distinguish between electromagnetic and hadronic components of a shower and to approximately correct for the recombination effects.

Calorimetry in imaging, fully sensitive liquid Argon

Quenching correction

Let assume that each elementary cell contains only one crossing track, the recombination effect can be unfolded using the collected charge and cell width to construct the observed dQ/dx and solving the recombination expression for the "actual" dE/dx. *Despite its simplicity, the procedure is very effective in recovering most of the recombination, particularly when the Argon is doped with TMG*

Compensation correction

Let us assume that electromagnetic energy deposition can be distinguished from hadronic one, the total energy of a shower is obtained as the sum of two terms $E = w \times (Q_{em} + \alpha \times Q_{had})$, where α is the compensation factor. *For pure argon,* α *is about* 1.5 (2.8) *with and without quenching corrections respectively. The same figures for TMG-doped argon are* 1.5 *and* 2.0

ICARUS: resolutions for pions

Expected hadronic resolution for pions

Medium	Compensation	Quench corr.	Resolution
Pure argon	no	no	$27\%/\sqrt{E} \oplus 8\%$
	yes	no	$24\%/\sqrt{E} \oplus 4\%$
	no	yes	$18\%/\sqrt{E} \oplus 6\%$
	yes	yes	$16\%/\sqrt{E} \oplus 1\%$
TMG doped argon	no	no	$20\%/\sqrt{E} \oplus 6\%$
	yes	no	$16\%/\sqrt{E} \oplus 2\%$
	no	yes	$15\%/\sqrt{E} \oplus 5\%$
	yes	yes	$12\%/\sqrt{E} \oplus 0.2\%$
No quenching	no	–	$15\%/\sqrt{E} \oplus 5\%$
	yes	–	$12\%/\sqrt{E} \oplus 0.1\%$

Expected resolution in the liquid target for pions with and without TMG doping, showing the effect of the offline compensation and quench correction. For reference, the resolution that would be obtained with no recombination effects is also listed.

Neutrino interactions in PEANUT: the *NUX-FLUKA* event generator

Authors: A. Ferrari (CERN/INFN), A. Rubbia (ETH Zurich), P.R. Sala (ETH/INFN)
Features:

- Full use of all sophisticated nuclear physics of PEANUT
- Quasielastic event generator built-in
- RES and DIS: nucleon density, position and Fermi motion via PEANUT $\rightarrow$ νN interaction via *NUX* (A.Rubbia, originally developed for NOMAD), $\rightarrow$ all secondaries propagated with PEANUT. Fully integrated one in the other in a single code $\rightarrow$ "correct" account for kinematical effects on cross section due to Fermi motion and for Pauli blocking

The comparison with NOMAD data are due to A. Bueno, A. Rubbia, ETH Zurich

Neutrino quasi-elastic events

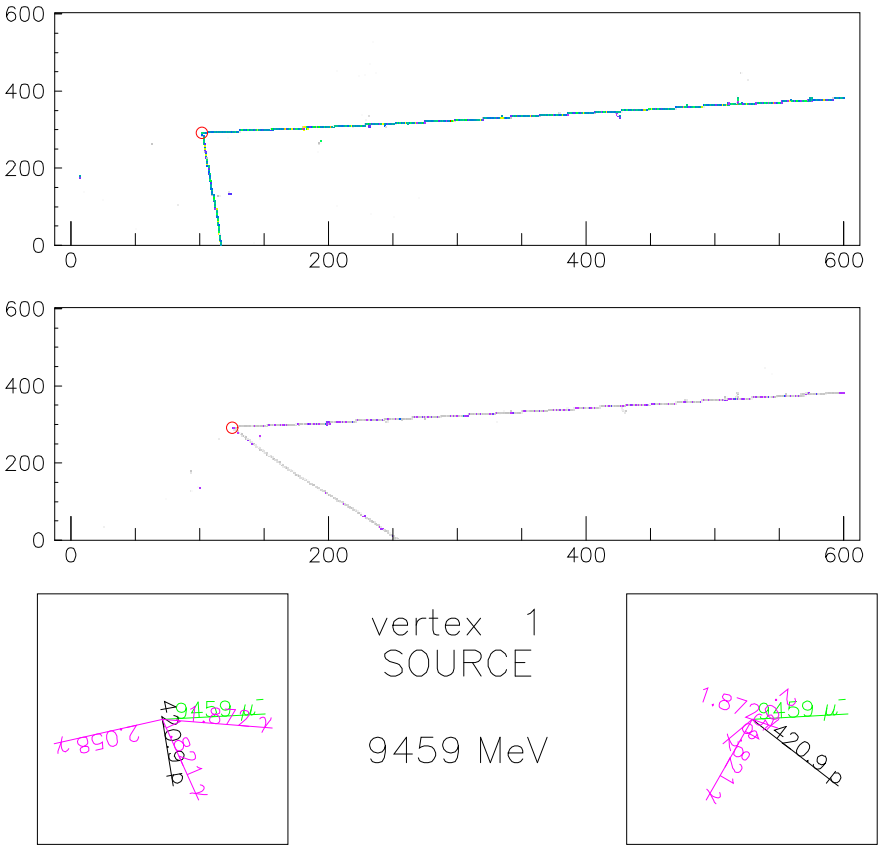

ICARUS prototype: two views in Liquid Argon, 10 GeV ν_μ CC

"Clean" event :

$$\nu_\mu \; n \rightarrow \mu^- \; p$$

$$\downarrow$$

$$\mu^- \quad \mathrm{p} \; \gamma$$

Neutrino quasi-elastic events

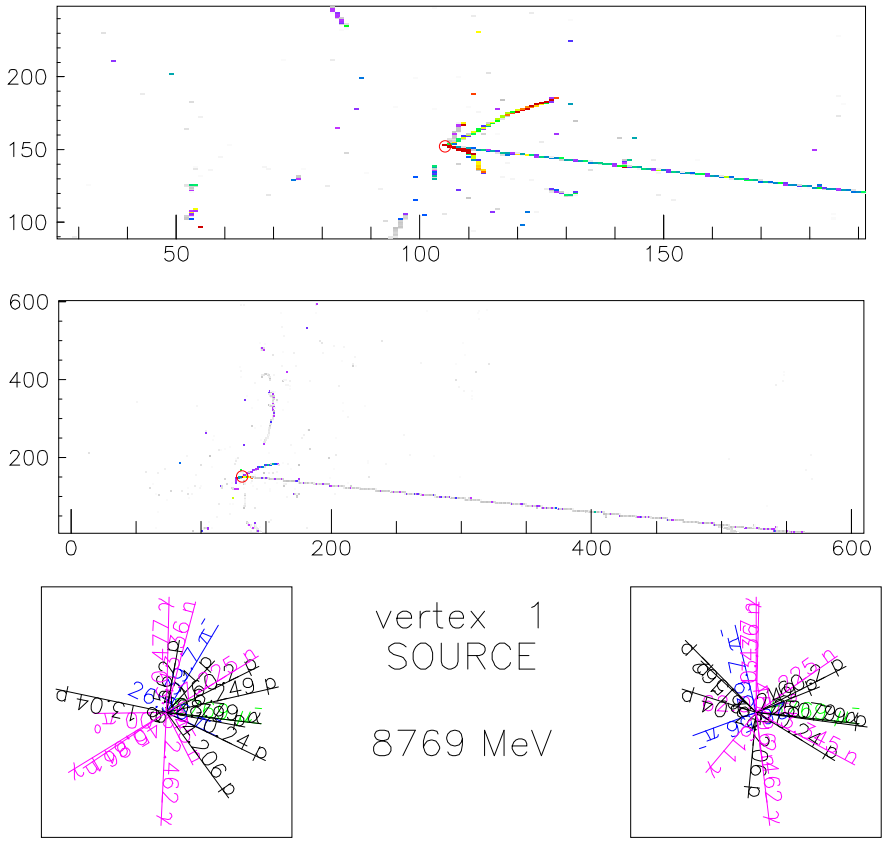

ICARUS prototype: two views in Liquid Argon, 10 GeV ν_μ CC

Complex event :

$$\nu_\mu\, n \rightarrow \mu^-\, p$$

$$\downarrow$$

1 μ^-, 8 p, 2 π^-, 1 π^0, 4 n, 1 α, 3 γ

The *NUX-FLUKA* event generator: comparison with NOMAD

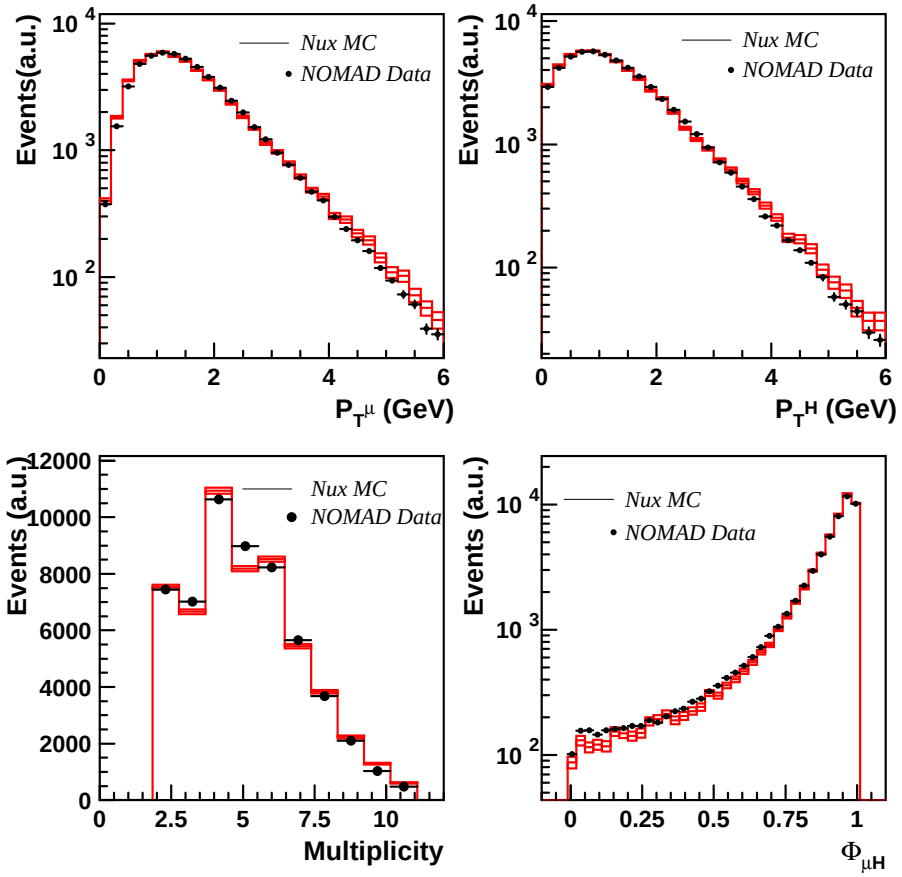

Neutron production: TARC (PLB458 (1999) 167, NIMA478 (2002) 577)

Experiment

Protons from the CERN PS , 2.5 or 3.57 GeV/c

Lead target , 334 ton , 99.99% purity

64 Instrumentation holes, different detectors to measure neutrons from thermal to MeV

Simulations: EA MC

Spallation and transport down to 19.6 MeV : FLUKA

Neutron transport and interactions, and target evolution: new code (C.Rubbia et al)

Neutron production examples: TARC (PLB458 (1999) 167)

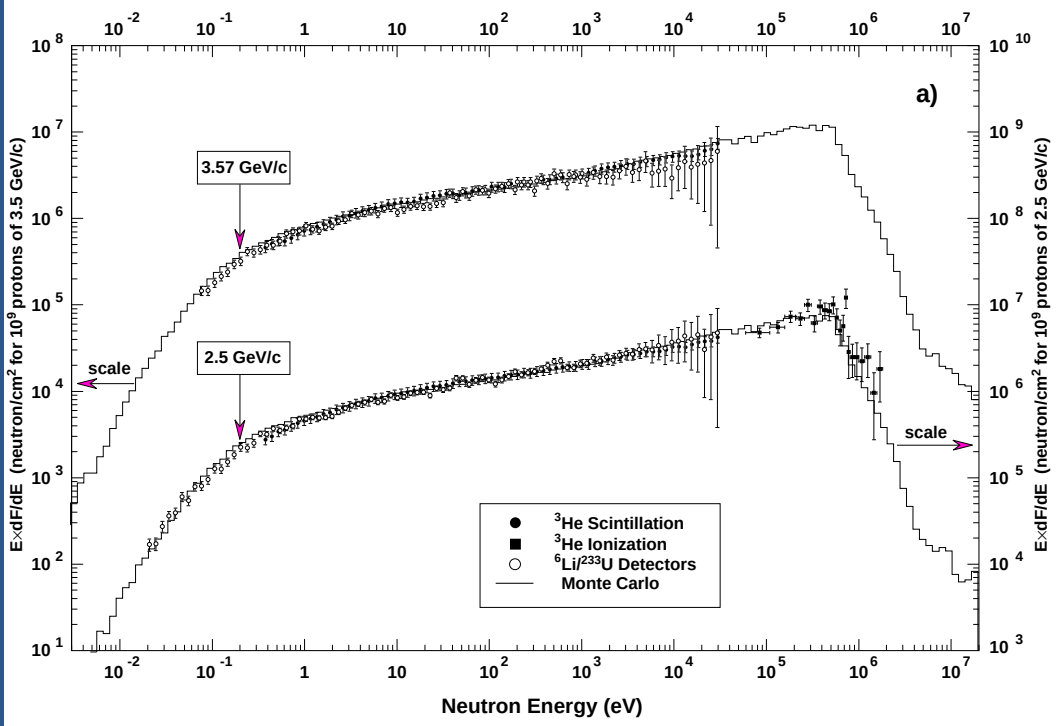

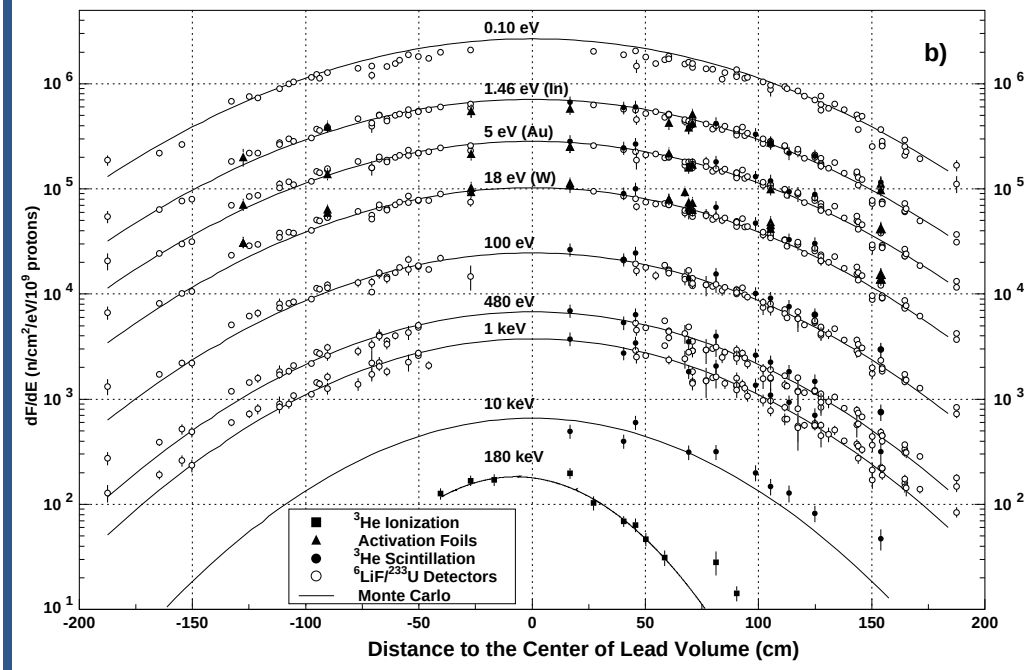

The CERN reference radiation facility – CERF

- A reference radiation facility (called CERF) for the calibration and intercomparison of dosimetric devices in high energy stray radiation fields is available at CERN since 1993, on the H6 beam line in the North Area.
- Hadron beams with momentum of either 120 or 205 GeV/c are stopped in a copper target, which can be installed in two different positions. On top and on side of these two positions, the secondary particles produced in the target are filtered by a shielding made up of either concrete or iron.
- The facility is partially supported by the European Commission in the framework of a research program for the assessment of radiation exposure at civil flight altitudes.
- The composition of the CERF field is accurately known by means both of FLUKA calculations and measurements with several instruments which nicely agree each other. Some examples of comparisons of computed vs measured data are presented in the following.

Neutron detector calibration

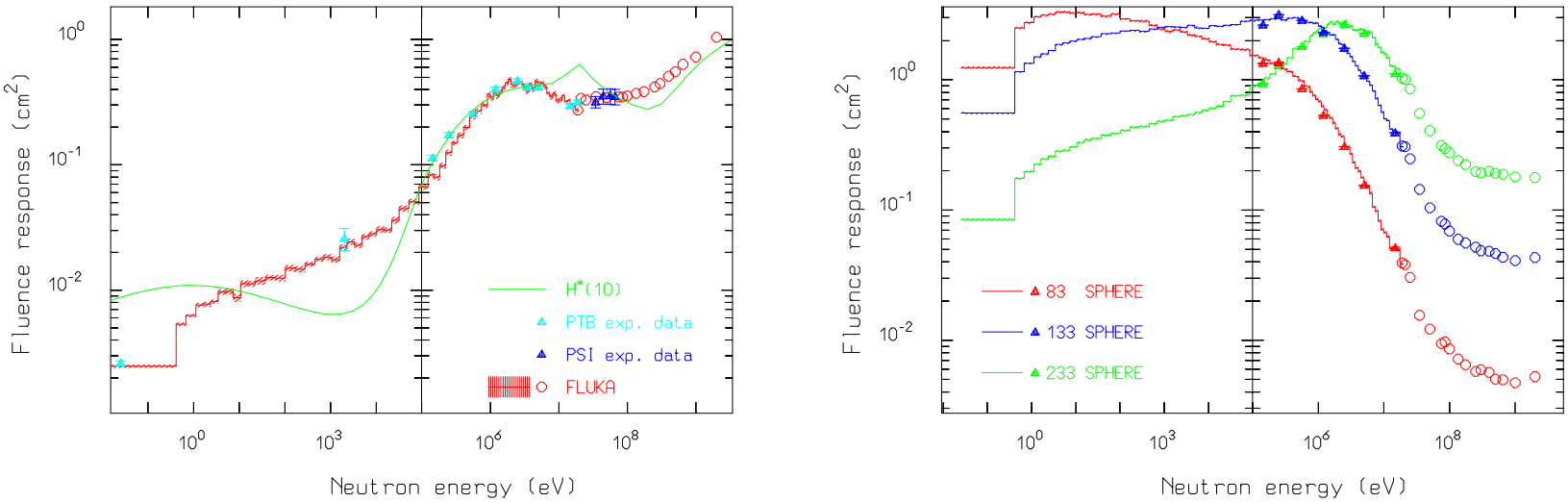

Calibration of the LINUS rem counter (left) and of three Bonner spheres (right) with monoenergetic neutron beams at PTB–Braunschweig and with semi–monoergetic neutron beams at PSI (full symbols), compared with simulations (dashed histos and open circles)

CERF: layout

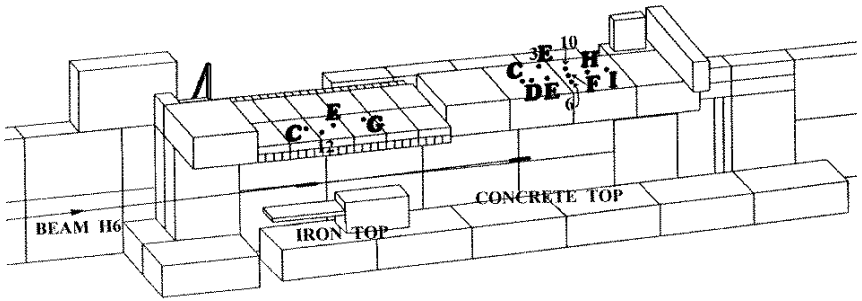

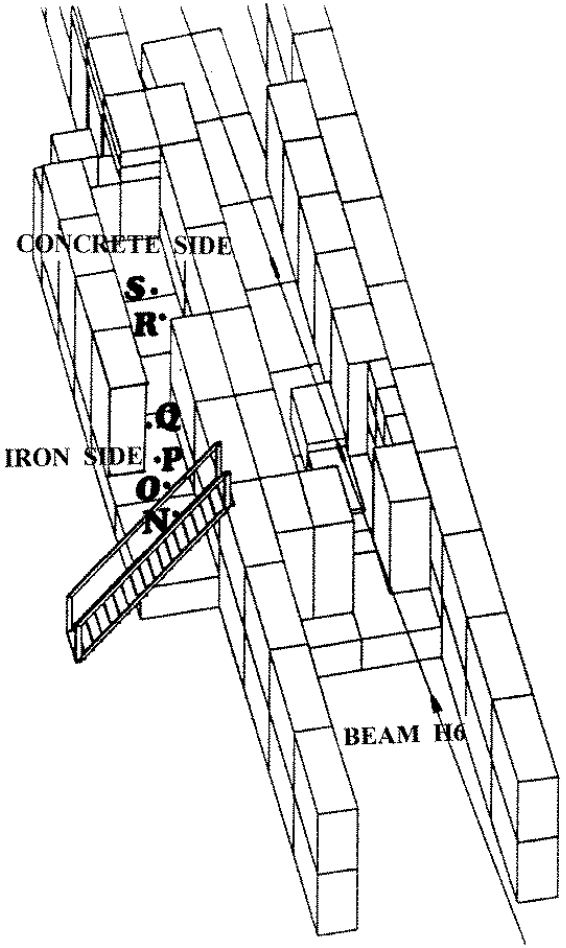

Top (left, one side removed) and side (right, roof removed) views of the CERF facility with the measuring positions.

CERF: some results

	experimental		FLUKA		experimental		FLUKA	
	cts/PIC	%	cts/PIC	%	cts/PIC	%	cts/PIC	%
	CONCRETE TOP "E"				IRON TOP "C"			
LINUS rem counter*	0.364	0.36	0.409	2.2	1.78	0.30	1.68	2.1
SNOOPY rem counter*	0.200	0.59	0.207	3.3	1.83	0.75	1.71	2.0
233 sphere	0.788	0.33	0.899	3.7	9.28	0.28	9.23	2.0
178 sphere	0.989	0.36	1.01	3.4	16.1	0.24	16.9	1.9
133 sphere	1.02	0.30	0.981	3.2	19.2	0.19	21.2	1.9
108 sphere	0.942	0.35	0.883	3.1	17.7	0.20	19.2	1.9
83 sphere	0.704	0.30	0.717	3.1	11.2	0.26	12.1	1.9

Comparison between the FLUKA predictions and the experimental response of the various detectors in stray radiation fields at CERN [6]. The percent statistical uncertainty (%) is indicated.

[6] C.Birattari et al., Rad.Prot.Dos.**76** (1998) 135

The OPTIS beam at PSI

Context : PSI therapy unit : 72 MeV proton beam, fully-modulated

Goal: Full understanding of its physical and radiobiological features

Emphasis: relationship between dosimetrical quantities and biological effects

Assumption: clustered DNA damage is an estimator for cell inactivation

Solution :Combined physical-biophysical simulation of the OPTIS beam

The input data used in the simulation were fixed a priori on the basis of informations provided by PSI.

No free parameter was introduced and no a posteriori fit to experimental data was performed.

The results were directly compared with the measurements of the physical dose and with experimental data on cell survival [7].

[7] M. Biaggi et al., NIMB **159** (1999) 89

The OPTIS beam at PSI II

Simulation approach:

- Full simulation of all beam line elements including the rotating beam shapers used for generating the Spread Out Bragg Peak (SOBP) and the actual beam emittance (technical part)
- Simulation of primary and secondary radiation fields associated with the proton beam and their interactions with the phantom tissue (physical part)
- "Weighting" of each track segment with the particle/energy dependent probability of inducing complex DNA lesions [8] (CL) as obtained from track structure simulations of DNA damage using the MOCA code [9] for the time being and the PARTRAC code [10] in the future (biophysical part)

[8] Operatively defined as two or more single-strand breaks on each DNA strand within 30 base pairs
[9] A. Ottolenghi, M. Merzagora, H.G. Paretzke, Radiat. Environ. Biophysics, **36**, (1997) 97
[10] W. Friedland et al., Radiat. Environ Biophys, **38** (1999) 39

Absorbed Dose and its components

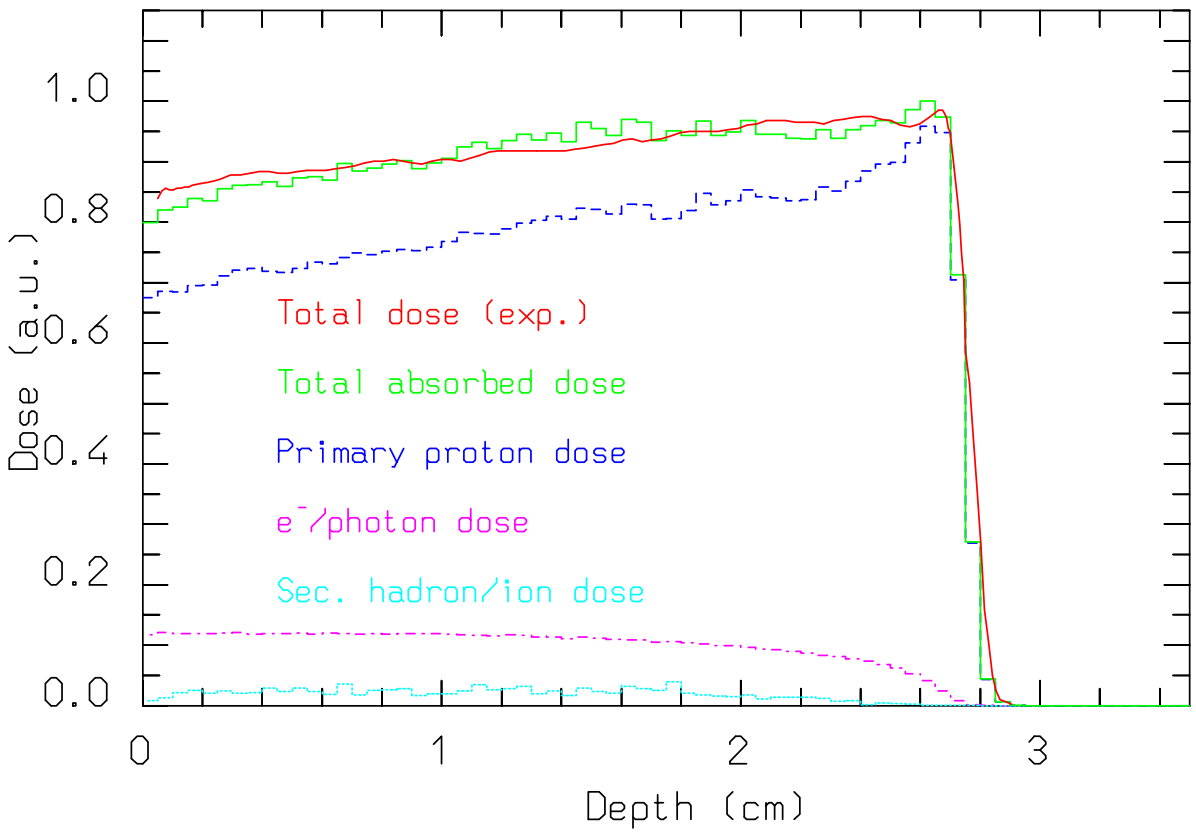

Measured (red) and calculated (green) depth-dose curves in perspex of 72 MeV modulated proton beam. The calculated dose is split into the contribution of primary protons (blue), electrons and photons (purple) and secondary hadrons including ions (cyan).

The Clustered DNA damage

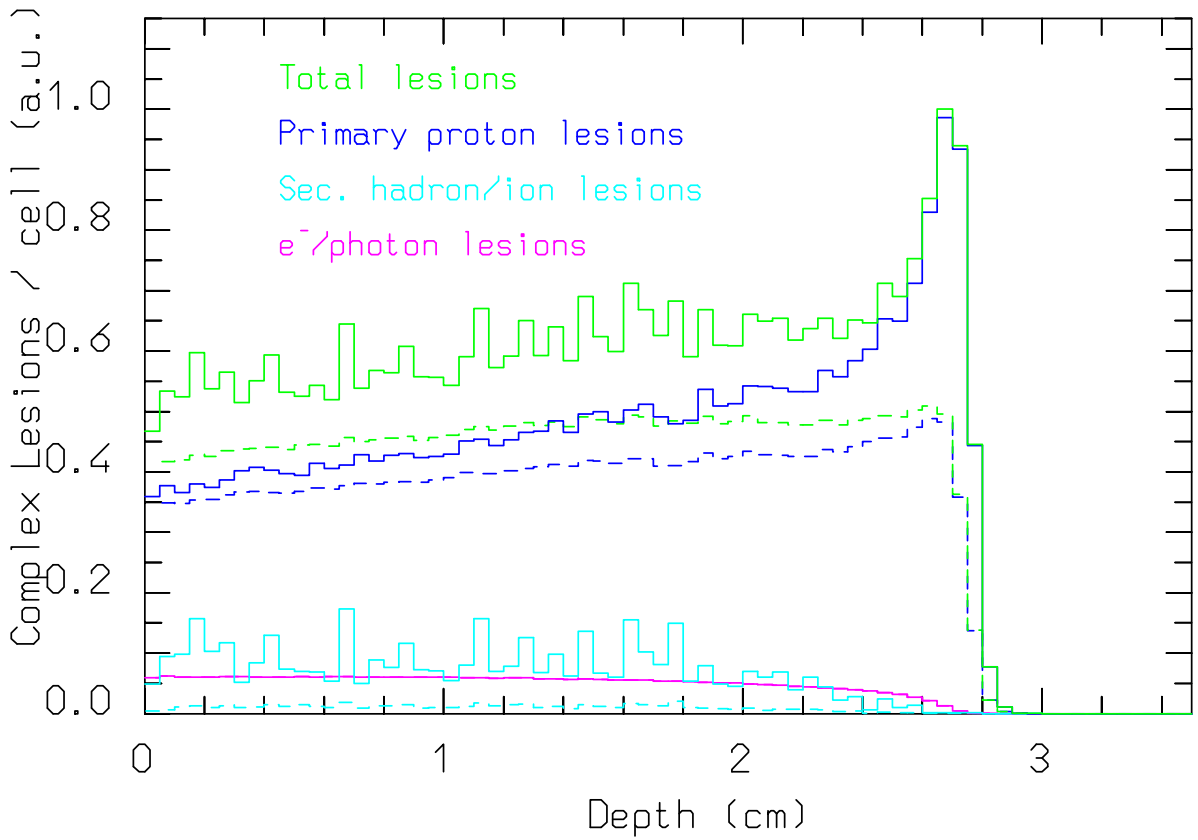

Calculated relative number of complex lesions per cell. For each component the upper (full) line represents the yield of complex lesions/cell, whereas the lower curve (dashed) represents the yield that one would obtain assuming an effectiveness equal to that of x-rays.

OPTIS: relative effectivness of protons wrt x-rays

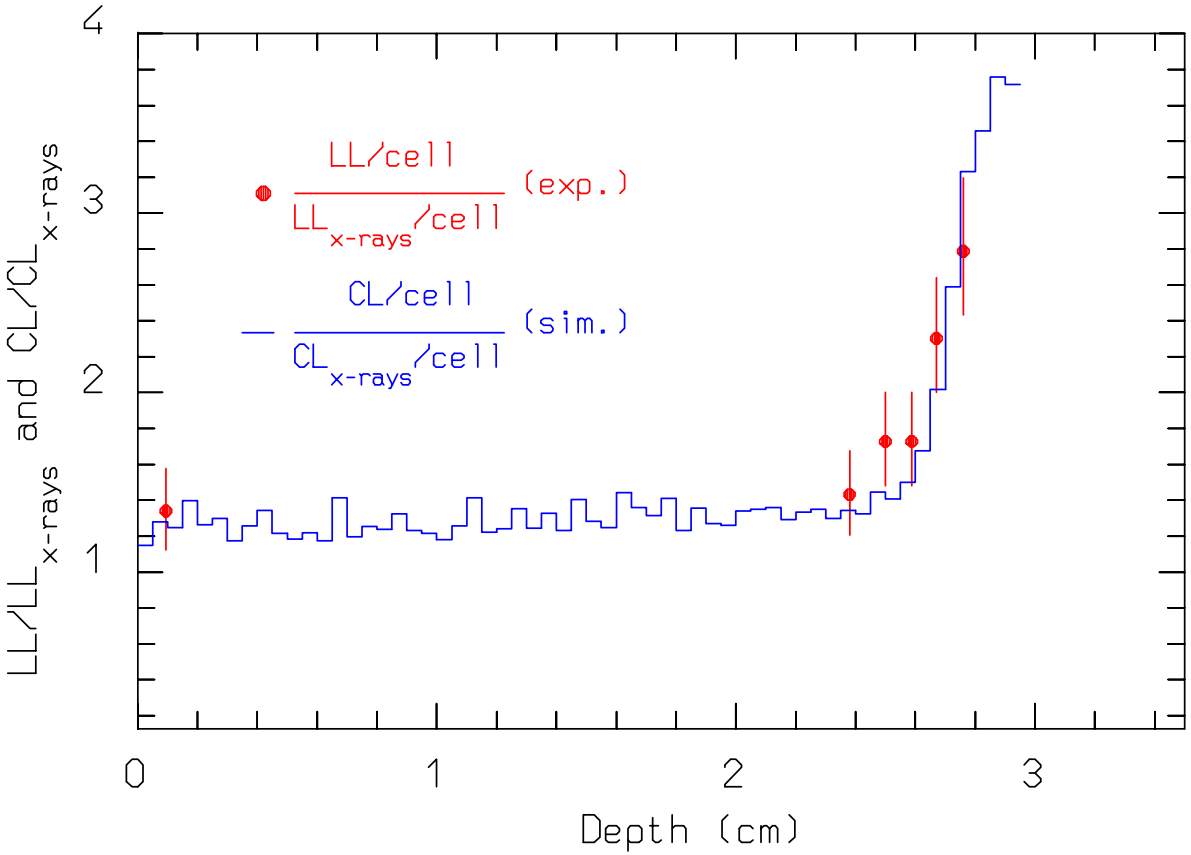

Simulation (blue curve): ratio between DNA complex lesions/cell (CL/cell) after irradiation with 2 Gy in the 72 MeV proton beam and with x-rays. Experimental data (red points): ratio between lethal lesions/cell (LL/cell) in V79 cells after irradiation with 2 Gy in the 72 MeV proton beam and with x-rays.

A Human Phantom for dosimetric calculations

For each organ:

- Spatial distribution of fluences of particles of different types and energies
- Estimation of radiation effects

Already in use for:

- Calculations of fluence-to-ambient dose equivalent and fluence to effective dose conversion factors for γ,$e^{+/-}$,p,n,π and μ up to very high energies (10 TeV).

Possible future applications:

- Estimation of protection properties of different shield designs in particular field conditions (aircrafts, spacecrafts)

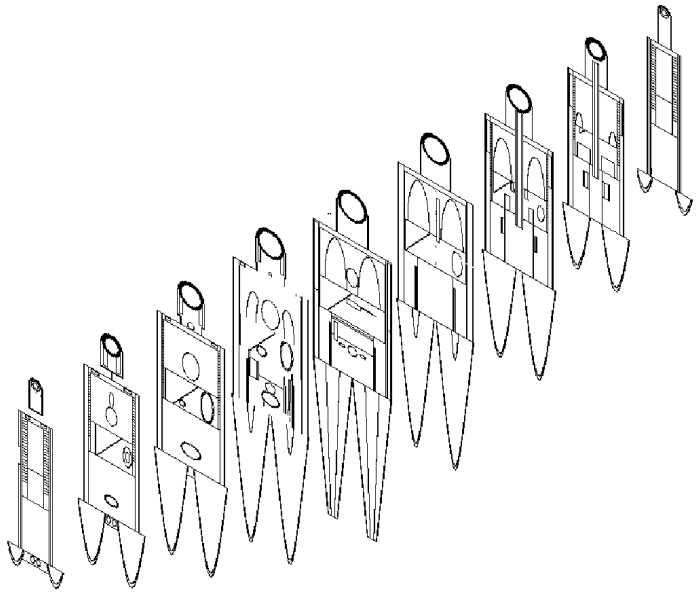

Sections of the antrophormic phantom used for conversion coefficient calculations

Cosmic Ray Showers

Motivation :Atmospheric neutrino fluxes (Astr. Phys. **12**, 315 (2000))

Benchmarks and Applications: Muon and hadron fluxes, Aircraft exposure

Ingredients

- Primary ray spectrum and composition, solar modulation
- Atmosphere description (3 Dimensional)
- Particle transport and decay (3-D)
- Hadronic interactions
- Geomagnetic effects

Up to now, primary nuclei are splitted into nucleons before interacting

3D effects in ν angular distributions

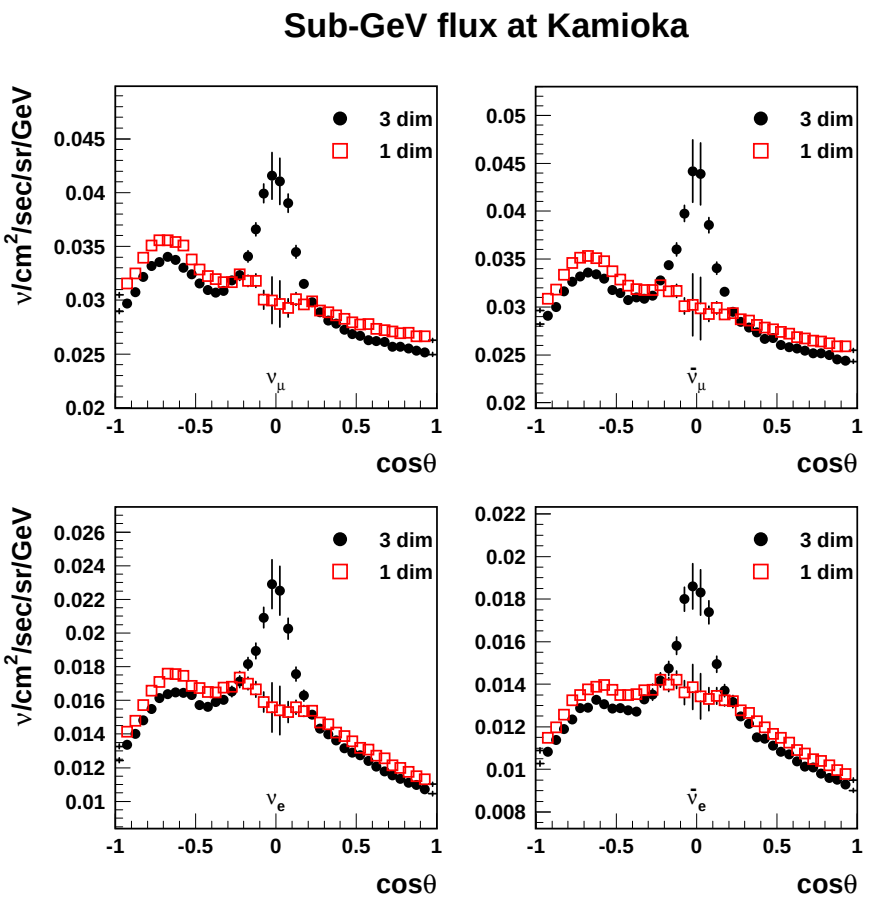

Hadron/muon fluxes in the atmosphere: μ^- Astropart. Phys. 17 477 (2002)

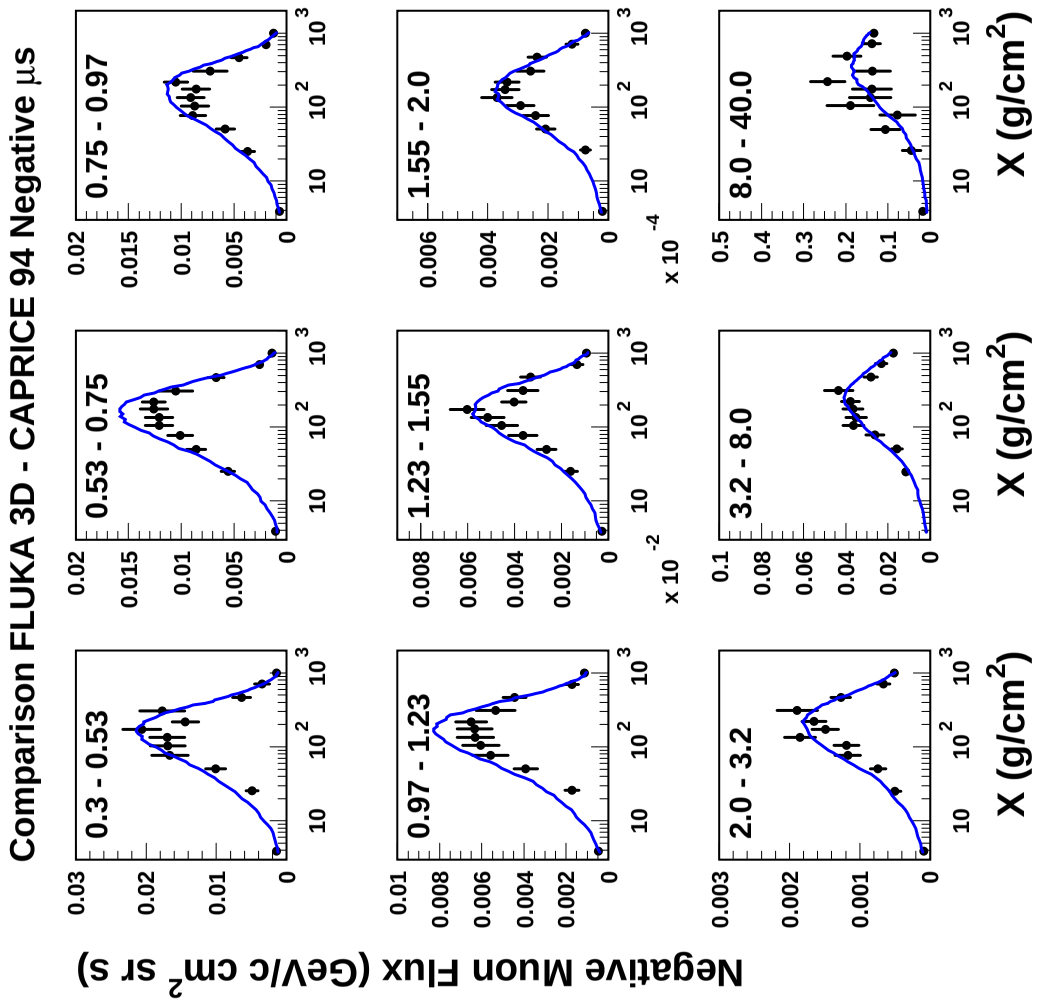

Hadron/muon fluxes in the atmosphere: μ^+ Astropart. Phys. 17 477 (2002)

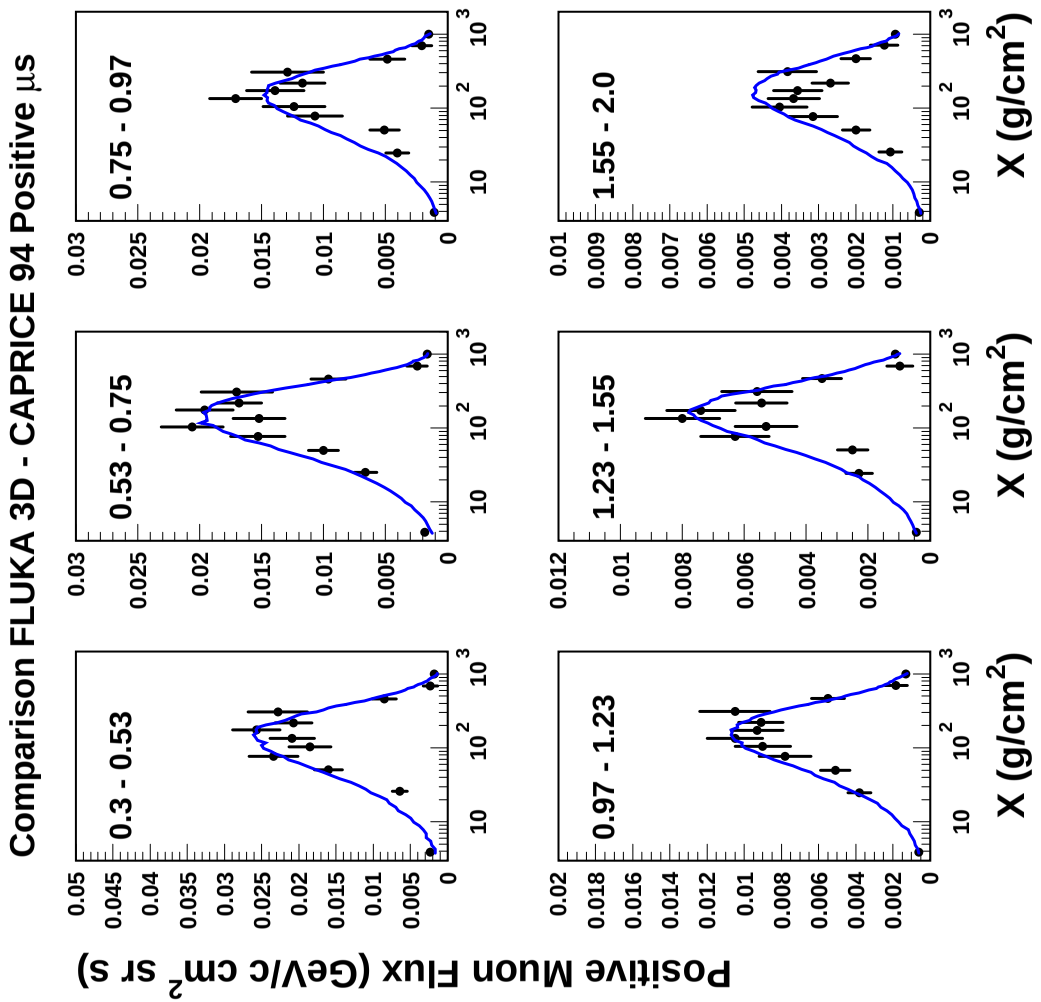

AMS (astro-ph/0111111)

Protons and leptons below the geomagnetic cutoff have been measured by the AMS experiment at altitudes 370-390 Km, latitude $\pm 51.7^o$.

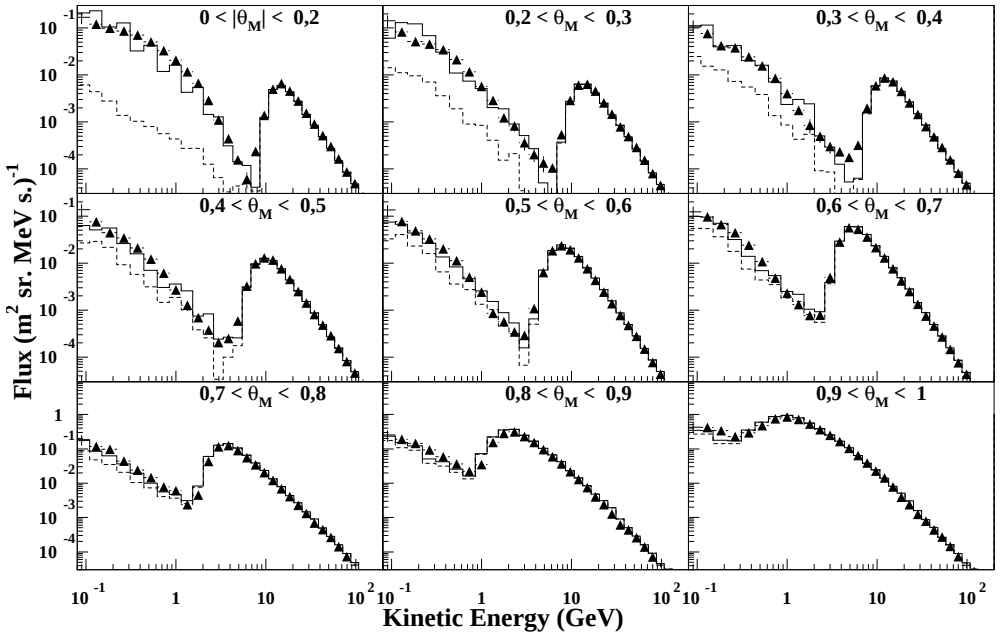

Downgoing proton flux, simulation(solid line) AMS data (triangles). Θ_M is the geomagnetic latitude in radians.

AMS

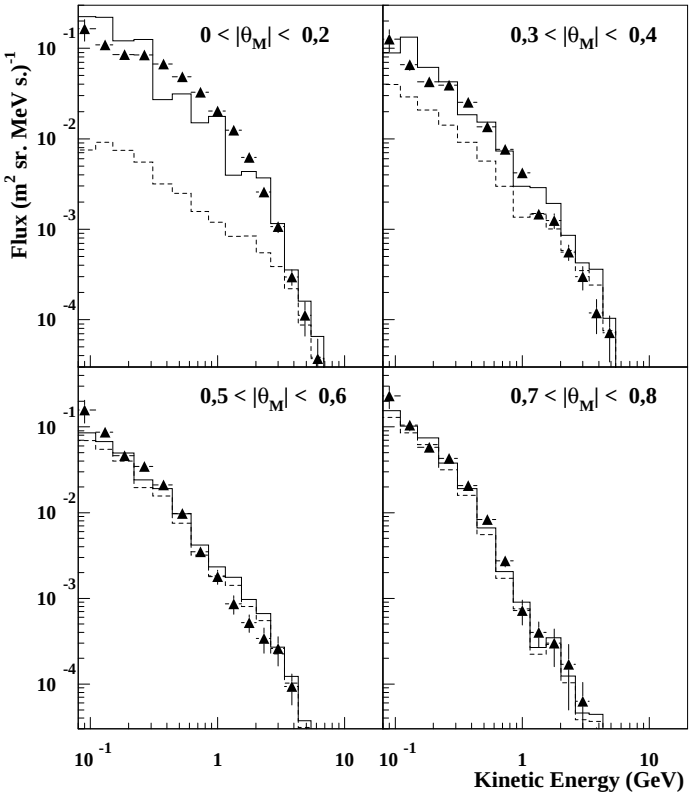

Upgoing Protons

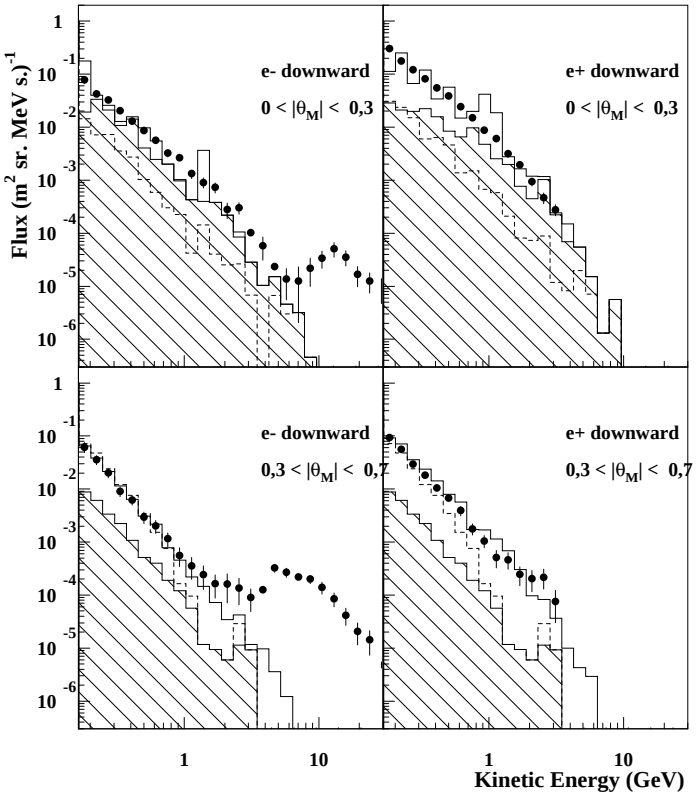

Downgoing $e^{\pm}$

Radiation Field at Aircraft altitudes

S. Roesler, W. Heinrich, H. Schraube, SLAC-PUB-8968

Courtesy of S. Roesler

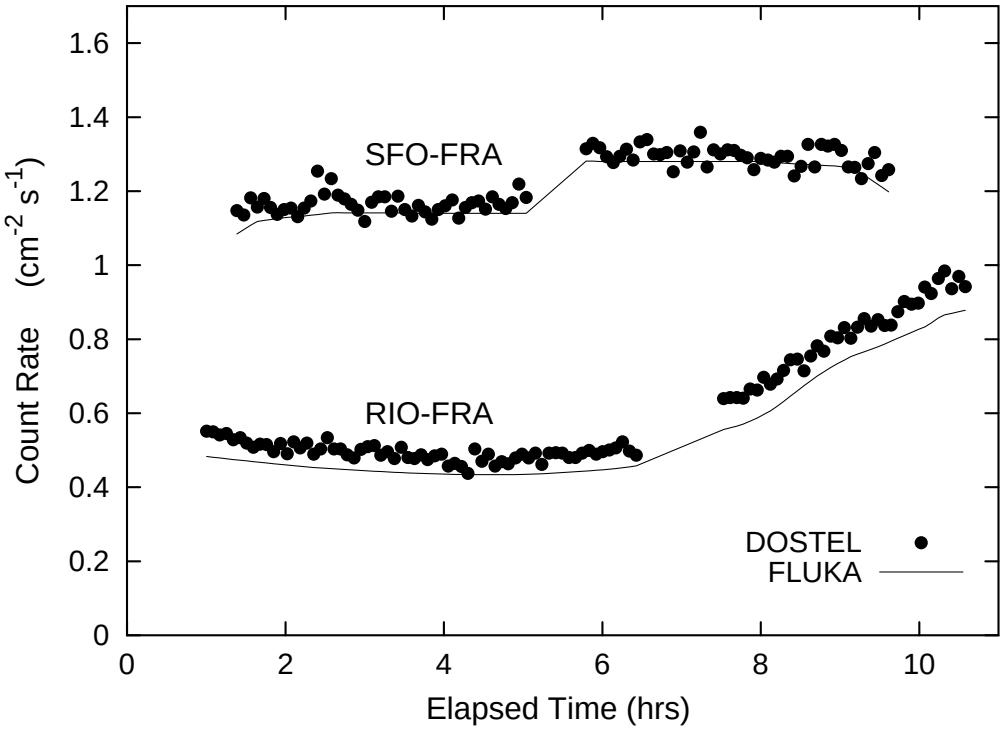

Ionizing radiation as a function of elapsed time after take-off, on commercial flights from San Francisco and Rio de Janeiro to Frankfurt

Data from R. Beaujean, J. Kopp and G. Reitz, Rad. Prot. Dosim 85,287 (1999)

Radiation Field at Aircraft altitudes

S. Roesler, W. Heinrich, H. Schraube, SLAC-PUB-8968

Courtesy of S. Roesler

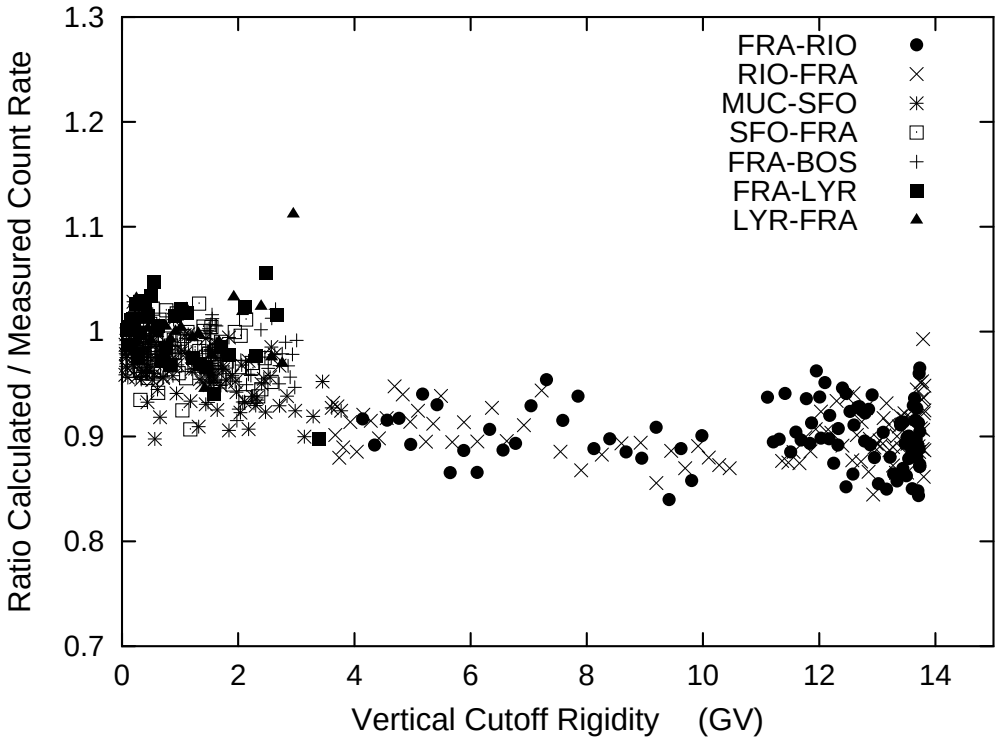

Ionizing radiation as function of vertical rigidity cutoff on commercial flights.

Data from R. Beaujean, J. Kopp and G. Reitz, Rad. Prot. Dosim 85,287 (1999)

Neutron Spectra at Ground level

S. Roesler, W. Heinrich, H. Schraube, SLAC-PUB-8968 Courtesy of S. Roesler

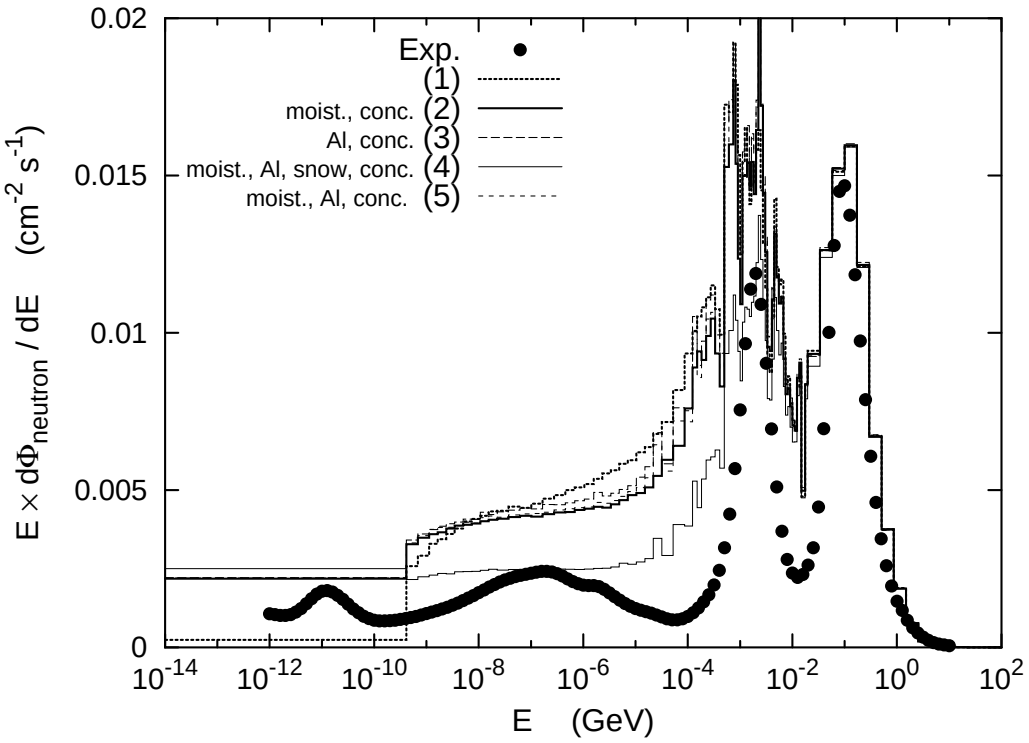

Ground-level neutron spectra at the Schneefernerhaus (2660 m a.s.l). Calculations with different humidity and soil

Data from H. Schraube et al., Rad. Prot. Dosim. 86,309(1999) and Rad. Prot. Dosim. 70,405 (1997)

Doses to commercial flight crews (Rad. Prot. Dosim. 93 101 and 96 219 (2001))

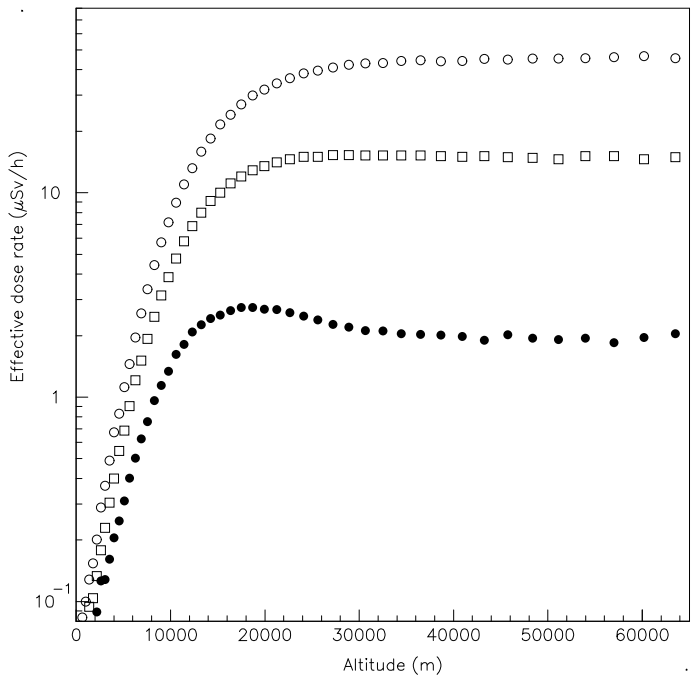

Calculated effective dose as a function of altitude for a vertical rigidity cutoff of 0.4 GV at solar minimum (open circles), and at solar maximum (open squares), and for a cutoff of 17.6 GV (black circles)

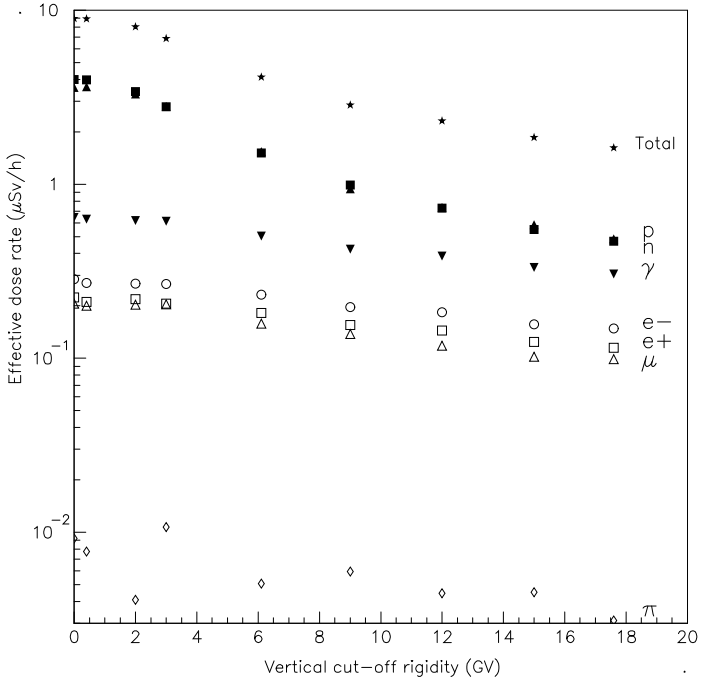

Contributions of various radiation components to the effective dose rate as a function of the vertical cut-off rigidity at solar minimum, and for an altitude of 10580 m

A. Ferrari, M. Pelliccioni and T. Rancati , Rad. Prot. Dos. 2001

A comparison of calculated ambient dose equivalent rates with in−flight measurements for different altitudes and geomagnetic latitudes (μSv/h).

B_m (°)	Vertical cut−off (GV)	FL 310 (9450 m)	FL 330 (10060 m)	FL 350 (10670 m)	FL 370 (11280 m)	FL 390 (11890 m)
−25.98	6.1	2.4 2.7	2.7 3.0	3.1 3.5	3.4 3.8	3.7 4.1
− 22.43	12.0	2.2 1.6	2.5 1.8	2.8 2.0	3.2 2.4	3.5 2.5
− 9.42	12.0	1.7 1.6	1.9 1.8	2.3 2.0	2.6 2.4	2.9 2.5
− 0.18	17.6	1.5 1.1	1.8 1.3	2.0 1.4	2.2 1.5	2.5 1.6
4.18	15.0	1.5 1.3	1.7 1.5	1.8 1.7	2.1 1.9	2.4 2.0
11.27	15.0	1.4 1.3	1.7 1.5	1.7 1.7	1.9 1.9	2.3 2.0
15.23	15.0	1.5 1.3	1.7 1.5	1.9 1.7	1.9 1.9	2.3 2.0
17.53	15.0	1.5 1.3	1.6 1.5	2.0 1.7	2.0 1.9	2.3 2.0
29.67	9.0	2.0 2.0	2.4 2.2	2.3 2.5	2.5 2.8	3.2 3.0
33.40	9.0	2.2 2.0	2.6 2.2	2.7 2.5	2.7 2.8	3.9 3.0
33.49	9.0	2.2 2.0	2.6 2.2	2.7 2.5	2.7 2.8	3.9 3.0
34.64	6.1	2.6 2.7	2.7 3.0	2.7 3.5	2.7 3.8	4.0 4.1
45.57	3.0	3.8 4.4	4.2 4.9	4.1 5.6	5.3 6.5	6.7 7.2
65.49	0.4	4.5 5.5	5.4 6.4	6.2 7.4	7.3 8.5	8.2 9.5

Differences < 20 % for 78% of data, <34 % for all

Data (upper lines) : U.J. Schrewe, NIM A422, 621 (1999)

The TIARA neutron propagation experiment

- Source term: neutron spectra generated by 43 and 68 MeV protons on a ^{7}Li target, carefully measured with TOF tecniques
  Quasi-monoenergetic neutrons of **40 MeV** and **65 MeV**
- Attenuation of the neutron beam at different depths in concrete and iron shields, both on axis and off-axis (*critical for elastic scattering!!*)
- Emerging neutron spectra measured with liquid scintillator detectors (the high energy component) and Bonner spheres (the low energy component)

H. Nakashima et al. Nucl. Sci. Eng. **124** (1996) and N. Nakao et al. Nucl. Sci. Eng. **124** (1996) 228

The TIARA exp.: FLUKA vs exp. data (concrete on axis)

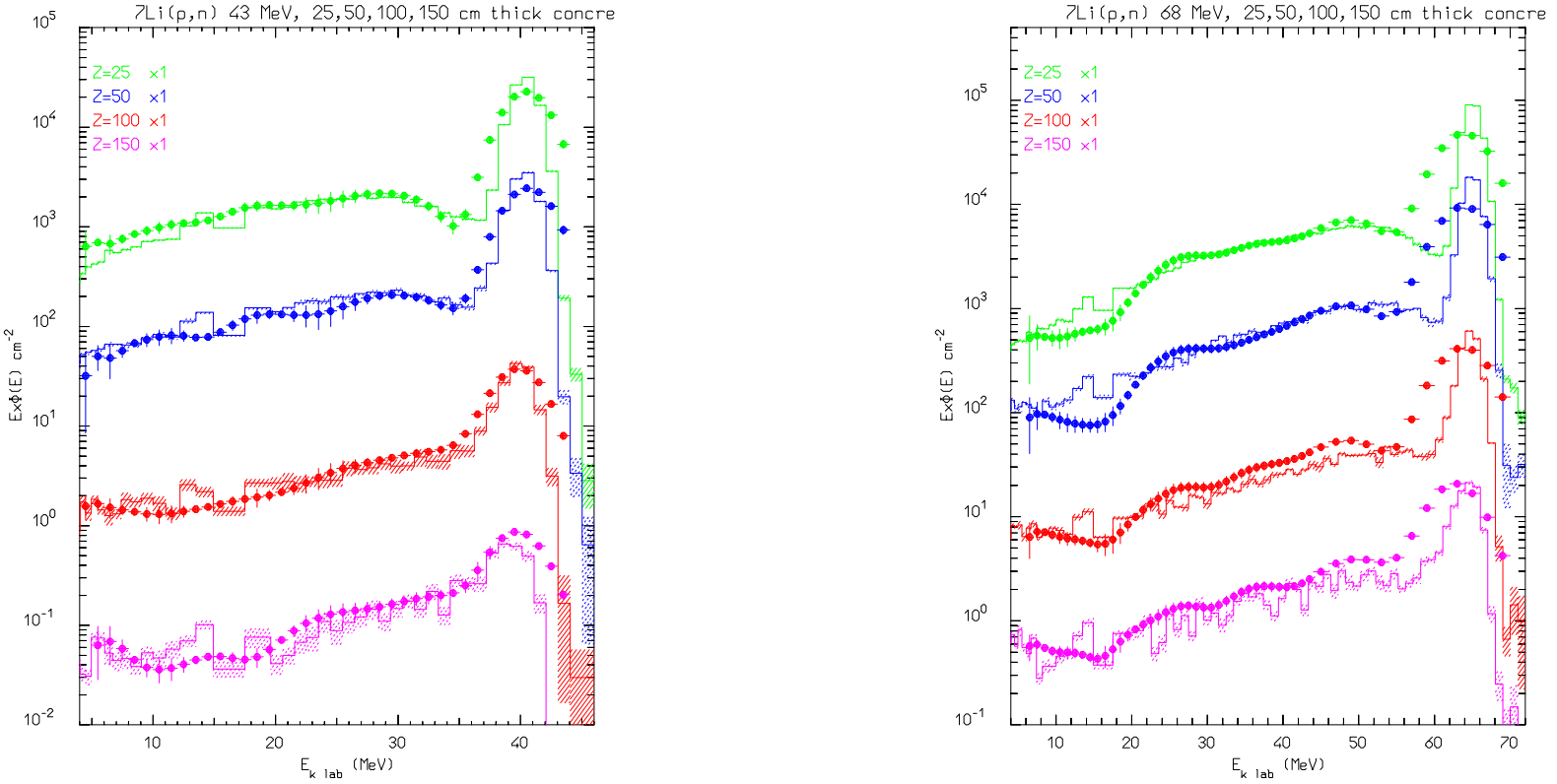

Comparison of simulated (dashed histogram) and measured (symbols) neutron spectra after different concrete thicknesses (from 25 to 150 cm), on axis. The neutrons are generated by ^{7}Li(p,n) at 43 (left) and 68 MeV (right)

The TIARA exp.: FLUKA vs exp. data (iron on axis)

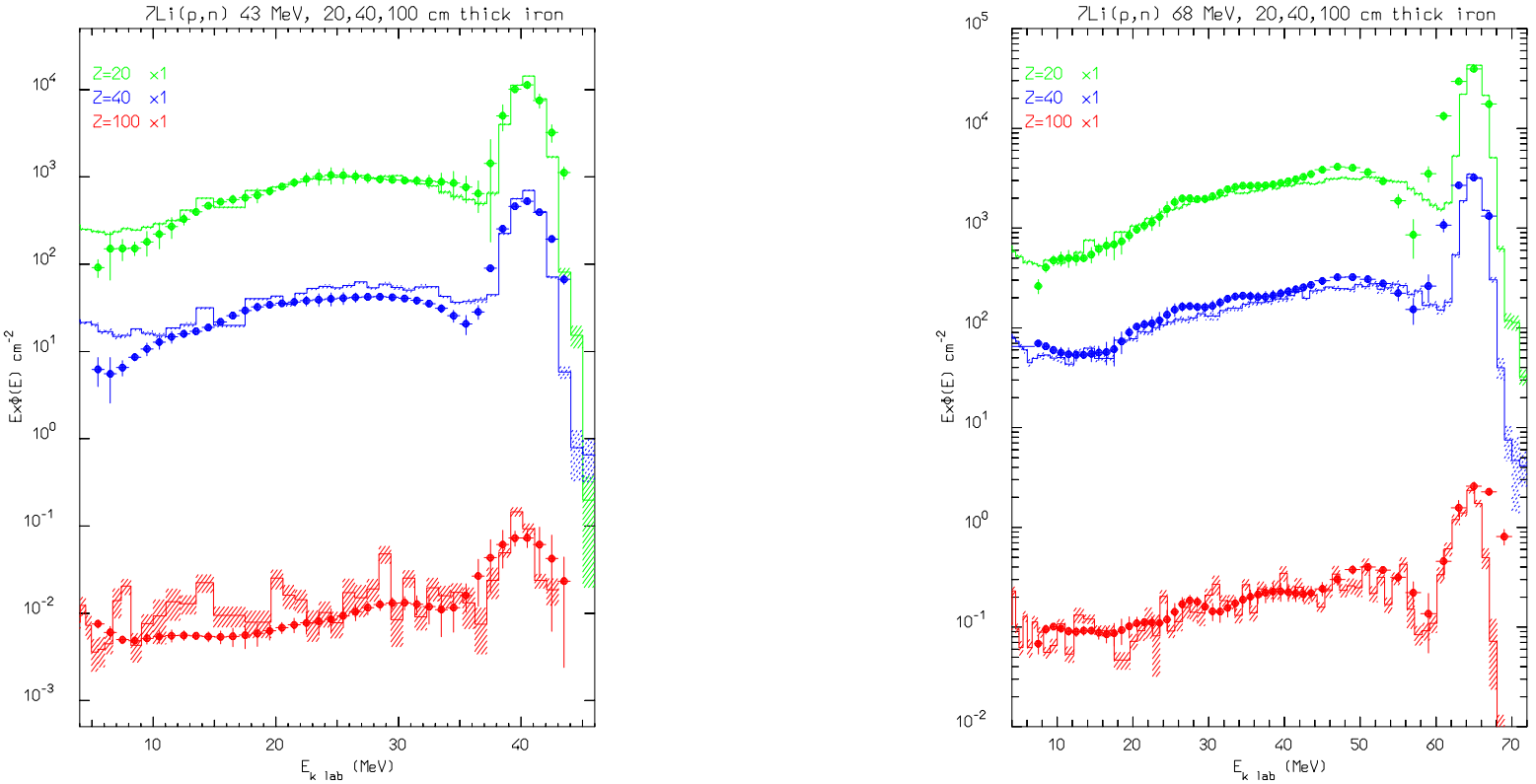

Comparison of simulated (dashed histogram) and measured (symbols) neutron spectra after different iron thicknesses (from 20 to 100 cm), on axis. The neutrons are generated by ^{7}Li(p,n) at 43 (left) and 68 MeV (right)

The TIARA exp.: FLUKA vs exp. data (concrete off axis)

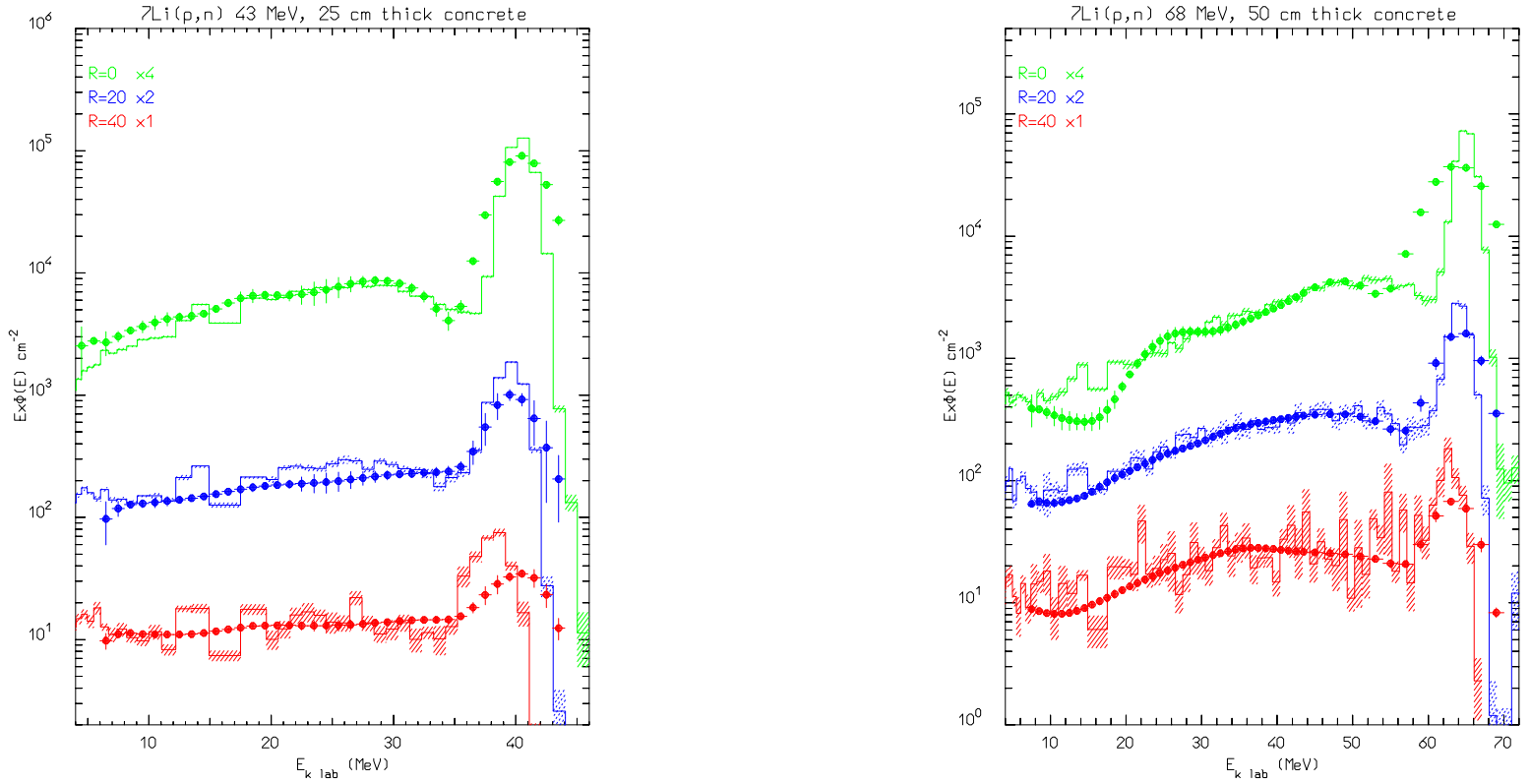

Comparison of simulated (dashed histogram) and measured (symbols) neutron spectra off axis (from 0 to 40 cm) after 25 (left) and 50 cm thick concrete shields. The neutrons are generated by ^{7}Li(p,n) at 43 (left) and 68 MeV (right)

The TIARA exp.: FLUKA vs exp. data (iron off axis)

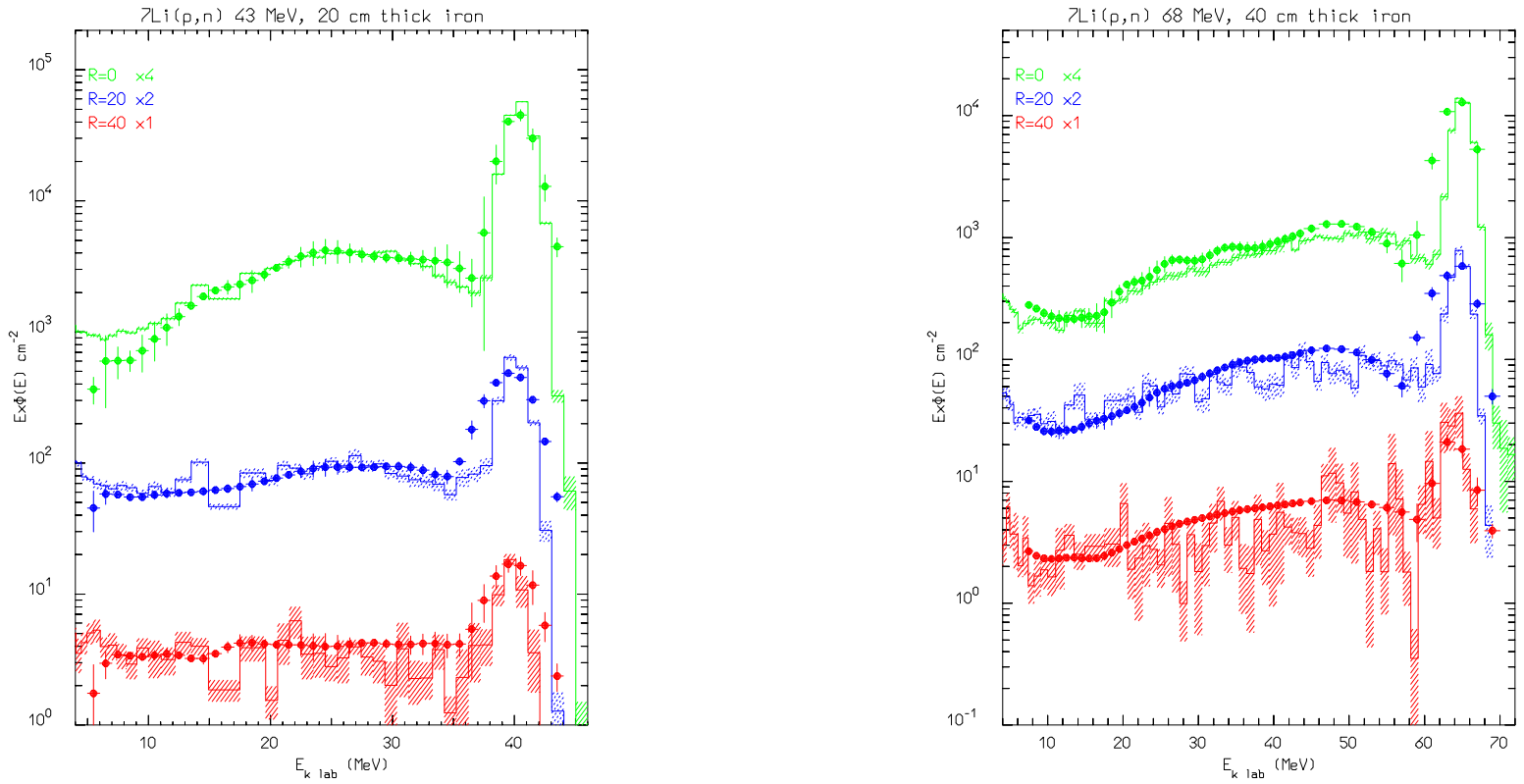

Comparison of simulated (dashed histogram) and measured (symbols) neutron spectra off axis (from 0 to 40 cm) after 20 (left) and 40 cm thick iron shields. The neutrons are generated by ^{7}Li(p,n) at 43 (left) and 68 MeV (right)

ATLAS combined calorimeter test beam

Layout of the experimental set-up (NIM A387,333(1997), NIM A449,461 (2000))

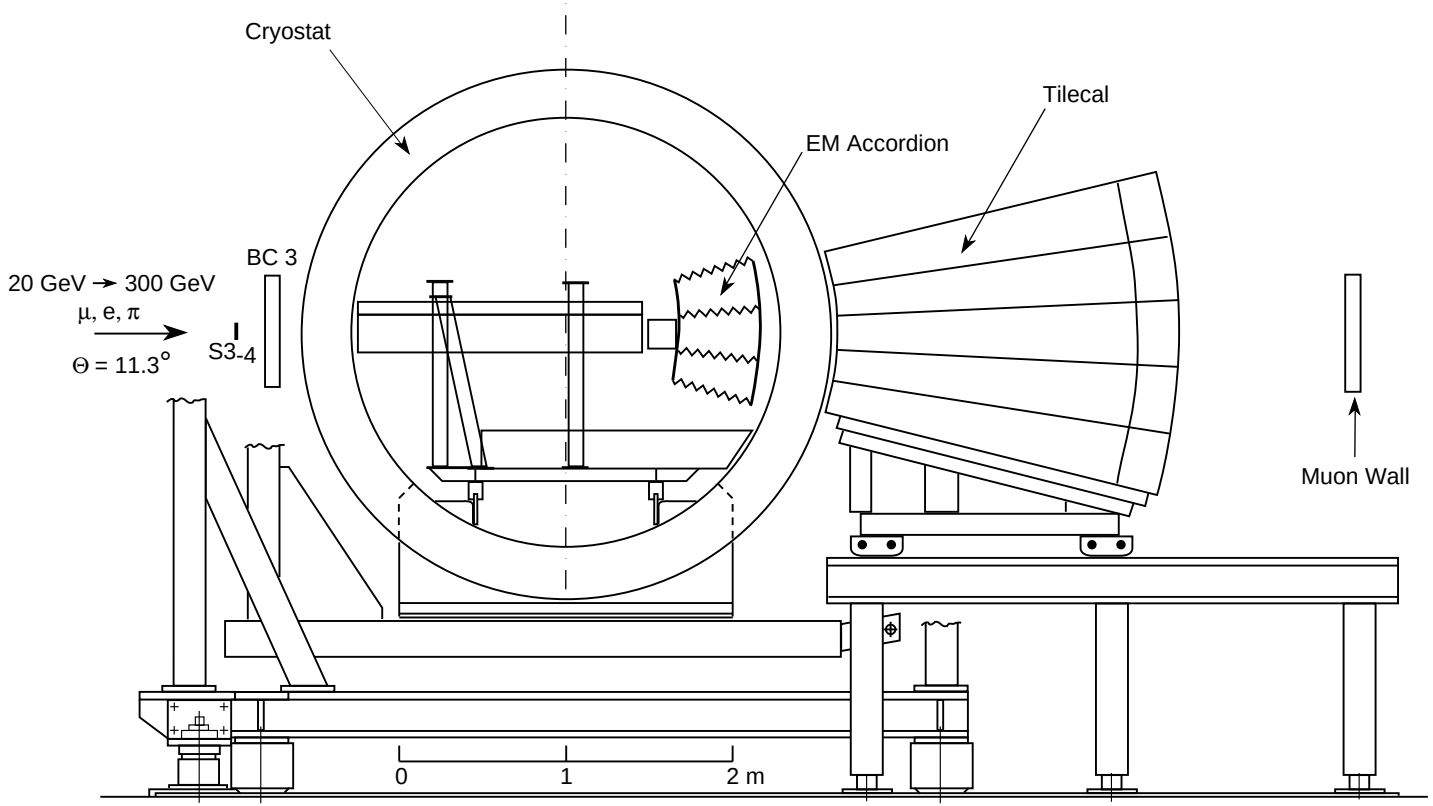

LAr electromagnetic calorimeter

Detail of the accordeon structure

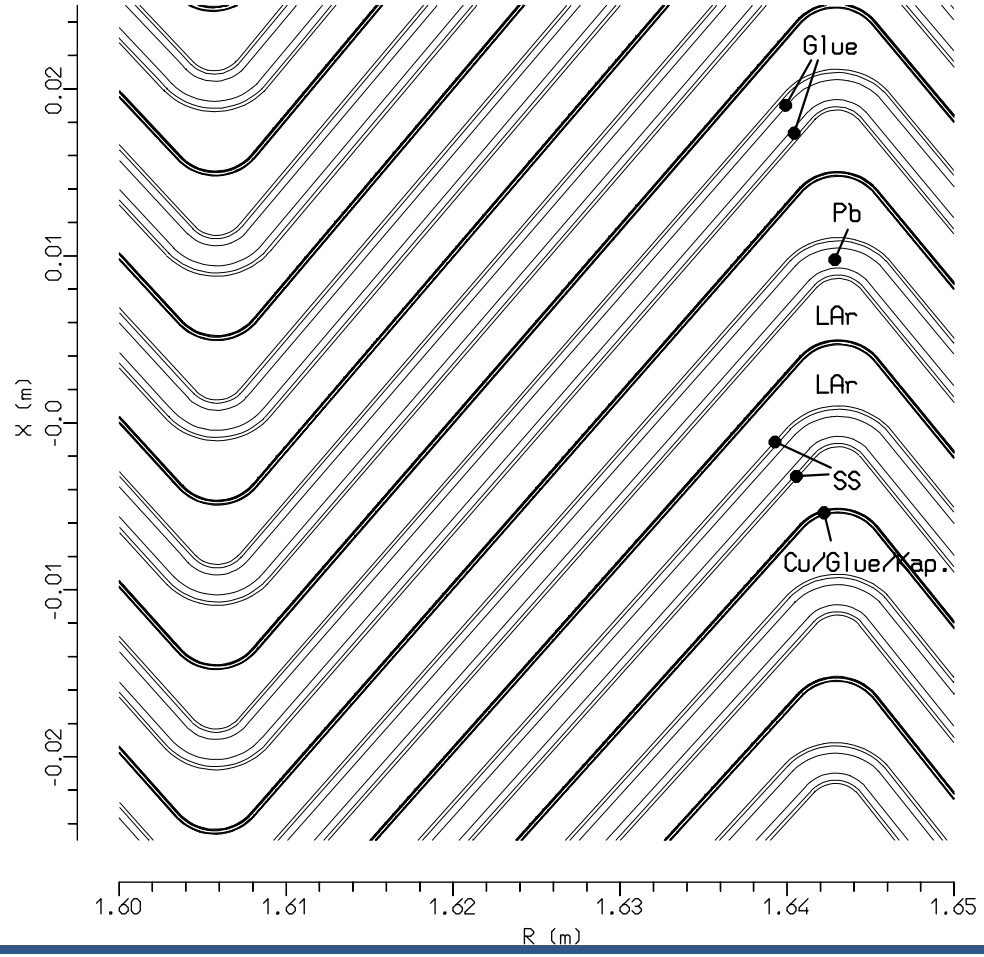

Sampling term :

e at $\eta = 0.28$

MC at 10 and 100 GeV

$$\text{Exp. :} \frac{\sigma}{E} = \frac{9.8 \pm 0.4\%}{\sqrt{(E)}}$$

$$\text{FLUKA :} \frac{\sigma}{E} = \frac{9.2 \pm 0.3\%}{\sqrt{(E)}}$$

LAr electromagnetic calorimeter

Phi modulation of the response

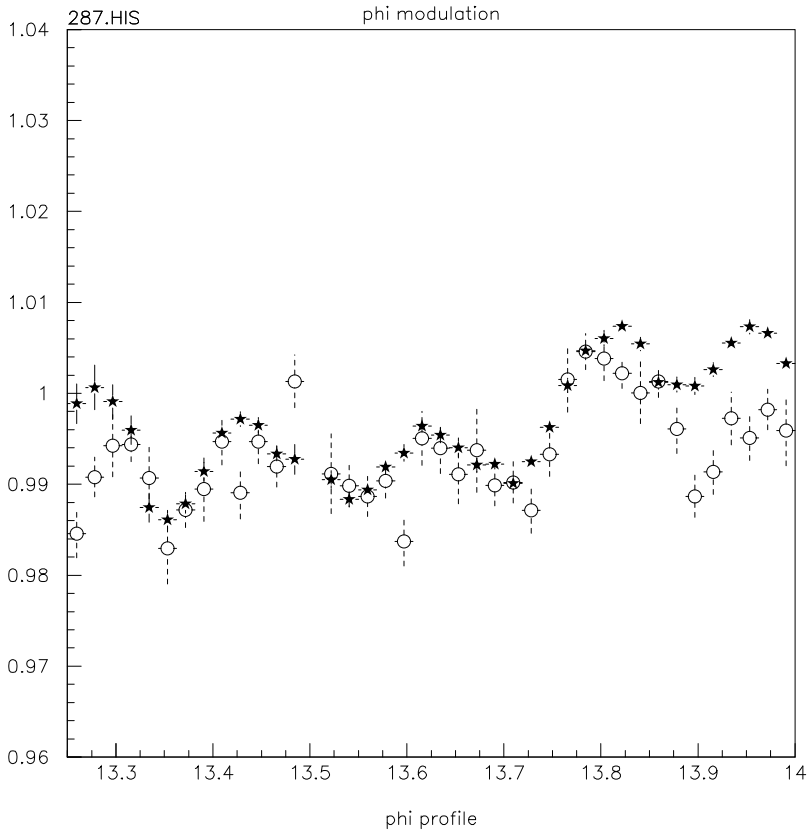

Longitudinal Development:

e at $\eta = 0.28$

Energy in sampling 1 / total

E	E1/E		r.m.s.	
GeV	Data	Fluka	Data	Fluka
100	0.68	0.69		
287	0.61	0.58	.091	.094

300 GeV μ in ATLAS combined calo

Calibration in electron scale
electronic noise added

E.M. Calorimeter

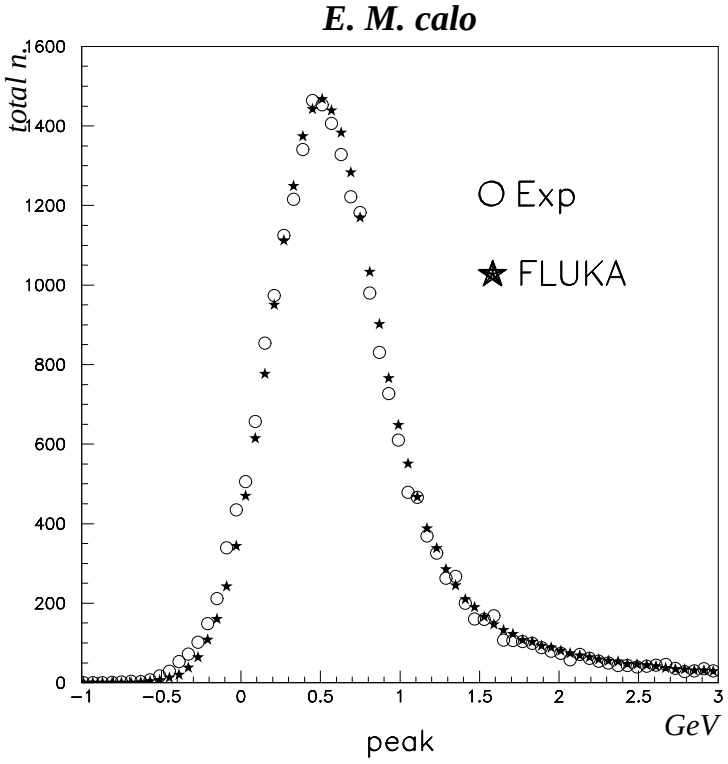

Tile Calorimeter

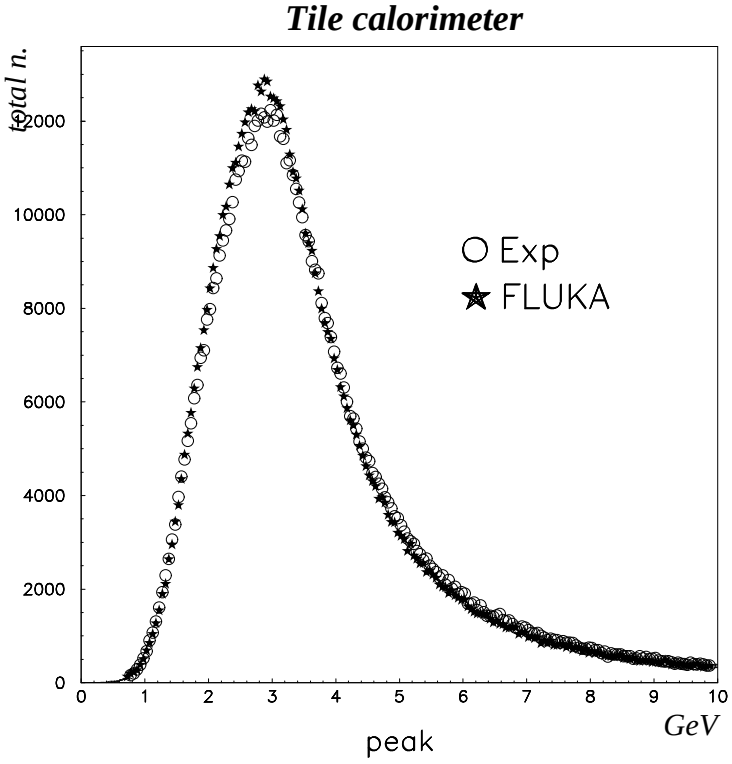

300 GeV μ in ATLAS combined calo

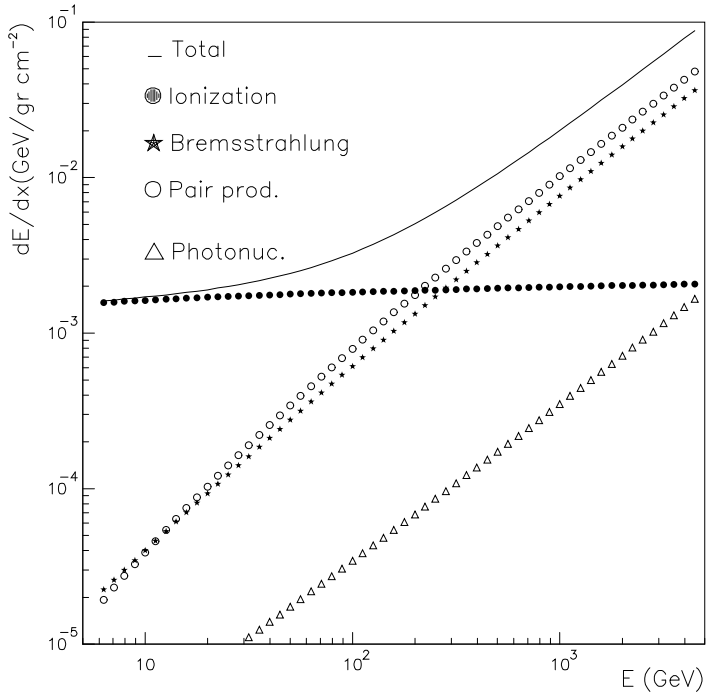

Total and partial energy losses for muons in lead as a function of muon energy

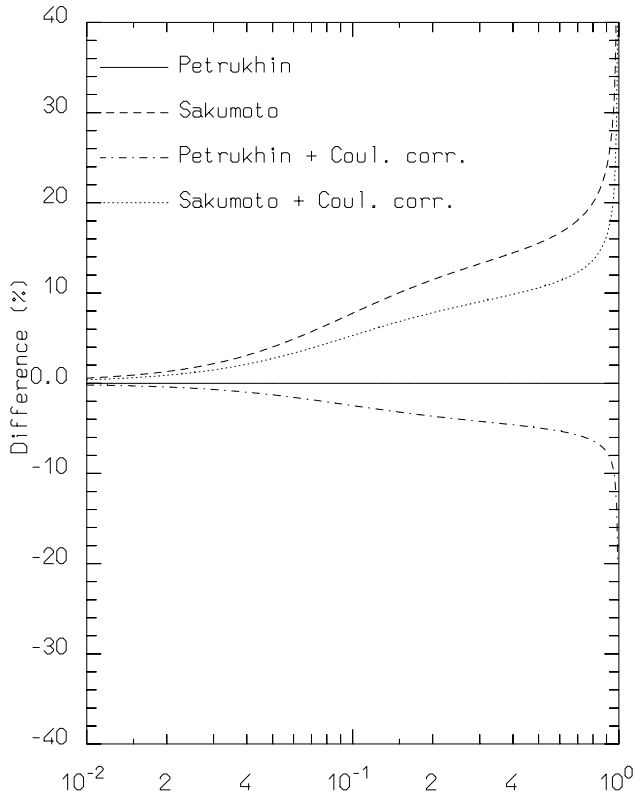

Energy loss difference for 300 GeV muons in lead using different formulations for bremsstrahlung.

300 GeV μ in ATLAS combined calo

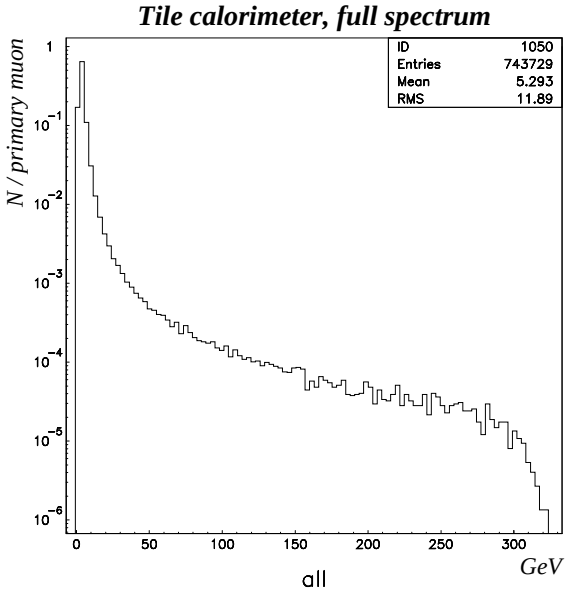

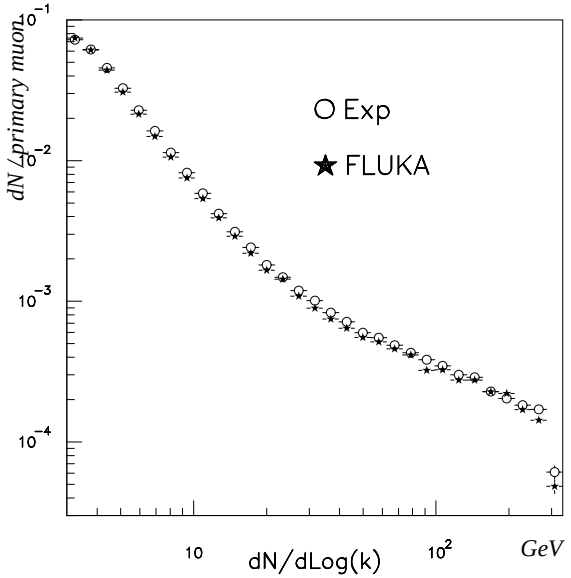

Total experimental spectrum in the Tile calorimeter.

Comparison between calculated and experimental spectra in the tile calorimeter for $v > 0.01$

Comparison with PION data

Cut on mip in presampler Cut on beam position (beam chambers)

FLUKA: Calibration in electron scale

FLUKA: Scintillator quenching included, Noise added

FLUKA: Proton contamination taken into account

Energy reconstructed using the "benchmark" technique:

$$E_0 = E_{em} + a \cdot Q_{had} + b \cdot \sqrt{|E_{em_3} \cdot a \cdot Q_{had_1}|} + c \cdot E_{em}^2 \qquad (1)$$

All parameters fixed to minimize $\frac{\sigma}{E_0}$ *at 300 GeV*

1994 Data: **Experimental electron scale calibration available**

	a (GeV/pC)	b	c (GeV^{-1})
FLUKA	0.172(2)	0.38(2)	-0.00038(10)
EXP	0.172	0.44	-0.00038

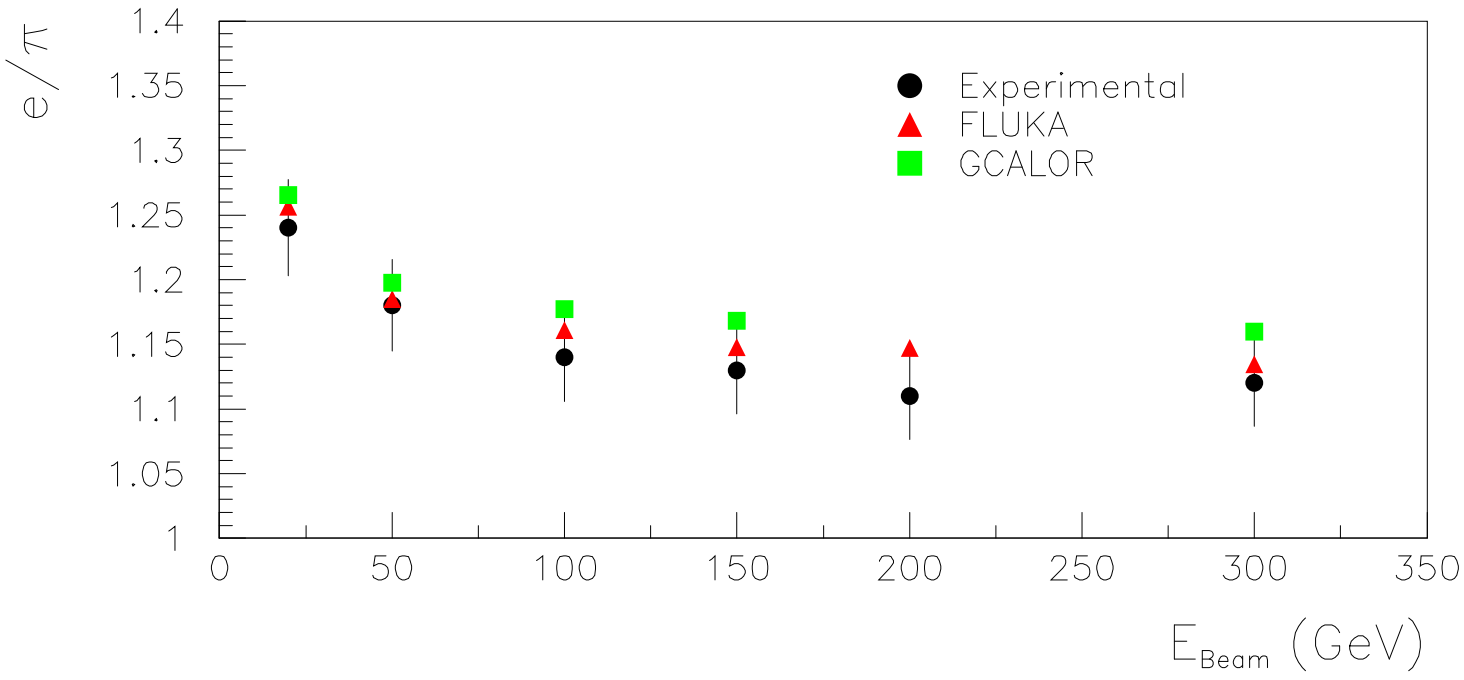

Comparison with PION data

1994 Data

Longitudinal shower development

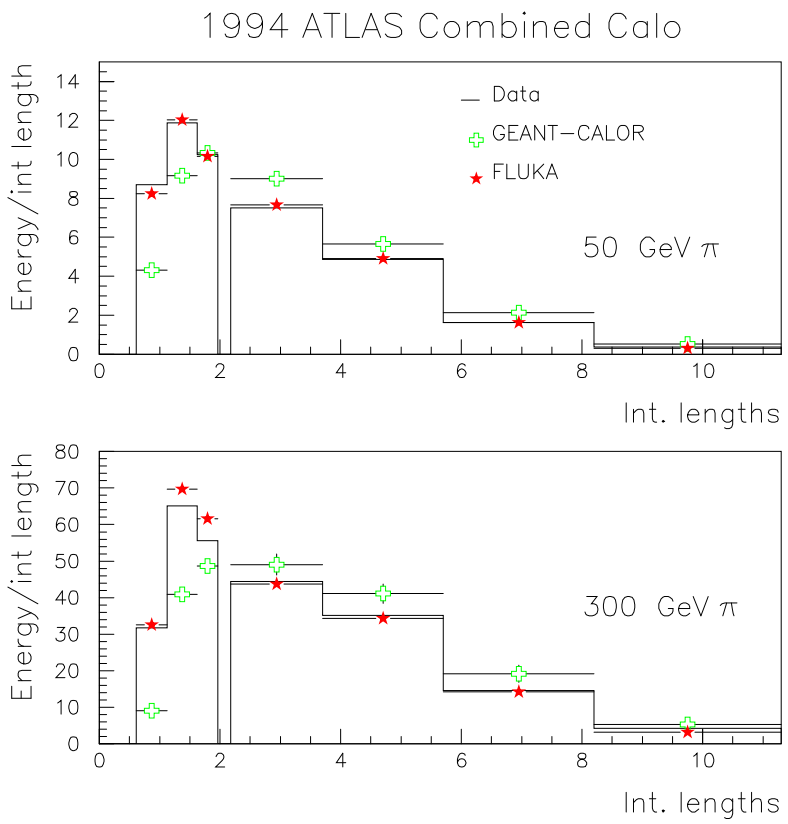

Energy spectrum in E.M. calo

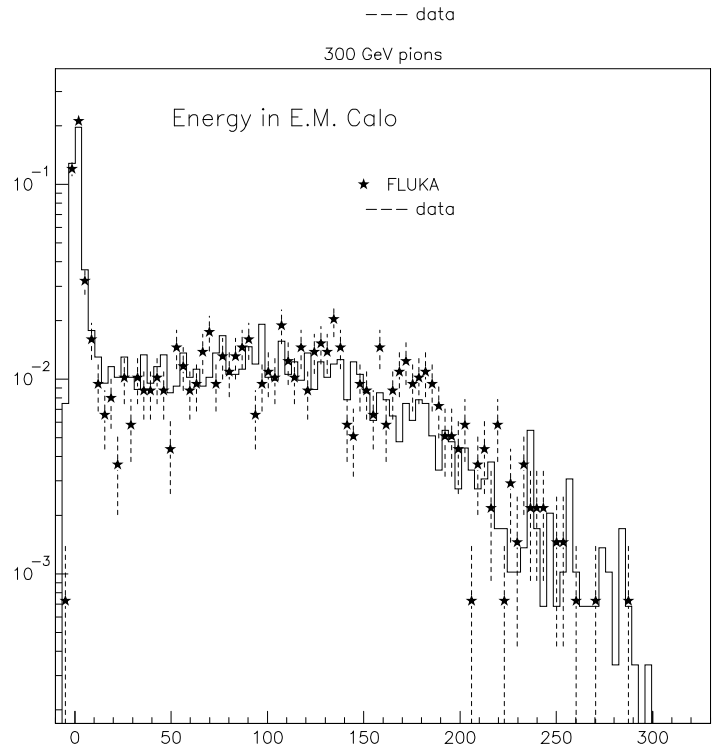

Comparison with pion data

Energy Resolution

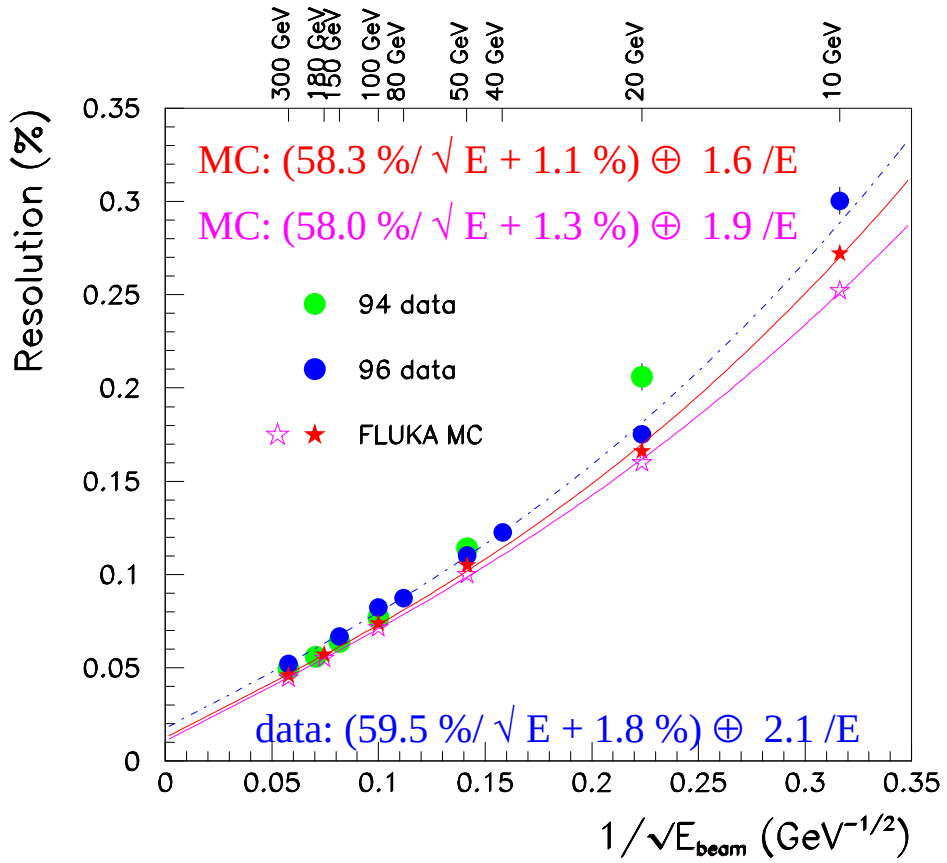

1996 Data :

Less electronic noise

Better presampler

No electron calibration

Comparison with pion data

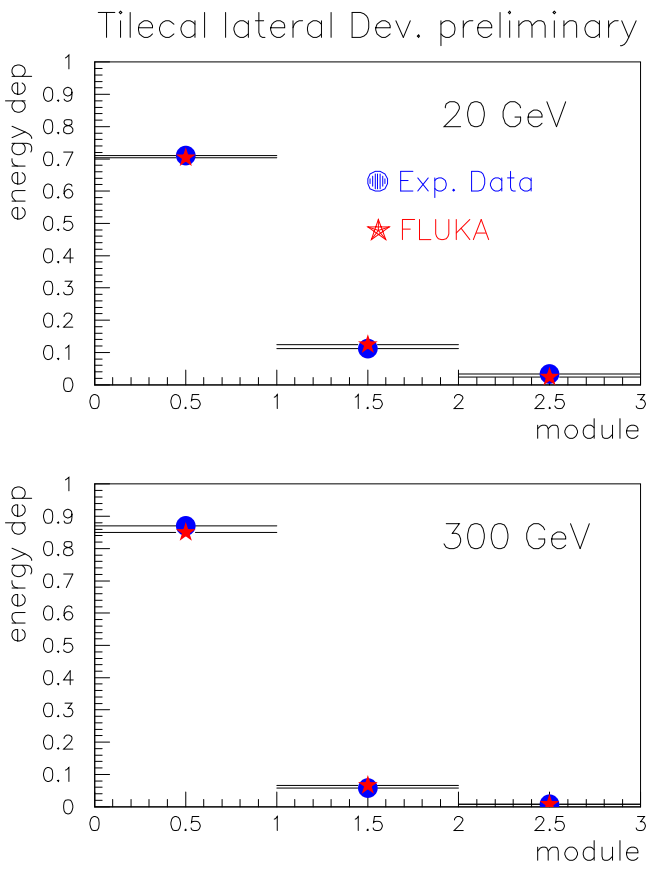

Linearity

1996 Combined Calo Test Beam

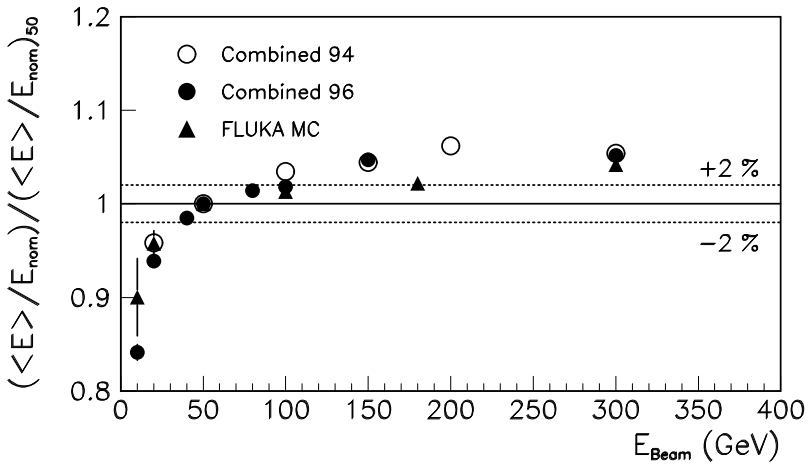

The effect of energy non-conservations

Include in each FLUKA interaction an energy non-conservation similar to the one observed in the old GEANT3-GHEISHA package as a function of projectile/energy

Simulation: Positive Pions in the ATLAS 1996 Combined Calo set-up

E(GeV)	Per Interaction		Per Event		σ/E	
	E_{miss}	rms	E_{miss}	rms	FLUKA	FLUKA+E_{miss}
10	0.094	0.25	2.1	0.93	24%	35%
100	0.070	0.28	12.7	5.3	7.2%	11.4%

$\Downarrow$

To enforce energy and momentum conservation at each step is as important as having sound physical models!!

The background in the ATLAS hall

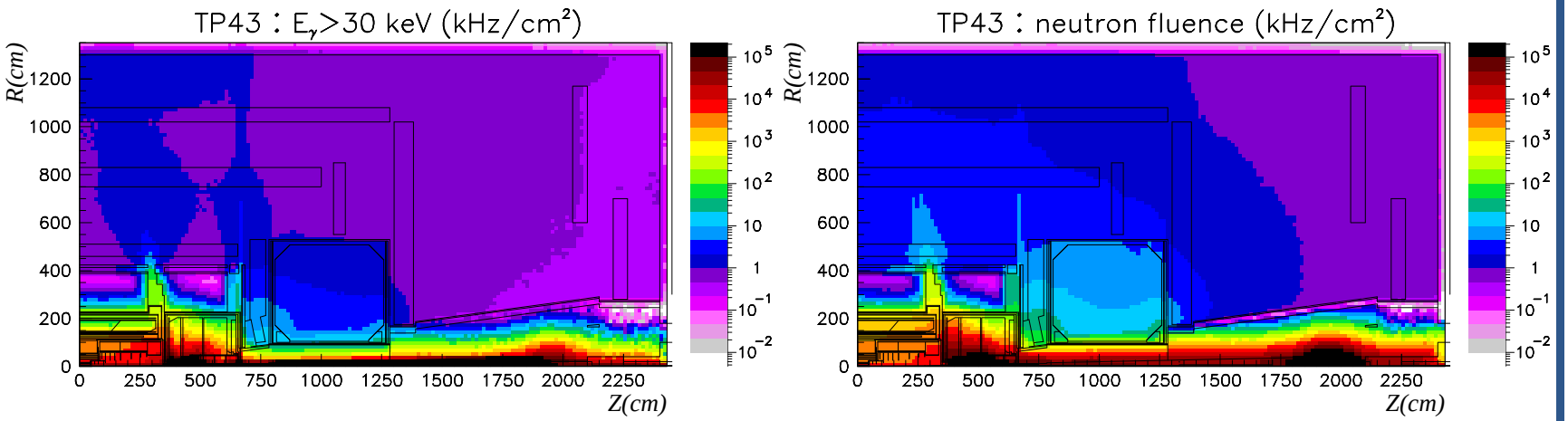

Computed photon (right) and neutron (left) background in the ATLAS experiment at LHC

LHC background benchmarking

Absolute yield and spectral measurements of photons and neutrons emanating from the final stages of hadronic showers have been checked with a $Bi_4Ge_3O_{12}$ detector with 40 and 120 GeV/c beams on 11 λ (200 cm) and 14 λ (240 cm) thick cast iron targets

The results were intended to verify or disproof the simulations used for assessing the soft particle background at LHC experiments

(E. Gschwendtner, H. Vincke, C.W. Fabjan, N. Hessey, T. Otto, CERN-EP/2001-025, submitted to NIMA)

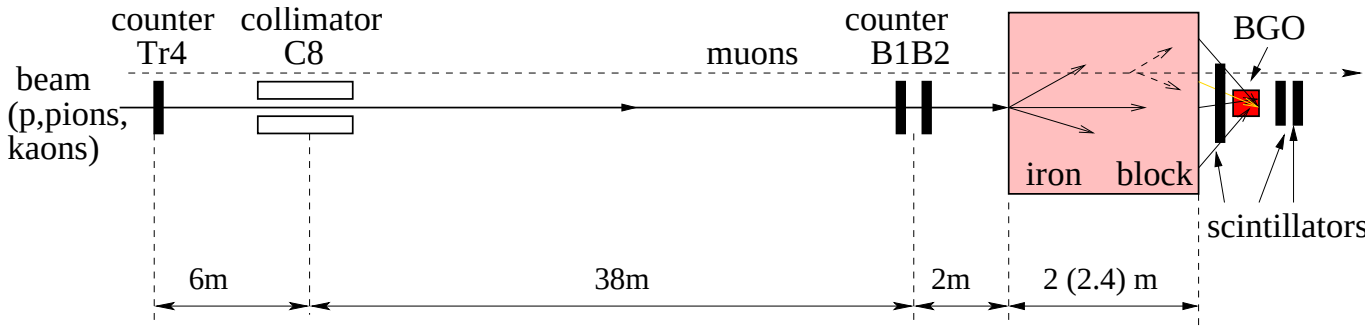

LHC background benchmarking

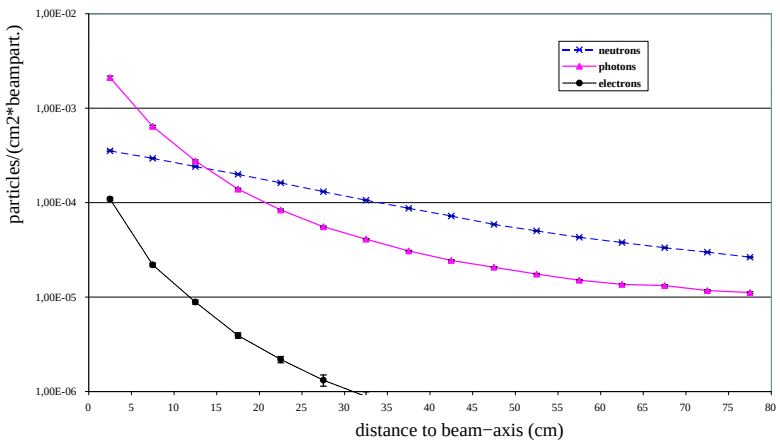

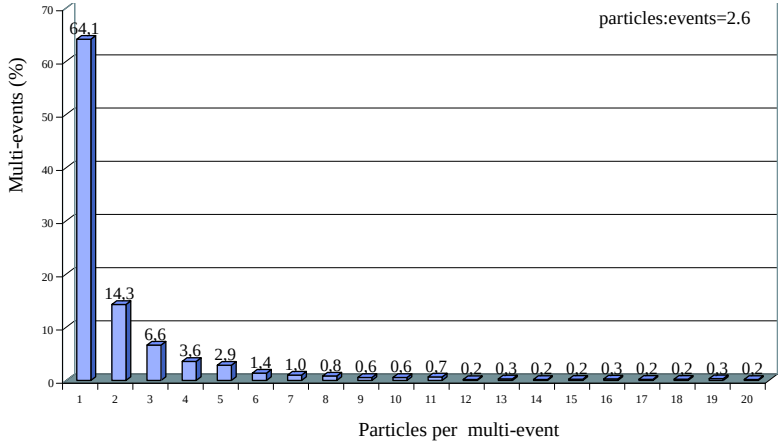

Computed shower composition at 40 GeV/c, 240 cm thickness (left), and computed event multiplicity in the BGO (right)

Showers are still dominated on axis by late π^0 !!

⇓

The event multiplicity and possible accompanying charged particles must be accounted for in order to repoduce properly the experimental conditions and vetos

LHC background benchmarking II

Measurement set-up	Signal rate $\times 10^{-4}$		Ratio
	Measured	Simulated	meas./sim.
$p_{\mathrm{beam}} = 40\,\mathrm{GeV}/c$			
200 cm on-axis	76.2 ± 0.4	$71.8\,^{+\,6.7}_{-\,14.9}$	$1.06\,^{+\,0.10}_{-\,0.22}$
200 cm off-axis	6.8 ± 0.2	$6.1\,^{+\,0.8}_{-\,0.7}$	$1.12\,^{+\,0.14}_{-\,0.13}$
240 cm on-axis	23.0 ± 0.4	$15.8\,^{+\,2.7}_{-\,3.6}$	$1.46\,^{+\,0.25}_{-\,0.33}$
240 cm off-axis	2.3 ± 0.1	$1.9\,^{+\,0.3}_{-\,0.2}$	$1.24\,^{+\,0.19}_{-\,0.15}$
$p_{\mathrm{beam}} = 120\,\mathrm{GeV}/c$			
200 cm off-axis	26.3 ± 0.4	$26.0\,^{+\,3.0}_{-\,2.9}$	$1.01\,^{+\,0.12}_{-\,0.12}$
240 cm on-axis	93.5 ± 1.7	$78.6\,^{+\,9.6}_{-\,11.1}$	$1.19\,^{+\,0.15}_{-\,0.17}$
240 cm off-axis	9.7 ± 0.6	$7.8\,^{+\,1.4}_{-\,1.3}$	$1.24\,^{+\,0.24}_{-\,0.21}$
		Weighted average	1.13 ± 0.06

Summary of measured and simulated signal rates in the energy interval $0.35\,\mathrm{MeV} < E < 9\,\mathrm{MeV}$ per incident beam particle

LHC background benchmarking III

Measurement set-up	$\langle E$-deposition$\rangle$ [MeV]	
	Measured	Simulated
$p_{\text{beam}} = 40\,\text{GeV}/c$		
200 cm on-axis	2.045 ± 0.018	2.057 ± 0.174
200 cm off-axis	1.615 ± 0.004	1.618 ± 0.041
240 cm on-axis	1.923 ± 0.009	1.824 ± 0.073
240 cm off-axis	1.666 ± 0.003	1.530 ± 0.021
$p_{\text{beam}} = 120\,\text{GeV}/c$		
200 cm off-axis	1.572 ± 0.009	1.805 ± 0.091
240 cm on-axis	2.051 ± 0.020	2.058 ± 0.183
240 cm off-axis	1.649 ± 0.006	1.687 ± 0.051

Summary of measured and simulated averaged energy depositions in the energy interval $0.35\,\text{MeV} < E < 9\,\text{MeV}$

LHC background benchmarking IV

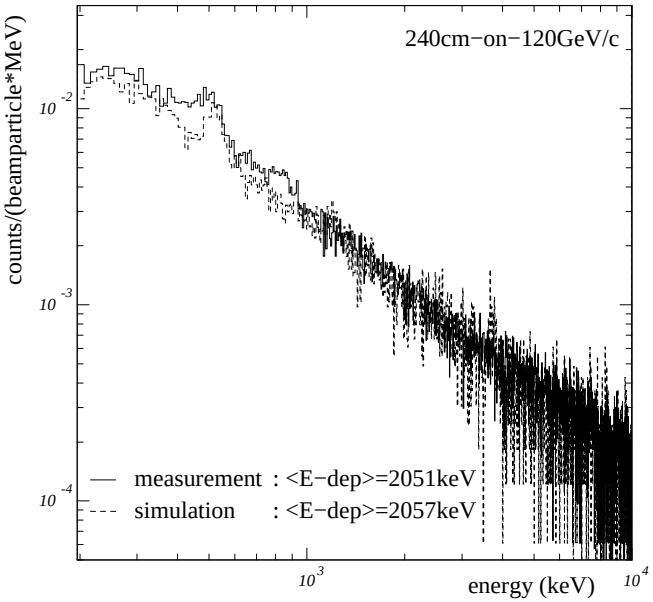

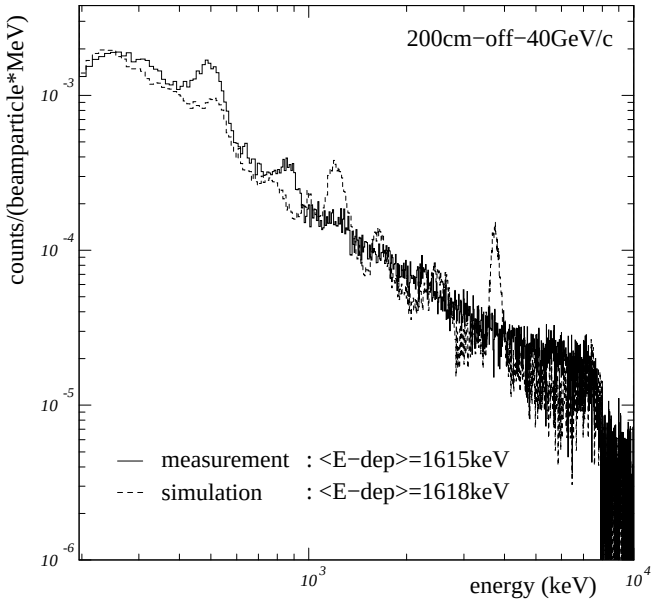

Computed and measured total spectra for two different beam energy, thickness and position combinations

Future developments:

- Ion interactions:
  - Consolidation and benchmarking of the interface with DPMJET
  - Extension of the present nuclear models to handle light ions in the intermediate energy range
- A new powerful and user friendly interface through the ROOT system
- Residual activity and dose rates: *Online use of databases for:*
  - *Cooldown* calculations (already implemented offline)
  - γ, β *and* α radiation emission and transport online.
- DPM: add multi-Pomeron exchanges
- PEANUT extension to high energy
- Refinements to evaporation, inclusion of heavy fragment emission
- New low energy neutron library